Proportional, Simultaneous and Independent Control (PsiCon) of Upper-Limb Prostheses for the Limb-Absent Population

by

Ziling Zhu

A Thesis
Submitted to the Faculty
of the
WORCESTER POLYTECHNIC INSTITUTE
in partial fulfillment of the requirements for the
Degree of Doctor of Philosophy
in
Electrical and Computer Engineering

May, 2021

APPROVED:

Professor Edward A. Clancy, Major Advisor, WPI ECE

Professor Xinming Huang, Committee Member, WPI ECE

Todd Farrell, Ph.D., Committee Member, Liberating Technologies, Holliston, MA

Abstract

The bioelectrical signal generated by muscle activities is the electromyogram (EMG). EMG is a powerful tool utilized in various medical assessments, rehabilitation, and myoelectric control of prostheses and orthoses. Continuing previous study by our group, this dissertation focused on three main topics in upper-limb myoelectric prosthesis control: offline testing of EMG signals and force control under mirrored movement, including direct mechanical comparison of bilateral forces; online testing of prosthesis control performance under different real-time control strategies; and online performance during 2-degree of freedom (DoF) dynamic target tracking.

The first topic of the thesis was a study of EMG-force and EMG-target performance during hand-wrist contraction in both able-bodied and limb-absent subjects in force-varying tasks, especially in bilateral mirror tasks. In order to solve the problem that limb-absent subjects have no end-effector force available as the supervisory output in EMG-force models, different kinds of feedback, such as contralateral force and target movement, were provided as alternatives in EMG-force models. We initially tested these alternative models offline on able-bodied subjects and compared to the true EMG-force model which we could measure only on able-bodied subjects, then applied the results to limb-absent subjects to contrast performance. The benchmark errors of relating EMG to dominant force on able-bodied subjects were ~10 percent maximum voluntary contraction (%MVC). Errors when using either contralateral force or target movement in bilateral tracking as alternative outputs were 12–16 %MVC, while no-feedback in unilateral tracking produced errors of 25–30 %MVC. This project explored the influence of different feedback conditions on the models, and effectively provided some calibration protocols than can be adopted in actual prosthetic control.

This first topic was extended to document normative force/moment tracking performance during bilateral symmetric hand-wrist tasks. In this aspect of the project, we measured the force /moment from both limbs to test the tracking accuracy under different conditions. This project provided some useful results of how intrinsic characteristics and external visual conditions jointly influenced bilateral synergies on able-bodied subjects, and thus, to better provide data support for the study of limb-absence device control from a biological perspective.

The second project involved online testing of prosthesis control to complete standardized (SHAP) tests for both able-bodied and limb-absent subjects. The project integrated the design of prosthesis

hardware, software, algorithms and thresholding. Three different control strategies were studied: conventional 2-site control (2 electrodes) with co-contraction switching, 2-DoF direct control (6 or 12 electrodes) and 2-DoF mapping control (6 or 12 electrodes) during three tasks: 1-DoF box-block test, 2-DoF clothespin refined test and 2-DoF doorknob test. The project investigated the actual ability of limb-absent subjects to control a multi-DoF prosthesis, and the superiority of new 2-DoF control algorithms over traditional control methods.

The third project explored the feasibility of 2-DoF EMG-force models for the wrist only, and also the wrist-hand, and found the minimum number of electrodes required for hand-wrist control in both 1-DoF and 2-DoF tasks by backward stepwise selection. The results showed as few as two electrodes for 1-DoF and four electrodes for 2-DoF could achieve the best performance, with an average RMS error of 6.0–16.3 %MVC for wrist only, and 8.3–9.2 % MVC for wrist and hand.

Other co-participated projects complemented the above projects. The first project focused on efficient training of 2-DoF EMG-force models, finding that a minimum training data length of approximately 40–60 s is the best, and proposed a new universal EMG-force filter across all subjects (as an alternative to subject-specific models or DoF-specific models), which was 15–21% better than original subject-specific models. The second project was a transition between offline testing and prosthesis control. Subjects controlled the cursor on the screen to reach different target position. The count of the number of correct target acquisitions, overshoot rate, path efficiency and stability for each DoF combination were tested to exhibit the performance of real-time 2-DoF control. The third project explored optimization of EMG processing in additive noise with root-difference-of-squares (RDS) and whitening methods.

In summary, this thesis provides a systematic study on prosthesis control. It starts with offline EMG-force model and optimization for able-bodied subjects. It then investigates the problems which limb-absent subjects face with respect to alternative feedback selection in bilateral tasks design. Finally, it tested algorithm performance when subjects directly used a prosthesis to complete some daily tasks.

Acknowledgement

In this thesis I describe the research I conducted in pursuit of my Doctor of Philosophy in Electrical and Computer Engineering in Worcester Polytechnic Institute.

Foremost, I would like to offer my deepest gratitude to my academic advisor, Dr. Edward A. Clancy. He not only inspires me by his profound knowledge and passion to the research, but also shares his experience and provides support to my life and study. It is my honor to have him as my PhD advisor.

Thanks to my committee members, Dr. Xinming Huang and Dr. Todd Farrell. Dr. Xinming Huang is a great professor that provides a lot of instructions and help to me on campus; Dr. Todd Farrell is an expert on prosthesis design, and his technical and intelligent guidance provides a great help to my research.

Besides, I feel grateful to have the whole LTI team's support during the PsiCon project. Specially, thanks to Carlos Martinez Luna for his strong technical support for the experiment. Without his help, the experiment would not proceed so smoothly.

Thanks to my senior alumnus Chenyun Dai. His guidance and support are the biggest motivation for me to advance in this field. Thanks to my senior alumnus Berj Bardizbanian. I am very happy to have this unforgettable experience to work with him.

Thanks to my beloved parents Yonghua Zhu and Wei Jiang. They are the most important people in my life; not only gave me life, but taught me all I need to know, loved me no matter what, and supported as I grew.

I also want to thank to all the partners in the lab, Jianan Li, He Wang, Haopeng Wang, William J. Boyd and Kiriaki J. Rajotte. Thanks so much for their help on my research, and the harmonious laboratory atmosphere as a big family. I am very happy to have all of you working in a group during my PhD study.

Contents

Chapter 1: Introduction

The introduction includes two main parts: background and the contribution of my Ph.D. work. The background part firstly describes the basic biomedical knowledge of EMG and its processing techniques, and then shows the development of prosthesis design. The contribution part separately talks about the current research field and my contribution of that field included in each subsequent chapter.

1.1 EMG and Processing Techniques

Electromyography (EMG) is a technique to record and evaluate the electrical activities of skeletal muscles. When muscles cells activate and contract, an electric potential is generated. This signal can be detected and analyzed for biomechanical movement, medical abnormalities and so on.

1.1.1 Structure of Skeletal Muscle

Skeletal muscle is one of the major muscle types in the human body. Most skeletal muscles are attached to bones by bundles of collagen fibers. These muscle groups are mainly responsible for human movement and exercise by producing voluntary contraction (Kamen 2004). The whole of skeletal muscle is comprised of muscle fascicles, which are a collection of muscle fibers (Fig. 1.1). There are two types of fibers: "slow-twitch" fibers (Type I) produce slower, less forceful contraction which need more generation of ATP from

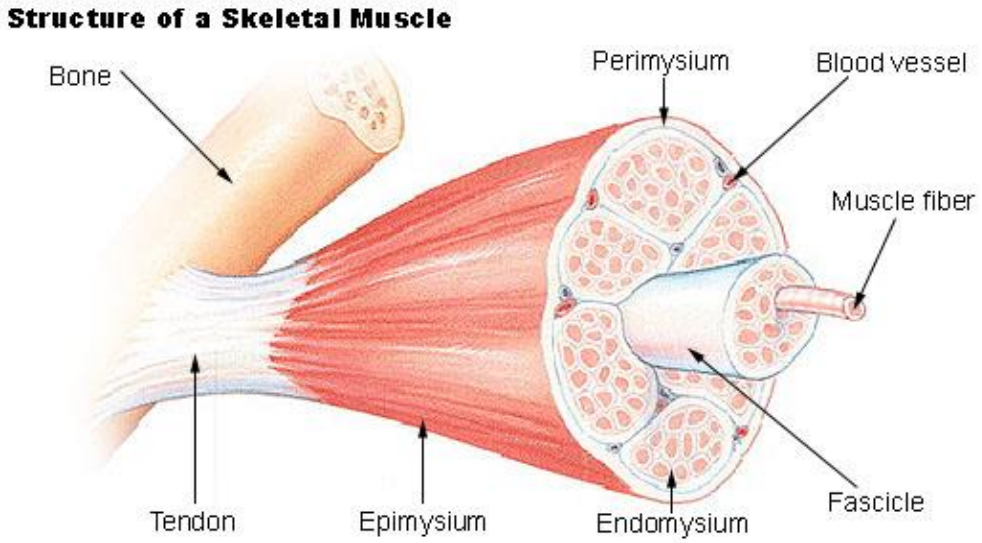

Fig. 1.1

aerobic metabolism. These fibers are usually slow to fatigue. The "fast-twitch" fibers (Type II) produce quicker and more forceful contraction, and need more generation of ATP from glucose. These fibers are fast to fatigue (Burke, Levine et al. 1971, Barry 1992).

When muscles are stimulated by their motor neuron, the muscle fibers contract. A motor neuron is a neuron whose cell body is located in the motor cortex, brainstem or the spinal cord, and the axon projects to the outside to directly or indirectly control muscles or organs (Georgopoulos, Kalaska et al. 1982, Graziano and Aflalo 2007). When the brain sends commands to the muscles, the motor neurons transmit the electrical signals to the muscle to electro-chemically activate muscle fibers. Under the excitation of a motor neuron, muscle fibers depolarized to create contraction, which also creates an electromagnetic field. This field can be recorded within muscle or on the skin surface.

1.1.2 Motor Unit and Action Potential

The motor unit consists of a motor nerve and all its innervated muscle fibers (Buchthal and Schmalbruch 1980) (Fig. 1.2). The muscle contraction, microscopically, is the motor units exhibiting mechanical twitch by stimulation. At the macro level, the force generated by muscle contraction is

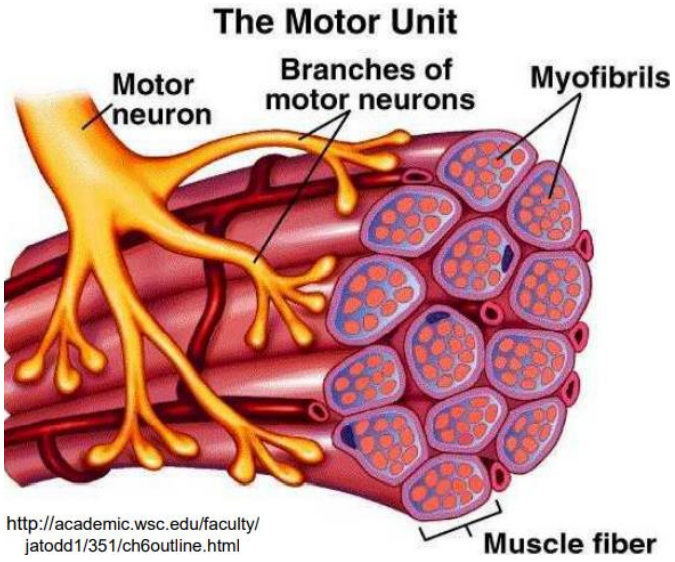

Fig. 1.2

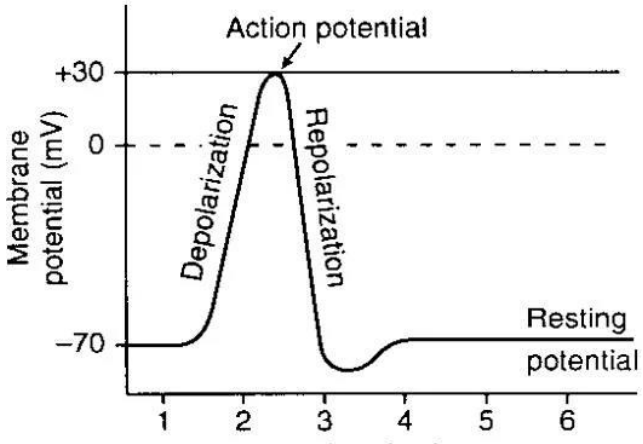

Fig. 1.3

determined by two factors: number of active motor units and firing rates. As the force increases, the number of active motor units, also called recruitment, gradually increases. When initially recruited, the firing rate is by 5–10 pulses/sec, and increases with force to 20 pulses/sec or more. For each motor unit, the time course of an electrical "action potential" is shown in Fig. 1.3. For a typical transmembrane potential of a muscle cell, the potential is initially resting at -70 mV, and then depolarizes to reach a voltage peak of +30 mV, which is the action potential. Then after a quick repolarization, the potential returns to the resting voltage. A complete action potential duration is 2–4 ms or longer. For one (healthy, non-fatigued) motor unit, the shape of its action potential is generally relatively fixed, while different motor units have different action potential shapes.

A recorded electrical signal from the muscle, as EMG, is a combination of action potentials from many different motor units, with different shapes and firing rates.

1.1.3 EMG Recording

To detect EMG muscle activity, two main recording techniques are used: indwelling (intramuscular) EMG recordings and surface EMG recordings (Fig. 1.4). In indwelling EMG recordings, needle electrodes are inserted directly into a muscle through the skin to record the electrical activity in that muscle. Because the needle electrode has a small area and is located close to the motor units, the recordings usually look like a series of individual spikes, which are the firings of a few motor units. Indwelling EMG has a wide use for clinical diagnosis and management of nerve or muscle diseases. In surface EMG recordings, some surface electrodes are secured over a large area of the skin surface and the recorded signal looks like an amplitude-modulated random signal which is modulated by effort level; a lot of undistinguished spikes from many motor units are mixed with noise, motion artifacts and so on. Compared with indwelling EMG recordings, surface EMG does not involve piercing the skin and does not hurt, and its modulation has a strong relationship with the force effort level. Therefore, in establishing the relationship between EMG and force and EMG's control of prostheses, many scholars prefer to use surface EMG, which is more acceptable to the public.

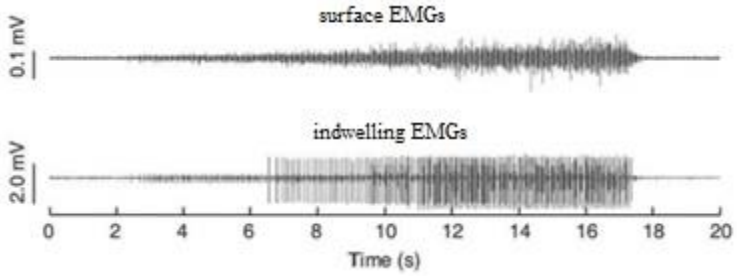

Fig. 1.4

1.1.4 EMG Signal Processing

Based on different uses of EMG recordings, a variety of EMG signal processing techniques are utilized to extract useful features. For indwelling EMG, since it is mainly used in medicine for diagnosis and disease recovery, researchers use classification or clustering methods to decompose spikes into different groups, detect some abnormalities in EMG signals and locate to the corresponding muscle tissue.

For surface EMG recordings, the EMG amplitude (EMGamp) is an important estimator of the intensity of the EMG signal (Fig. 1.5). EMGamp is the time-varying standard deviation of the EMG signal, and it varies with muscle tension or localized muscle fatigue. If we model the recorded surface EMG as an amplitude modulated, zero-mean random process, the raw EMG signal can be written as:

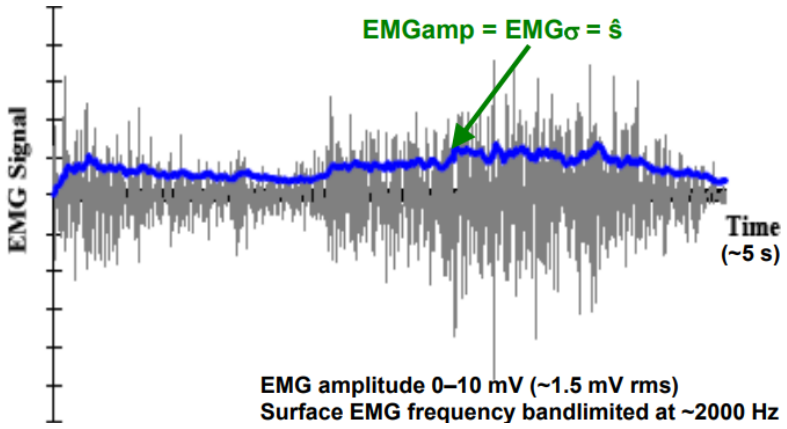

Fig. 1.5

$$m_i = s_i \cdot w_i$$

where i is the discrete-time sample index, m_i is the raw EMG signal, s_i is EMGamp (modulation) and w_i is a random process. The PDF for N samples m_1, m_2,..., m_N and quasi-constant effort is:

$$p_{m_1,\dots m_N}(M_1,\dots M_N|\hat{s}) = \frac{1}{(2\pi\hat{s}^2)^{N/2}} e^{\frac{-\sum_{i=1}^{N} M_i^2}{2\hat{s}^2}}, -\infty \le M_i \le \infty$$

If the random process is Gaussian distributed and the samples are independent, the optimal (ML) solution for $\hat{s}_i$ is the RMS:

$$\hat{s}_i = \left[\frac{1}{N}\sum_{i=1}^{N} M_i^2\right]^{1/2}$$

which is a moving average filter. EMGamp can be improved by some techniques such as noise cancelling, EMG signal whitening (when the samples not independent), and multiple EMG channels for large muscles. Nowadays, a complete set of EMGamp processing procedures includes the following steps (Fig. 1.6): 1) since most useful EMGamp information is below ~10 Hz, a high-pass filter to remove noise and motion artifacts; 2) EMG whitening to reduce variance of the amplitude estimate; 3) rectify to demodulate the standard deviation (Vredenbregt and Rau 1973, Weir, Wagner et al. 1992); and 4) a low-pass filter to smooth the signal (Clancy and Hogan 1994, Clancy, Morin et al. 2002, Clancy, Negro et al. 2016).

Other features such as waveform length, zero-crossing rate and slope-sign change rate have good performance under some special needs and can be used as an auxiliary tool to help EMGamp better realize some functions.

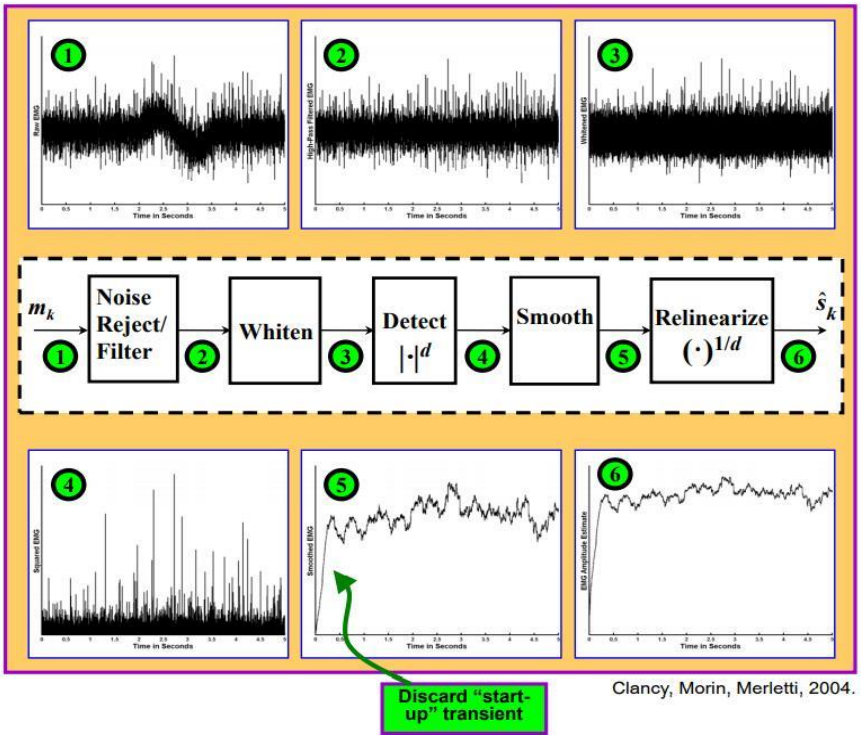

1.1.5 EMG-Force Model

In general, when the brain sends commands to muscles, motor unit firing cause electrical changes that can be measured as the EMG signal, and physiologically, leads to force/moment change at the muscle and joint. Since EMGamp has strong relationship with the force change, we assume that the EMG signal contains sufficient information to estimate joint force/torque.

Because the EMG-force relationship is affected by many factors including: 1) kinematics, including different kinds of contraction, fatigue, dynamic changes in joint angle, muscle co-contraction, 2) anatomy and physiology difference person to person, and 3) electrodes/hardware design; a general EMG-force model is proposed as:

$$F[m] = \sum_{d=1}^{D} \sum_{q=0}^{Q} \sum_{e=1}^{E} c_{q.d} EMG\sigma_e^d [m-q]$$

where F is the estimated force, m is the sample index, D is the polynomial nonlinear order, Q is the number of time lags, EMGσ = EMGamp, and subject-specific coefficients $c_{q.d}$ are calculated by a least-squares fit procedure (Clancy 1991).

1.2 Prostheses Development

A prosthesis is an artificial device to replace a missing body part. Body parts can be missing due to accidents, disease or congenitally., Especially when a limb is absent, a prosthesis can restore some functions of their absent body part. The development of prostheses plays an important role in rehabilitation for the limb-absent population, bring them a more normal life.

1.2.1 History of Prostheses

Fig. 1.7

The first confirmed use of a prosthetic device is from 950–710 BC (Finch 2011). Due to wars, many people lost their limbs and thus procured some kind of body/limb shape prosthetics by wood or metal to realize some basic functions. Examples include a prosthetic leg to stand, or a prosthetic hand/arm to hold a weapon (Friedmann 1978) (Fig. 1.7). Most of these prostheses had no mechanical structure to drive them and simply look like a model, and only wealthy people or armies could afford them. Most prostheses didn't look like a real body shape. For example, hand prostheses looked like a hook or even a knife instead of a 5-finger hand, since these shapes were enough to complete most necessary tasks, while a fake anatomically-shaped hand looked very delicate and might not be able to hold a glass of water steadily.

At the end of World War II, the NAS (National Academy of Sciences) began to advocate better research and development of prosthetics. And, in the following decades, the prostheses gradually developed in three directions:

1. Besides the use of prostheses by military, soldiers and scientific studies, more commercial prostheses were provided to the public.
2. The appearance of prostheses became more realistic as a real body shape, and the mechanical structure was more ergonomic and kinematic in design.

3. More advanced algorithms allowed prostheses to have more precise and functional control, to deal with complex tasks.

There are three main categories of prostheses: passive prostheses, body powered prostheses and myoelectric prostheses. For passive prostheses such as a passive hand, the force to adjust the grasping mechanism is applied externally. Most passive prostheses have no moving parts and can be adjustable by external force. These prostheses are very useful in bimanual tasks that require fixation or support of an object (Maat, Smit et al. 2018). Body powered prostheses rely on a system of cables or a harness to control the limb itself. Essentially, people operate and control the prostheses by other parts of the body, such as the shoulder, elbows etc. Myoelectric prostheses are controlled using electric signals that are created by muscles. As a hot topic to current scholars and one of the best type of development prospects, myoelectric prostheses fully use the residual limbs to obtain electrical signals (EMG) from these muscles, translate the signals into movement and execute the demands properly (Wirta, Taylor et al. 1978).

1.2.2 Modern Control of Myoelectric Upper-Limb Prostheses

Nowadays, more than 2 million people live with limb absence in the US, and this number increases by an average of 185,000 each year (Dillingham, Pezzin et al. 2002, McGimpsey and Bradford 2008). A high demand for high performance, multifunctional, and affordable prostheses brought more support from government and growth of the market.

Although upper-limb prostheses hooks or gripper can handle most daily or special tasks, some modern prostheses are also moving toward more diversified functions (Fig. 1.7). Instead of conventional opening and closing in one dimension, the new prosthetic hands have different grip pattern hand positions which can perform activities such as eating meals, carrying bags, opening doors, or even controlling a mouse. This kind of prosthesis based on EMG signal control can realize proportional control, which enable people to adjust the speed and force by the intensity of muscle contraction.

The techniques of controlling myoelectric prostheses have also been gradually developed with the development of computer and microelectronics technology.

Two-site control: The conventional and most typical myoelectric hand prostheses are designed with two bipolar electrodes separately contacting the flexors and extensors to control hand close and open, respectively. Limb-absent people only need to learn how to separately contract the flexor or extensor of their residual limb, and prosthesis movement is based on the contrast of two EMG signals. Two-site control is simple but mature, and still the most used technique in commercial prostheses. The limitation of this technique is that only one degree-of-freedom (DoF) can be controlled.

Co-contraction control: An advanced version of 2-site control allows users to control multi-DoF movement, such as open-close and pronation-supination. This technique is a sequential controller, in which the user controls one-DoF at one time, and switches to another DoF by a quick co-contraction of both flexor and extensor muscles. This is a relatively cumbersome technique, and highly influenced by a user's residual limb condition, since muscle contraction imbalance or neuron damage make it hard to trigger a co-contraction.

Learning-based control: Features of EMG signals are extracted and put into a learning system. These features will be trained by models for estimating the user's intent. Classification and regression are two main techniques researchers are most interested in. The classification method recognizes different patterns of EMG signals and their corresponding motions in the training phase, and predicts the motions by EMG signals in the testing/use phase. Classification is a highly efficient and precise method if the EMG pattern is repeatable. However, in real life, a large variety of conditions such as noise, skin condition, and motion artifacts seriously affect prostheses control, which can make the results of classification unreliable. The regression method is a continuous mapping between EMG signals and force (or movement) to predict continuous output values, compared with a finite number of pre-trained patterns in classification. This is more robust to some unpredictable variations in EMG signals, and has better performance during untrained conditions (Fougner, Stavdahl et al. 2012, Hahne, Biessmann et al. 2014, Hahne, Dahne et al. 2015). The advantage of learning-based control removes the restrictions of 1-DoF control, but needs more electrodes (channels) recorded and more complicated processing.

1.3 Current State of My Research Field and My Contribution

This section describes the main research wors I completed during my Ph.D. study. The entire work followed the outline of the PsiCon project supported by the U.S. Eunice Kennedy Shriver National Institute of Child Health & Human Development. The project had 4 phases, and I was the lead student researcher on phases B and D. Phase B focused on the characteristics of EMG and force in bilateral mirror tasks. Phase D focused on real-time prosthesis control to complete daily tasks. Additionally, I focused on dynamic target tracking projects for both wrist-only and wrist-hand prior to the PsiCon project.

1.3.1 EMG Mirror Project

Current research field: System identification models relating EMG signals to force are now widely use in myoelectric upper-limb prostheses research. A variety of supervised system identification models have been used to model EMG-force, mainly approached by two techniques: classification and regression. Both techniques have their advantages, and now regression is more acceptable by part of the researchers as its robustness to instability and susceptibility to external influences of EMG signal (Hahne, Markovic et al.

2017). Most research on EMG-force models were tested on able-bodied subjects since both EMG and force could be measured and put into a training system, and then use recorded EMG signals to estimate the force.

Since both the input and output signals could be measured, and the estimated force could be compared with the true force when doing testing, this model had "truth" values that can reflect the performance on able-bodied subjects. However, this approach is hampered by lack of supervised force/moment output signals in limb-absent subjects. Since we could not measure the force from their missing limb, the training model had no output, and even when we estimated a force, we had no reference to compare.

My contribution to this field: To deal with this problem, target tracking strategies with mirror therapy techniques were applied to find a solution. We provided alternative feedbacks for different tasks. Three substitute output signals were: (1) contralateral (to the limb-absent side) force from the sound side recorded during symmetric movement, (2) target movement when the unilateral limb-absent side tracked the target without visual feedback, (3) target movement in bilateral tracking with mirror visual feedback from the contralateral side. We firstly trained models to relate EMG to three alternative outputs on able-bodied subjects, and tested the performance vs. true dominant force (which could be measured) with an average RMS error of 10 %MVC for all DoF. We then tested them vs. the respective feedback signals (other than dominant force) on able-bodied subjects to imitate the limb-absent condition. Finally, we extended the analysis to limb-absent subjects to test if the alternative signals could be good measurements for EMG-force system identification models. For able-bodied and limb-absent subjects, using target as feedback in both unilateral (no-feedback) and bilateral (mirror feedback) tasks had 15–20 %MVC RMS error which is significantly higher than using contralateral force as feedback with an error mostly ranging over 10–15 %MVC. We also recorded the forces from both limbs in mirror movement tasks for able-bodied subjects. The between limb difference and respective tracking accuracies of two forces were tested under different visual feedback types and motions. The goal of this part is to assess the normative performance of bilateral symmetric movement under different visual feedback.

1.3.2 Real-time Prostheses Control Project

Current research field: As millions of people in the US suffer from limb-absence, there is a high demand for prostheses development to improve their living quality. Although new algorithms based on machine learning were generated for lab-based research for myoelectric prostheses, 2-site control is still the most widely used myoelectric prosthetic control technology. This technique is simple by using only 2 electrodes contacting extensor and flexor muscles, but can only control prosthetic hand open and close (1-DoF). Thus, the co-contraction method was enrolled to control multiple DoFs, by triggering co-contraction

mode switching. Essentially, this is still 2-site, sequential 1-DoF control. In addition, some prior lab-based prostheses testing of multi-DoF control needs a large number of electrodes, which is not feasible in existing commercial prostheses. Thus, new system identification algorithms such as regression-based 2-DoF control with a small number of electrodes is necessary to development.

My contribution to this field: We developed a complete prosthesis real-time control system based on a regression algorithm. We tested 2-DoF control with three different control strategies: mapping control, direct control (each with 6 or 12 electrodes), and conventional 2-site control with co-contraction mode switching. Both able-bodied and limb-absent subjects were enrolled in this research. Three tasks were tested to judge the performance with different control strategies and different number of electrodes: in 1-DoF box-block test, conventional 2-sites control had twice the number of blocks transported than 2-DoF methods; in 2-DoF clothespin refined test and 2-DoF door-knob test, either MapCon or DirCon used shorter time to complete the task than conventional 2-sites control (with co-contraction switching).

1.3.3 Two-DoF Dynamic Target tracking Project

Current research field: Most commercial hand-wrist prostheses currently use 2 electrodes to only control hand open and close for trans-radial limb-absent people. When facing some complex tasks in daily life which need multiple joint synergies (wrist and hand), or multiple DoFs in one joint (extension and rotation of the wrist), a more functional 2-DoF prostheses is required to deal with simultaneous activities.

In order to realize 2-DoF control, researchers have tried different approaches including recognizing different patterns by classification models, or modelling continuous EMG-force by regression models. Most methods need a large number of electrodes to obtain high precision, which is not feasible in commercial prostheses design, since the high cost of more channels and its corresponding computing hardware system is not affordable for most people and insurance companies.

My contribution to this field: This study exhibited the feasibility of 2-DoF control on wrist extension & flexion, radial & ulnar deviation, and pronation & supination, as well as simultaneous wrist & hand use. To explore the minimum number of electrodes that are required for either 1-DoF or 2-DoF control by regression models, backward stepwise selection of EMG channels was applied. We gradually reduced the number of electrodes until finding the minimum number that still had similar performance to all 16 electrodes. For the wrist only, the minimum number of electrodes for 1-DoF was two and for 2-DoF was four. The average RMS errors ranged from 6.0–16.3 %MVC. For wrist and hand, the minimum number of electrodes for 1-DoF was two with the average RMS errors ranging between 8.3%–9.0 %MVC, depending on the DoF; the minimum number of electrodes for 2-DoF was four with 9.2 %MVC RMS error for each DoF pair.

1.4 Collaborative Projects and My Contribution

During my Ph.D. study, I was also involved in other collaborative projects. For PsiCon phase A, we improved the EMG-force model by reducing the training duration and generated a universal filter as a substitution for subject-specific EMG-force models. Phase C used computer-based myoelectric cursor control to reach targets, which is a transition between offline testing and embedded prostheses control.

1.4.1 Efficient EMG-Force Training Project

Current research field: More and more researchers study dynamical system models to relate the surface EMG signal to muscle force. These supervised EMG-force models are used in various areas, including ergonomics assessment, clinical biomechanics, and motor control research. Recently, this research expanded from 1-DoF to multiple joint applications. In previous studies, researchers required a long training duration (larger training set) to make accurate EMG-force models. Reducing EMG-force training duration is meaningful when this technique is applied to practical applications such as calibration in prostheses control.

My contribution of this field: This study explored the necessary duration of training data used to build the EMG-force model in 2-DoF dynamic target tracking tasks. Hand open & close was always combined with one of three wrist DoFs: extension & flexion, radial & ulnar deviation, or pronation & supination. Furthermore, we investigated efficient training models by generating a "universal" filter across all subjects, and compared this approach with conventional subject-specific and DoF-specific models.

1.4.2 Computer-Based Real-time Cursor Control Project

Current research field: There are a large group of upper limb-absent people who still have residual forearm muscles which produce EMG signals and make it possible to control prosthetics to improve their daily life. However, for most amputees, a prosthetist determines the best electrods locations once. Control performance can drift day-to-day, which can lower the precision of the model's output. Hence, a method for rapid calibration is desired. Newer commercial products support pattern recognition/classification as the control algorithms, which can distinguish ifferent gestures or hand movements. But, such systems limit the user to one hand movementat a time, which makes it impossible to perform a natural hand gesture or movement. Recently, two novel classification methods were used to extend this limitation of the traditional method. The first one is combining the classification method with contraction level to estimate continuous gestures with variable movement velocity; but the numbers of gestures are still limited. The second is to combine multiple individual gestures as one output to achieve simultaneous prothesis control. However the total number of classes would dramatically increase and the output accuracy would drop a lot. As an alternative, the regression-based method has the ability to provide independent simultaneous control with

proportional output levels, which is better for natural multiple DoFs' hand movements or gestures. However, the traditional regression method heavily depends on the training data. Most EMG training data need the EMG signal to be paired with the force level or movement. However, for amputees, it's hard to gather the accurate force level or movement.

My contribution of this field: We investigated a novel method to rapidly calibrate myoelectric control with no force feedback, which could solve the problems. This project represents a transition between offline testing and embedded prosthesis control. Different DoF pairs: [extension & flextion + radial & ulnar deviation], [open & close + pronation & supination] were tested with different control strategies could be applied in future prostheses controllers. Subject's real-time myoelectric signal controlled the cursor on the screen to reach different random-generated target positions. Furthermore, subjects were asked to hold constant 2-DoF force efforts for a period of time. The count of properly acquired targets, overshoot rate, path efficiency of target tracking, and stability when holding a constant force for each DoF pair were tested to exhibit the performance of real-time 2-DoF control.

1.4.3 Optimal EMGσ Estimation Project

Current research field: Surface EMG is usually modeled as an amplitude-modulated random process. The most common information extracted from the signal is an estimate of its time-varying standard deviation (EMGσ). During the processing, a moving average root mean square (RMS) or moving average mean absolute value (MAV) are two different approaches to smooth the signal. While RMS processing is the optimal estimate of EMGσ if the noise-free EMG is modeled as Gaussian distributed, MAV processing is optimal if the noise-free EMG signal is modeled as Laplacian distributed.

In practice, EMG is always measured with additive measurement noise from apparatus, radiated electromagnetic interference, electrode-to-skin contact resistance, etc. The root difference of squares (RDS) is an efficient approach for noise reduction, which is better than standard deviation subtraction.

My contribution of this field: This project derived the RDS processing of EMG in additive noise separately for the Gaussian model and Laplacian model. Then, we evaluated the optimal results as a function of two factors: whitening/unwhitening, and with/without RDS processing.

1.4.4 Summary of My Ph.D. Work and Introduction of Remaining Chapters

The remaining chapters introduce all of my Ph.D. projects in detail according to their completion order. Each chapter is a published or submitted paper to a journal or conference.

Chapters 2–4 describe the EMG-force with/without mirror feedback project. First, in Chapter 2, we focus on testing alternative EMG-force and EMG-target models for limb-absent subjects. This chapter was

published as a journal paper in *IEEE Transactions on Neural Systems and Rehabilitation Engineering*. Second, in Chapter 3, we extend the prior work and purely compare the force from both limbs under different feedback conditions. This chapter is in preparation as a journal paper submission. Third, in Chapter 4, we briefly discuss the EMG-force performance using alternative feedbacks for limb-absent subjects in calibration protocols. This Chapter was published as a conference paper in the *2019 IEEE Signal Processing in Medicine and Biology Symposium*.

Chapter 5 describes the real-time prostheses control project. This chapter is still in preparation and is expected to be submitted as a journal paper.

Chapters 6–7 focus on the 2-DoF dynamic target tracking project. Chapter 6 focuses on wrist-only EMG-force models and explores the minimum number of electrodes. This chapter was published as a conference paper in the *2017 IEEE Signal Processing in Medicine and Biology Symposium*. Chapter 7 focuses on hand-wrist EMG-force models and explores the minimum number of electrodes. This chapter was published as a journal paper in *Journal of Electromyography and Kinesiology*.

Then in Chapter 8, we discuss the efficient EMG-force training project. This chapter is published as a conference paper in the *2020 42nd Annual Internation Conference of IEEE Engineering in Medicine & Biology Society*. Second, in Chapter 9, we focus on the computer-based real-time cursor control project. This chapter is still in preparation and expected to be submitted as a journal paper. Third, in Chapter 10, we discussedthe optimal EMGσ estimation project. This chapter was published as a journal paper in *IEEE Transactions on Neural Systems and Rehabilitation Engineering*.

Chapter 2: EMG-Force and EMG-Target Models During Force-Varying Bilateral Hand-Wrist Contraction in Able-Bodied and Limb-Absent Subjects

This chapter has been published as: Ziling Zhu, Carlos Martinez-Luna, Jianan Li, Benjamin E. McDonald, Chenyun Dai, Xinming Huang, Todd R. Farrell, and Edward A. Clancy, "EMG-Force and EMG-Target Models During Force-Varying Bilateral Hand-Wrist Contraction in Able-Bodied and Limb-Absent Subjects," *IEEE Transactions on Neural Systems and Rehabilitation Engineering*, Vol. 28, Issue:12, Dec. 2020. Color Versions of one or more of the figures in this paper are available online at https://ieeexplore.ieee.org/abstract/document/9260149.

***Abstract*—System identification models relating forearm electromyogram (EMG) signals to phantom wrist radial-ulnar deviation force, pronation-supination moment and/or hand open-close force (EMG-force) are hampered by lack of supervised force/moment output signals in limb-absent subjects. In 12 able-bodied and 7 unilateral trans-radial limb-absent subjects, we studied three alternative supervised output sources in one degree of freedom (DoF) and 2-DoF target tracking tasks: (1) bilateral tracking with force feedback from the contralateral side (non-dominant for able-bodied/ sound for limb-absent subjects) with the contralateral force as the output, (2) bilateral tracking with force feedback from the contralateral side with the target as the output, and (3) dominant/limb-absent side unilateral target tracking without feedback and the target used as the output. "Best-case" EMG-force errors averaged ~ 10% of maximum voluntary contraction (MVC) when able-bodied subjects' dominant limb produced unilateral force/moment with feedback. When either bilateral tracking source was used as the model output, statistically larger errors of 12-16 %MVC resulted. The no-feedback alternative produced errors of 25-30 %MVC, which was nearly half the tested force range of ±30 %MVC. Therefore, the no-feedback model output was not acceptable. We found little performance variation between DoFs. Many subjects struggled to perform 2-DoF target tracking.**

***Index Terms*—Amputee, biological system modeling, biomedical signal processing, electromyogram, electromyography, EMG-force.**

2.1 Introduction

Limb-absent subjects can generate motor commands that are communicated to remnant muscle tissue, which contracts and provides a measurable electromyogram (EMG) (Ramachandran and Rogers-Ramachandran 1996, Reilly, Mercier et al. 2006). This remnant muscle EMG is used to command myoelectric prostheses (Parker, Englehart et al. 2006). Proportional myoelectric control of one degree of freedom (DoF) prosthesis tasks has been available commercially for decades—including systems which support sequential switching between distinct DoFs (Mann 1981). So-called seamless sequential control has been achieved via pattern recognition (Hudgins, Parker et al. 1993) and recently commercialized. Simultaneous, independent and proportional control of multiple DoFs is mostly found in research systems and is primarily limited to 2-DoFs. Such control has typically been facilitated via multiple EMG sites (Kuiken, Li et al. 2009) or advanced machine learning algorithms (Hahne, Wilke et al. 2020). Our research described herein is applicable to simultaneous, independent and proportional 2-DoF hand-wrist prosthesis control.

In able-bodied subjects, biomedical signal processing and modelling methods have been used to map EMG to force (Buchanan, Lloyd et al. 2004, Parker, Englehart et al. 2006, Jiang, Englehart et al. 2009, Staudenmann, Roeleveld et al. 2010, Clancy, Liu et al. 2012, Liu, Liu et al. 2015), and to mechanical impedance about a joint (Abul-Haj and Hogan 1990, Popat, Drebs et al. 1993, Kawase, Kambara et al. 2012, Golkar, Tehrani et al. 2017, Dai, Zhu et al. 2019). Historically, such modeling has a goal of improving myoelectric prosthesis control (Abul-Haj and Hogan 1990, Popat, Drebs et al. 1993, Parker, Englehart et al. 2006). Numerous supervised system identification methods have been used to model the EMG-force (or, EMG-kinematics) relationship (see (Buchanan, Lloyd et al. 2004, Staudenmann, Roeleveld et al. 2010) for reviews). All methods use an estimate of the EMG standard deviation (EMGσ, a.k.a. processed EMG) as input (Hogan and Mann 1980, Clancy and Farry 2000), and may use other features extracted from the EMG signal, such as zero crossing rate, slope sign change rate and waveform length (Hudgins, Parker et al. 1993, Dai, Bardizbanian et al. 2017). Regression approaches have been common, with studies using standard (un-regularized) linear regression to fit the model (Messier, Duffy et al. 1971, Smith, Kuiken et al. 2016). Recent work has used various forms or regularized regression, such as ridge (Clancy, Liu et al. 2012), Moore-Penrose pseudo-inverse (Clancy, Liu et al. 2012) and support vector (Ameri, Kamavuako et al. 2014) regression approaches, to improve robustness of the model and reduce its error. Non-linear models have also been shown to reduce error somewhat, from implementations of the EMGσ-force power law observation reported by Vredenbregt and Rau (Vredenbregt and Rau 1973, Dai, Bardizbanian et al. 2017), to neural networks (Liu, Herzog et al. 1999, Luh, Gwo-Ching et al. 1999), to parallel cascade structures (Hashemi, Morin et al. 2012), amongst many others. Some modeling approaches that require limited supervision are also emerging,

including nonnegative matrix factorization (Jiang, Rehbaum et al. 2014, Lin, Wang et al. 2018) and population-based assignment of dynamics (Pan, Crouch et al. 2018, Bardizbanian, Zhu et al. 2020). Of course, a classic approach with limited supervision is to insert dynamics in the form of a conventional linear lowpass filter (e.g., 2nd-order with cut-off frequency ~1.5 Hz) (Winter 2009, pp. 250–280, Koirala, Dasog et al. 2015). Note that each of these less-supervised approaches still must calibrate a gain to each EMG channel.

A fundamental challenge for developing EMG-force models in limb-absent subjects is that end-effector force is not available as the output of supervised model training. As one alternative, EMG from remnant muscles of the absent limb are used to estimate the force (or kinematics) from the contralateral limb when performing bilateral symmetric (mirror) contractions (Muceli, Jiang et al. 2010, Nielsen, Holmgaard et al. 2011, Muceli and Farina 2012). This model is then used as the EMG-force relationship in the absent limb. Mirror-provided optical reflection of contralateral-side movement creates a visual illusion that builds awareness of phantom limb movement (and may relieve phantom limb pain) (Ramachandran and Rogers-Ramachandran 1996, Mercier, Reilly et al. 2006, Chan, Witt et al. 2007, Andison 2011). Bilateral symmetric mirror tracking experiments on able-bodied subjects have found that relating dominant-limb EMG to contralateral hand position is slightly worse than relating it to dominant hand position (Muceli and Farina 2012). However, experiments on amputees led to different results, as they had overall poorer performance than able-bodied subjects, but equal or better performance for some specific motions and their combinations (Jiang, Vest-Nielsen et al. 2012). The individual differences within limb-absent subjects was another important factor, as different kinds of limb-absence (i.e., congenital, traumatic), residual-limb length, or other conditions (e.g., neuron damage, contraction imbalance) may affect performance. Accordingly, some researchers prefer to individualize control methods for each specific subject (Jiang, Vest-Nielsen et al. 2012).

An alternative approach is for limb-absent subjects to directly activate their phantom limb to track a target on a computer screen, then relate EMG to this target (Ameri, Kamavuako et al. 2014, Ameri, Scheme et al. 2014). This solution avoids the need for a physical feedback source (also applicable to those with bilateral limb-absence). However, this approach provides no physical measure of actual achieved remnant muscle force and always produces some amount of tracking error. For example, visual tracking incurs a pure reaction time delay between the target and the produced force (i.e., an average delay of 0.268 s (Luce 1986, p. 209–210)).

Our research extends prior EMG-force study in several manners. First, in able-bodied subjects, we compare and contrast different visual feedbacks within one study: dominant limb force, contralateral limb force with mirror feedback, and no force feedback. Second, in limb-absent subjects, the feedbacks studied

were: contralateral[1] side using mirror feedback and no force feedback. Third, our novel methods include instrumenting hand open-close (Opn-Cls) forces *as well as* wrist forces/moments, and doing so simultaneously on *both sides* of able-bodied subjects. We are not aware of any previous applicable studies that have simultaneously measured hand-wrist forces on *both* sides of able-bodied subjects. This instrumentation provided unique insights into evaluation of EMG-force models, including a direct measure as to how well forces in the contralateral limb are representative of forces in the dominant limb of able-bodied subjects. Our results have important implications for the calibration of myoelectric control algorithms, in particular the extent to which these measures can serve as surrogate supervised output sources for limb-absent subjects.

2.2 Methods

2.2.1 Experimental Apparatus

Experimental data were collected from 12 able-bodied subjects (6 males, 6 females; aged 18–55 years) and 7 trans-radial unilateral limb-absent subjects (4 males, 3 females; aged 27–61 years; see Table 2.1) at Worcester Polytechnic Institute (WPI) and approved by the WPI Institutional Review Board (IRB Protocol #17-155). All limb-absent subjects routinely use myoelectric-controlled upper-limb prostheses and all, except subject 27, were known to have previously participated as subjects in upper-limb myoelectric control studies. All subjects provided written informed consent. Able-bodied subjects had no deficits involving their upper limbs or vision and were right-hand dominant. Limb-absent subjects had no deficits involving their contralateral limb or vision, and the residual limb on the affected side was at least 5 cm in length with

Fig. 2.1. Experimental apparatus. Subjects (limb-absent subject shown) sat in a chair with each able hand secured into force measurement devices, facing the computer screen which displayed a target and real-time force/moment feedback.

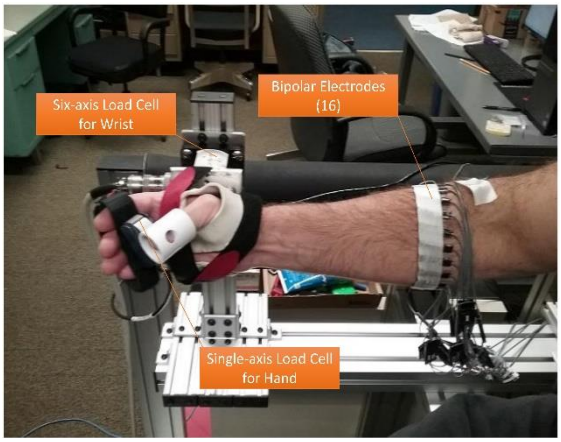

Fig. 2.2. Experimental apparatus at the hand-wrist. Each able hand was separately secured via Velcro to a thermo-formable plastic glove that was bolted to a six-axis load cell to measure the moment at the wrist. Fingers were secured to a single-axis load cell to measure hand grip force. Sixteen EMG electrodes were secured around the dominant/limb-absent forearm.

[1] The term "contralateral" will be used to refer to the non-dominant side of able-bodied subjects and the sound side of limb-absent subjects.

functional muscle contraction. One additional limb-absent subject was excluded due to neural damage on the limb-absent side.

TABLE 2.1
TRANS-RADIAL LIMB-LOSS SUBJECT INFORMATION.

Sub. Num.	Sex	Age (years)	Type of Limb-Loss	Side	Time Limb Absent (years)	Residual Length (cm)	Circ. (cm)
21	F	61	Congenital	R	61	5.5	19
22	M	27	Congenital	L	27	15	24
23	M	30	Congenital	L	30	13.5	25.5
25	F	49	Traumatic	R	32	10.5	22
26	M	54	Traumatic	R	37	14	20.8
27	F	58	Traumatic	R	33	13	19.6
28	M	36	Congenital	L	36	11	23

Subjects were seated at the experimental apparatus (Fig. 2.1). The palm of each hand (sound side only for limb-absent subjects) was separately aligned and secured via Velcro straps to a thermo-formable plastic mold which was rigidly connected to a six-DoF load cell (MC3A-100 transducer, Gen 5 signal conditioner, AMTI, Watertown, MA) to measure radial-ulnar deviation (Rad-Uln) force along one force axis and pronation-supination (Pro-Sup) moment along one moment axis. Rad-Uln force was measured directly. However, this force is not produced at the axis origin of the load cell (which exists within the body of the load cell, approximately 6.3 cm from the center of mass of the palm). Hence, Rad-Uln forces also produced an artifactual Pro-Sup moment. Thus, Pro-Sup moment was computed as the moment measured by the load cell, less the product of the Rad-Uln force times the 6.3 cm moment arm. To measure hand grip force during attempted hand Opn-Cls, each hand (sound side only for limb-absent subjects) additionally gripped a single-axis load cell (LCR-150 with DMD-465WB amplifier, Omega Engineering, Inc., Stamford, CT) while the thumb was secured via a rigid tube and, separately, the proximal aspects of the four fingers were secured by Velcro on the opposing side of the cell. The palms of the hands were oriented perpendicular to the plane of the floor, facing inwards; the wrists were relaxed in a neutral position; and the shoulders were in the anatomical position (Fig. 2.2).

During unilateral tasks (Fig. 2.3, Tasks 1 and 2), a computer-controlled target guided the subject to complete different experimental tasks via a blue arrowhead on the computer screen in front of the subject, with up-down movement displaying wrist radial-ulnar deviation, rotation displaying Pro-Sup moment and arrowhead size displaying hand Opn-Cls force. (Wrist extension-flexion force was considered as an additional contraction dimension, but discarded due to the overall experimental protocol duration and its proximity to muscles used in hand Opn-Cls.) When desired, another red arrowhead displayed real-time force/moment feedback from both load cells on the dominant/affected or contralateral side, depending on the task being performed. During bilateral tasks (Fig. 2.3, Task 3), these displays were mirrored in two display panels on the screen.

One array of 16 bipolar EMG electrodes was secured to a subject's forearm (dominant side for able-bodied subjects, affected side for limb-absent subjects). Electrode gel was applied to a subject's forearm and

the electrodes were equally spaced about its circumference, with the midpoints of the bipolar contacts placed 5 cm distal to the elbow crease. Each electrode pair consisted of 5 mm diameter, stainless steel, hemispherical contacts separated 1 cm edge-to-edge, oriented along the forearm's long axis. A reference electrode was gelled and secured on the forearm, just proximal to the active electrodes. Each bipolar EMG signal was differentially amplified (Liberating Technologies, Inc. BE328 amplifier; 30–500 Hz pass band, CMRR>100 dB over the pass band) and then selectable gain was applied. All EMG channels and load cell signals were sampled at 2048 Hz with 16-bit resolution, and target movement was recorded at 800 Hz.

2.2.2 Experimental Protocol

All trials were constant-posture. To prevent cumulative fatigue, the interval between trials was at least two minutes. All limb-absent subjects were offered mirror-box training, using methods designed by a consulting occupational therapist, before tracking trials to help build a better sense of muscle contraction for the different tasks.

1) *MVC Trials*: After a warm-up period during which each task was introduced, able-bodied subjects performed bilateral maximum voluntary contraction (MVC) trials for each of wrist radial and ulnar deviation, wrist pronation and supination, and hand close and open. Limb-absent subjects only performed MVC trials for the sound side. All subjects took 2–3 seconds to ramp up to their MVC effort and then maintained this effort for 2–3 seconds. The plateau force/moment during the maintained period was recorded as the MVC. Lastly, rest trials with all muscles fully relaxed were recorded for EMG noise level evaluation.

2) *Force-Varying Target Tracking Trials*: Next, subjects performed force-varying target tracking Tasks 1, 2 and 3 (explained below) separately for 1-DoF Rad-Uln, Pro-Sup and Opn-Cls; and 2-DoF Rad-Uln & Opn-Cls and, separately, Pro-Sup & Opn-Cls. The 2-DoF tasks always included Opn-Cls, as this function is fundamental to a hand-wrist prosthesis. Only the utilized motions were enabled for visualization in the screen display (i.e., the remaining DoFs were locked out). The target was a 0.75 Hz band-limited, white and uniform random process [16] between ±30% MVC (independently generated for each DoF) corresponding to the utilized task. This bandwidth was the widest for which subjects could maintain target tracking for these tasks during preliminary testing. The order of presentation of DoFs, unilateral/bilateral and visual feedback condition (see below) was randomized and the subjects were told which side was controlling the feedback. Each trial was 40 s in duration and conducted twice per task. Before each trial, subjects were instructed about the range of target movements and allowed practice until they were comfortable. Unilateral and bilateral tasks were completed as described subsequently.

Task 1—Tracking with Dominant-Limb Force Feedback (Fig. 2.3a): Only able-bodied subjects performed these force-varying tracking tasks, using their dominant limb (with EMG electrodes). Feedback of dominant force/moment was provided for target tracking. The contralateral limb was fully at rest and not secured to the load cells. Off-line, EMG (which was acquired only from the dominant side) was related to force/moment on the dominant side. This task provides the best-case scenario for supervised learning of EMG-force models since EMG is recorded directly from the muscles producing the measured force/moment and, thus, represents the benchmark. Limb-absent subjects did not complete this task.

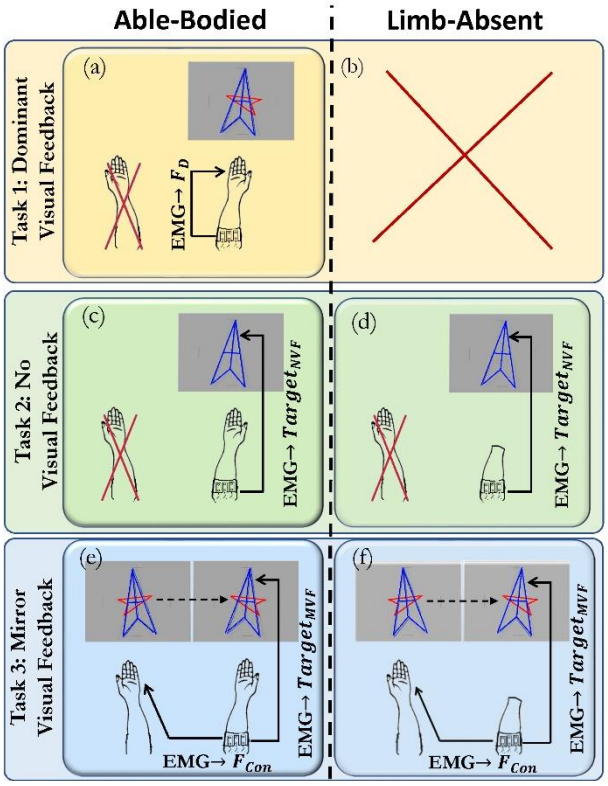

Fig. 2.3. Experiment Protocol. Blue arrowhead is target and red arrowhead is visual feedback. a) Task 1: able-bodied subjects tracked target with their dominant limb given real-time visual feedback of their dominant limb force (F_D); c, d) Task 2: subjects tracked the target with their dominant/limb-absent side with no visual feedback (NVF); e, f) Task 3: subjects tracked the target with both limbs given real-time feedback from their contralateral side and with mirror visual feedback (MVF).

Task 2—Unilateral Tracking with No Visual Feedback (Fig. 2.3c, d): Able-bodied subjects used their dominant limb (with electrodes) to track the target, with no real-time feedback provided. Only the target was shown on the screen. Limb-absent subjects used the limb-absent side (the only side with electrodes) to track the target, with no real-time feedback provided. For all subjects, the contralateral limb was fully at rest (not secured to the load cells). Off-line, EMG was related to the target. This task represents the no-feedback condition in which a dominant/limb-absent side model is built without feedback.

Task 3—Bilateral Tracking with Mirror Visual Feedback (Fig. 2.3e, f): Able-bodied subjects used both limbs to simultaneously track the target. Limb-absent subjects used their sound and phantom limbs to simultaneously track the target. For all subjects, feedback consisted only of the force produced by the contralateral-side limb. This force and its mirror force were simultaneously displayed, producing mirror visual feedback. Offline, EMG was related to contralateral-side force/moment. This task represents use of the force/moment in the contralateral side in order to build the dominant/limb-absent side model. We also related EMG to the target, for comparison.

2.2.3 Methods of Analysis

1) Data Pre-Processing: Data processing was performed in MATLAB 2018b (Mathworks, Inc., Natick, MA). All filters were implemented using the two-pass, zero-phase method, thus their effective filter orders are twice those listed herein. The forces/moments (Rad-Uln, Opn-Cls, Pro-Sup) were each lowpass filtered (fc=16 Hz; Chebyshev Type I filter, ninth-order, 0.05 dB peak-to-peak passband ripple) and then downsampled from 2048 Hz to 40.96 Hz. The wrist Rad-Uln data were normalized by $(|MVC_{Rad}|+|MVC_{Uln}|)/2$, and similar normalization was applied to the Pro-Sup and Opn-Cls data. All target data were identically lowpass filtered, then resampled to 40.96 Hz.

For each of the 16 EMG channels in a trial, an estimate of time-varying EMG standard deviation ($EMG\sigma[m]$, where m was the decimated discrete-time sample index) was computed. The raw EMG were highpass filtered (fc=15 Hz, fifth-order Butterworth filter) to remove motion artifact, then notch filtered (second-order IIR filter at 60 Hz, notch bandwidth of 1 Hz), rectified, lowpass filtered (fc=16 Hz, as above) and finally downsampled to 40.96 Hz. Note that additional lowpass filtering, typically with $fc \leq 1$ Hz, is optimized to each subject via the EMGσ-force/target model (Koirala, Dasog et al. 2015). Prior to further analysis, the initial and final 1 s of all signals were removed to avoid filter startup transients.

2) Latency Between Forces/Moments and the Target: For each able-bodied subject and DoF, we computed the cross-correlation coefficient function to estimate the latency between subject force/moment and the target (Azaria and Hertz 1984). For 2-DoF tasks, latency estimates were made independently for each DoF. The time location of the maximum of the cross-correlation coefficient function indicated the time delay (latency) ($\tau=k/F_s$, where k is the number of samples, F_s is the sampling frequency) at which the force/moment and the target were best aligned. The corresponding maximum cross-correlation coefficient function value (ρ) is a measure of the linear association of the target tracking, after accounting for the latency. It is invariant to gain and, as such, is a measure of timing accuracy in tracking. As the force will lag behind target movement due to the subject's reaction time, we only searched for the maximum ρ between a delay τ of 0 to 1 s. Note that our pre-processing of the force/moment data did not bias the latency estimates, since pre-processing filters were implemented with zero phase.

3) Dynamic EMGσ-Force/Target Modeling: When $EMG\sigma[m]$ was related to force (EMG-force), or when EMG was related directly to the arrowhead target (EMG-target), during 1-DoF trials, a linear, dynamic, finite impulse response relation was used, of the form:

$$F[m] = \sum_{q=0}^{Q} \sum_{e=1}^{E} c_{e,q} EMG\sigma_e[m-q-k],$$

where F was the force/target, m was the decimated discrete-time sample index, q and e were integer indexes, Q=20 was the order of the linear dynamic model, E = 16 was the number of electrodes used in the fit, and $c_{e,q}$ were the fit coefficients (Clancy, Martinez-Luna et al. 2017). Latency (k; in samples) was assigned to zero for EMG-force models (we observed that sufficient latency was provided by the frequency-dependent phase response of the linear models). For EMG-target models of able-bodied subjects, latency was taken from the same trial as the model fit, as this value was assumed to be most accurate; for limb-absent subjects (wherein latency cannot be measured on the limb-absent side), the latency used was the average latency from able-bodied subject trials from the same task and DoF. Fit coefficients were estimated via the linear least squares pseudo-inverse method, in which singular values of the design matrix were removed if the ratio of that singular value to the largest was less than a tolerance value (Tol=0.1, based on previous study (Clancy, Liu et al. 2012, Dai, Bardizbanian et al. 2017)). We chose this modeling method for its robustness, simplicity and because linear models capture most of the EMG-force/target relationship. In this manner, we could maintain our focus on the different feedback mechanisms.

Each task consisted of two trials. The first trial was used for coefficient training and the second for testing. Then, the training and testing trials were flipped for two-fold cross-validation and the average of the two RMS errors (RMSEs) reported. All RMSEs were in %MVC (normalized force/moment).

For 2-DoF trials, two EMGσ-force/target models were fit, one per DoF (each with its own coefficients). In this manner, each EMG channel contributed to each DoF. Again, one trial was used for training and one for testing, with two-fold cross-validation.

4) EMG-Force, EMG-Target Models Studied: For each experimental task, both 1- and 2-DoF trials had been performed. Thus, both 1- and 2-DoF EMG-force/target models were studied, respectively. From the Task 1 data, EMGσ was related to force in the dominant arm. These data were only available from the able-bodied subjects and represented the reference ("best-case") task. From the Task 2 data in which there was no visual feedback, EMGσ only was related to the target for all subjects. This analysis represents building models when no feedback is available during training (e.g., when building EMG-force style prosthesis control models for limb-absent subjects). From the Task 3 data that used mirror visual feedback, EMGσ was related to contralateral force (representing use of forces from the sound side to train models in unilateral limb-absent subjects); and EMGσ was related to the target for all subjects (for comparison to results from Task 2). Again, the average RMSEs from two-fold cross-validated results is reported.

2.2.4 Statistics

Our primary evaluation metrics were latency between forces/moments and the target, and maximum cross correlation coefficient/RMSE between measured/EMG-estimated forces/moments. Unless noted otherwise, performance differences were evaluated using repeated measures analysis of variance (RANOVA) in SPSS 22, using a significance level of p=0.05. Prior to RANOVA, the degree of sphericity (ε) was used to adjust the degrees of freedom by either the method of Greenhouse-Geisser ($\varepsilon < 0.75$) or the method of Hyunh-Feldt ($0.75 < \varepsilon < 1$). Unless stated otherwise, no interactions were found. Pairwise comparisons (post hoc or stand-alone) were conducted using paired t-tests with Bonferroni correction. We statistically analyzed 1-DoF tasks separately from 2-DoF tasks.

2.3 Results

2.3.1 Latencies Between Force/Moment and Target

Table 2.2 shows the mean ±std. dev. latencies between force/moment and target for each experimental task, for the able-bodied subjects. RMSE between force/moment and target was compared pairwise with vs. without latency adjustment. Pooling all conditions [288 1-DoF trials (12 subjects × 4 feedback types × 3 DoFs × 2 sets) and 384 2-DoF trials (12 subjects × 4 feedback types × 2 DoF pairs × 2 errors per DoF pair × 2 sets], the latency adjusted error was smaller (in 658 of 672 pairs) by an average of 4.60±2.91 %MVC, which was statistically significant ($p < 10^{-6}$, paired sign test). This result formed the basis for our step in the Methods section to latency-adjust all EMG-target models.

TABLE 2.2
ABLE-BODIED SUBJECTS, TRACKING LATENCY BETWEEN ACTUAL FORCE/MOMENT AND TARGET, FOR EACH DOF (MS)

1-DoF:	Rad-Uln	Pro-Sup	Opn-Cls
Task 1, Dominant	268±46	300±68	330±75
Task 2, Dominant	274±100	240±79	234±73
Task 3, Dominant	278±53	349±144	353±88
Contralateral	293±54	349±98	367±102

2-DoF:	Rad-Uln	Opn-Cls	Pro-Sup	Opn-Cls
Task 1, Dominant	242±37	491±90	289±38	485±100
Task 2, Dominant	431±171	458±192	263±72	509±189
Task 3, Dominant	270±30	524±94	325±51	528±94
Contralateral	297±40	523±120	364±49	535±92

2.3.2 RMSE, Dominant Force vs. Target, Able-Bodied Subjects

Before reporting EMG-force and EMG-target performance (see subsequent sub-sections), we describe the ability of able-bodied subjects to track the random target in Tasks 1–3. Fig. 2.4 shows summary RMSE

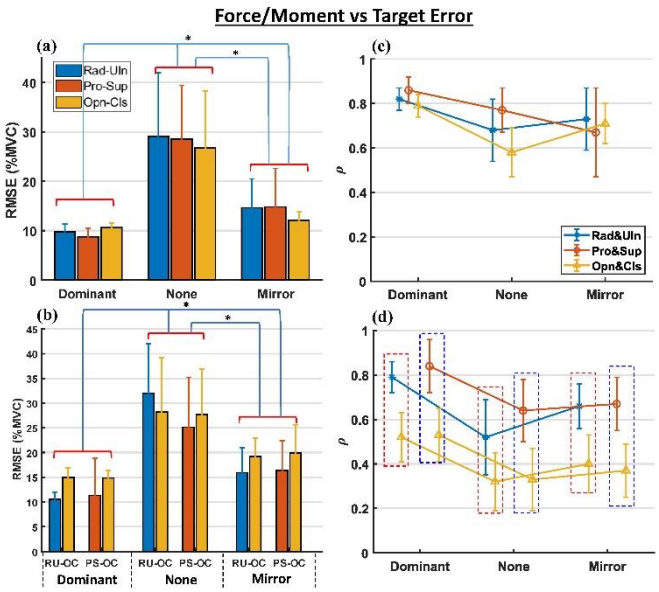

Fig. 2.4. Mean + std. dev. errors between dominant limb force/moment and *target* for able-bodied subjects, after adjusting for time latency. Statistically significant differences between feedback types indicated with "*". RMSE (left) with different feedback conditions [dominant (Task 1), none (Task 2) and mirror (Task 3)] as a function of DoF for 1-DoF tasks (top) and as a function of DoF pairs for 2-DoF tasks (bottom). Maximum cross-correlation coefficients (ρ) shown at right. Dash-line boxes in (d) group DoF pairs.

and ρ of dominant limb force in able-bodied subjects vs. *target* for the different feedback conditions (i.e., tasks), after adjusting for time latency. RMSE measures tracking error, while ρ provides an error measure that is invariant to gain (and provides our latency values).

In 1-DoF tasks, a two-way RANOVA of RMSE with the factors feedback (dominant, none, mirror) and DoF (Rad-Uln, Pro-Sup, Opn-Cls) found only feedback as significant [$F(1.1, 12.6) = 42$, $p_{GG} = 10^{-5}$. Pairwise comparison found RMSE in dominant feedback was significantly lower than none ($p = 10^{-4}$) and mirror ($p = 0.002$), and mirror had significantly lower error than none ($p = 10^{-4}$).

In 2-DoF tasks, a three-way RANOVA for tracking RMSE with the factors of feedback (dominant, none, mirror), DoF pair (Rad-Uln & Opn-Cls or Pro-Sup & Opn-Cls) and motion-within-DoF (wrist Rad vs. Uln, or Pro vs. Sup; or hand Opn vs. Cls) found only feedback was significant [$F(1.2, 13.0) = 40$, $p_{GG} = 10^{-5}$]. Pairwise comparison found RMSE in dominant feedback was significantly lower than none ($p = 10^{-4}$) and mirror ($p = 10^{-4}$), and RMSE in mirror was significantly lower than none ($p = 0.001$). <u>In both 1-DoF and 2-DoF tasks, the average error when using no feedback is nearly half the contraction range of ±30 %MVC, which seems unacceptable.</u>

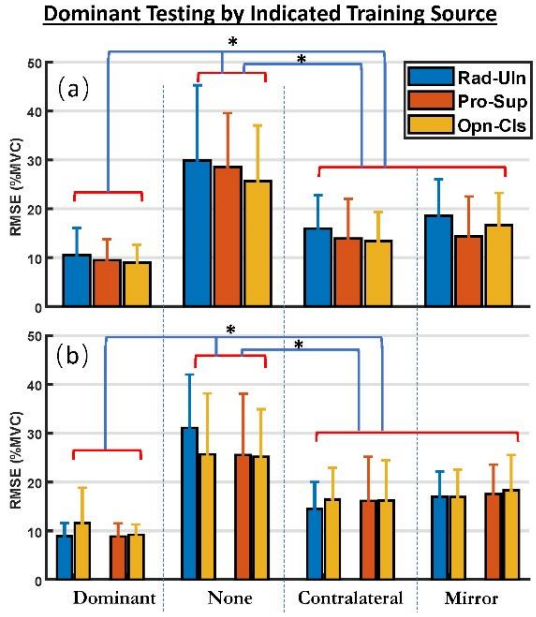

Fig. 2.5. Mean + std. dev. errors between dominant limb force/moment and *target* for able-bodied subjects, after adjusting for time latency. Statistically significant differences between feedback types indicated with "*". RMSE (left) with different feedback conditions [dominant (Task 1), none (Task 2) and mirror (Task 3)] as a function of DoF for 1-DoF tasks (top) and as a function of DoF pairs for 2-DoF tasks (bottom). Maximum cross-correlation coefficients (ρ) shown at right. Dash-line boxes in (d) group DoF pairs.

2.3.3 Train EMG-Force, EMG-Target: Test Using Dominant Limb <u>Forces</u> of Able-Bodied Subjects (Tasks 1–3)

Fig. 2.5 shows summary results of EMG-force/target models *trained* with the various indicated signal as the supervised output, but always *tested* using a distinct trial of able-bodied *dominant* limb forces. Thus, regardless as to whether the *training* set used force or target as the

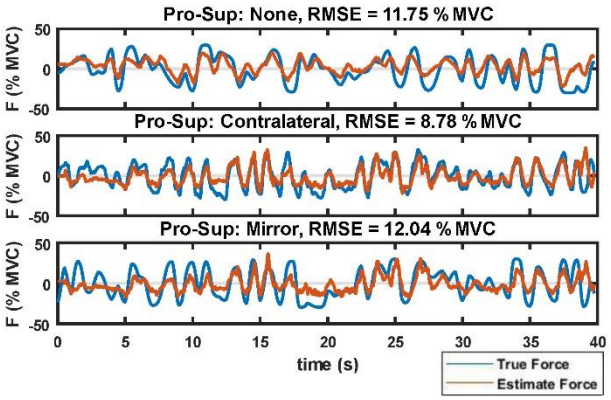

Fig. 2.6. Mean + std. dev. errors between dominant limb force/moment and *target* for able-bodied subjects, after adjusting for time latency. Statistically significant differences between feedback types indicated with "*". RMSE (left) with different feedback conditions [dominant (Task 1), none (Task 2) and mirror (Task 3)] as a function of DoF for 1-DoF tasks (top) and as a function of DoF pairs for 2-DoF tasks (bottom). Maximum cross-correlation coefficients (ρ) shown at right. Dash-line boxes in (d) group DoF pairs.

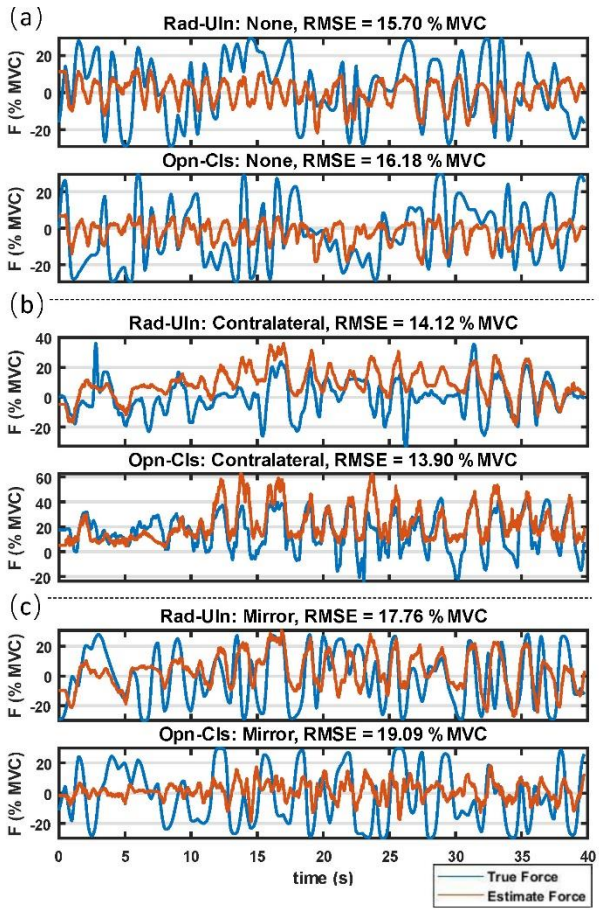

Fig. 2.7. Example 2-DoF EMG-force time-series results, limb-absent subject 21, Rad-Uln & Opn-Cls when using (a) no feedback, (b) contralateral feedback and (c) mirror feedback. EMG acquired from the affected side. Both true force and EMG-estimated force are shown in each plot.

output, the model was *tested* using dominant limb force as the output. When *training* did *not* use dominant limb force, then testing on the dominant limb best indicates if the supervised output is an acceptable surrogate for dominant limb force—which, of course, is not available in limb-absent subjects. Note that *training* with dominant force feedback (same side as the electrode array) represents the best-case EMG-force training condition (EMG recorded directly from muscles producing the measured force/moment).

In 1-DoF tasks, a two-way RANOVA with factors: DoF (Rad-Uln, Pro-Sup, Opn-Cls) and feedback (dominant, contralateral, none, mirror) found only feedba ck was significant [$F(1.3, 14) = 45$, $p_{GG} = 10^{-6}$]. *Post hoc* comparison found that dominant feedback had significantly lower RMSE than the others ($p < 0.002$), contralateral and mirror had no significant difference from each other, and both had lower RMSE than none ($p < 0.001$).

In 2-DoF tasks, a three-way RANOVA with factors: DoF pair (Rad-Uln & Opn-Cls, Pro-Sup & Opn-Cls), feedback (dominant, contralateral, none, mirror) and motion-within-DoF (wrist Rad-Uln vs. hand Opn-Cls, or wrist Pro-Sup vs. hand Opn-Cls) found only feedback was significant [$F(1.4, 16) = 37$, $p_{GG} = 10^{-6}$]. Pairwise comparison found that dominant feedback had significantly lower RMSE than the others ($p < 0.001$), contralateral and mirror had no significant difference from each other, and both had lower RMSE than none ($p < 0.004$).

2.3.4 Train EMG-Force, EMG-Target: Test Using Respective Feedback Signal—All Subjects (Tasks 2, 3)

Fig. 2.6 and Fig. 2.7 show example time-series results. Fig. 2.8 shows summary results of EMG-force/target models when the distinct train and test trials were from the *same* feedback signal *other* than dominant force. These three signals were available for both able-bodied and limb-absent subjects, so provide a more direct means of comparison between these subject populations which is not available from the prior results.

In 1-DoF tasks, a three-way RANOVA for RMSE with two subject-within factors: feedback (contralateral, none, mirror) and DoF (Rad-Uln, Pro-Sup, Opn-Cls); and one subject-between factor: group (able-bodied, limb-absent) found significant interactions. Thus, two-way RANOVAs were computed separately for able-bodied and limb-absent subjects. For able-bodied subjects, the two-way RANOVA found only feedback was significant [$F(2, 22) = 12.5$, $p = 10^{-4}$]. Pairwise comparison showed that contralateral feedback had significantly lower error than none ($p = 0.04$) and mirror ($p = 10^{-4}$). For limb-absent subjects, the two-way RANOVA found both feedback and DoF significant [$F(2, 22) > 4.0$, $p < 0.05$]. Pairwise comparison showed that contralateral feedback had significantly lower error than none ($p = 0.035$) and mirror ($p = 0.015$), and that Pro-Sup had better performance than Rad-Uln ($p = 0.021$). Alternatively, we fixed each of the DoFs in the original three-way RANOVA. Of these three two-way RANOVAs, only when Rad-Uln was fixed was a significant difference found in the group factor, with able-bodied subjects exhibiting lower error than limb-absent [$F(1, 17) = 10.8$, $p = 0.004$].

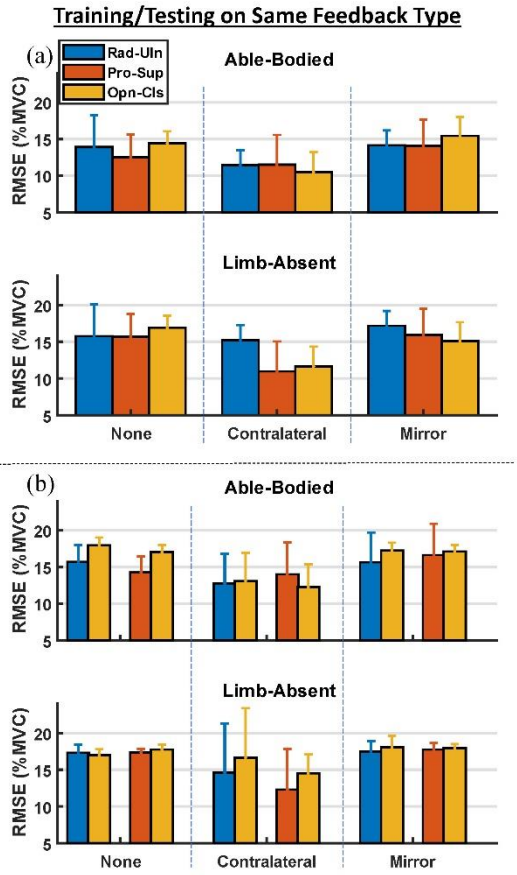

Fig. 2.8. Example 2-DoF EMG-force time-series results, limb-absent subject 21, Rad-Uln & Opn-Cls when using (a) no feedback, (b) contralateral feedback and (c) mirror feedback. EMG acquired from the affected side. Both true force and EMG-estimated force are shown in each plot.

In 2-DoF tasks, a four-way RANOVA for RMSE with three subject-within factors: feedback (contralateral, none, mirror), DoF pair (Rad-Uln & Opn-Cls; Pro-Sup & Opn-Cls) and motion-within-DoF (wrist Rad-Uln vs. hand Opn-Cls, or wrist Pro-Sup vs. hand Opn-Cls); and a subject-between factor: group (able-bodied, limb-absent) found DoF to not be significant [$F(1, 17) = 0.3$, $p = 0.6$], and the other three factors to interact. Continuing analysis of the three interacting factors, two three-way RANOVAs with factor group

fixed were computed. For able-bodied subjects, there was a two-way significant interaction of feedback×motion-within-DoF. Thus, pairwise comparison found that: for both motion-within-DoF wrist Rad-Uln and Pro-Sup, contralateral feedback had significantly lower RMSE than mirror ($p = 0.008$); for motion-within-DoF hand Opn-Cls, contralateral feedback exhibited significantly lower RMSE than both none ($p < 10^{-4}$) and mirror ($p = 0.001$). For limb-absent subjects, the three-way RANOVA found only feedback significant [$F(1.1, 6.4) = 9.4$, $p = 0.02$]. Pairwise comparison found contralateral feedback had significant lower RMSE than mirror ($p = 0.033$).

2.4 Discussion

2.4.1 Latencies Between Force/Moment and Target

The 1-DoF latencies between force/moment and target (Table 2.2) are generally consistent with those found in the literature, ranging in average from 234–367 ms (Luce 1986, p. 209–210). When tracking using the contralateral (i.e., non-dominant) limb of able-bodied subjects for feedback, the latencies tended to be longer.

Latencies for our 2-DoF tasks were not readily found within the literature, hence our results for these tasks may be novel. Across Tasks 1–3, the trend was for much larger average latencies (by a factor of ~2) for the Opn-Cls dimension within each 2-DoF task, while the other contraction dimension retained a latency similar to its 1-DoF task. Standard deviations were similar to the 1-DoF results. The only exception was Rad-Uln & Opn-Cls 2-DoF Task 2—in this case both constituent DoFs exhibited the higher average latencies. Anecdotal observation during the trials suggests that subjects struggled to perform the 2-DoF tracking, and may have concentrated their tracking focus on Rad-Uln/Pro-Sup at the expense of Opn-Cls. Additionally, use of arrowhead size as the feedback source for Opn-Cls may have been more challenging compared to the other DoFs. But, this issue is less likely, since no similar performance distinction occurred in 1-DoF. Note that in able-bodied subjects, each subject's latency was available, thus these subject-specific latencies provided the most accurate estimates. For limb-absent subjects, we resorted to using the average value from able-bodied subject trials from the same task and DoF. This approximation was necessary, but likely contributed more error to the limb-absent results.

2.4.2 Latencies Between Force/Moment and Target

The results in Fig. 2.4 depict the ability of forces/moments in the dominant arm of able-bodied subjects to track the target, as a function of three feedback sources. As expected, when dominant feedback is provided from the dominant limb, errors are statistically lower. Our results then show a hierarchy of performance, with

mirror feedback showing the next lowest error and no-feedback providing the highest error. These results are consistent both for 1- and 2-DoF tasks. Notably, the error between the target and the actual force produced by the dominant arm in the no-feedback condition averaged 25–30 %MVC, even though the full force range only spanned ±30 %MVC. Hence, this error was nearly half the available force range, which is quite large; suggesting that the target displayed during the no-feedback condition is quite a poor supervised output source for system identification purposes.

In contrast, the maximum cross-correlation results for all of these tasks are quite high (Fig. 2.4, right). The average value of ρ ranged from ~0.6 to over 0.8 for the 1-DoF tasks. As shown in the time-series plots of Fig. 2.6 and Fig. 2.7, subjects followed the *timing* of the extrema of target force quite well, but had difficulty in maintaining proper amplitude (especially for 2-DoF tasks).

2.4.3 Train EMG-Force, EMG-Target: Test Using Dominant Limb Forces of Able-Bodied Subjects

Fig. 2.5 shows the principal results of this study. Relating EMG from the dominant limb to forces in that limb, as expected, gives EMG-force models with the lowest errors— since EMG is recorded directly from the muscles producing the measured force/moment. The errors found herein are consistent in magnitude with those found in prior studies (Clancy, Martinez-Luna et al. 2017, Bardizbanian, Zhu et al. 2018). It is also encouraging that the EMG-force errors shown in Fig. 2.5 are similar in amplitude to the force tracking errors shown in Fig. 2.4. Thus, relating EMG to dominant side force has errors that are similar to those between dominant force and the target. But, when dominant limb forces are not available and a surrogate output is needed to train EMG-force for the dominant limb (e.g., limb-absent subjects), our results again found a hierarchy of statistically significant differences: bilateral tracking using contralateral force for training (with or without mirror visual feedback) performed somewhat poorer, while no feedback performed the poorest. Statistically, there was no performance distinction in bilateral tracking between feedback of contralateral force and mirror visual feedback. For both 1- and 2-DoF tasks, the EMG-force/target errors with no feedback were approximately half the available force range. These errors are so large that it is likely that population-based models of EMG-force dynamics (e.g., Hill-style muscle models (Hof and Van den Berg 1981) or generic EMG-force calibrations from a population (Pan, Crouch et al. 2018, Bardizbanian, Zhu et al. 2020), combined with estimation only of one gain parameter per EMG channel, would provide considerably better EMG-force estimation. For example, in a 2-DoF hand-wrist EMG-force task involving nine able-bodied subjects (Bardizbanian, Zhu et al. 2020), we replaced EMG-force dynamics calibrated to each individual with one universal model calibrated across the population. A single gain per EMG channel was still optimally estimated per individual. The population-based model performed nearly identically to those customized to

each individual. Of course, optimal gain selection still requires force estimation from the dominant limb. However, prosthetists are familiar with the subtleties of EMG channel gain selection.

Note that EMG-force calibration using contralateral force feedback (with or without mirror feedback) still requires use of a load cell. This option might be reasonable for use in a prosthetist's office, but does not seem reasonable for field calibration of a prosthesis control system.

2.4.4 Train EMG-Force, EMG-Target: Test Using Respective Feedback Signal—All Subjects

Finally, Fig. 2.6 and Fig. 2.7 show results when EMG-force/target models were trained and tested from the same signal source, excluding the previously shown Task 1 results from training using dominant limb force. These models importantly highlight results from the limb-absent subjects (whose anatomy does not permit measurement of affected-side limb forces). The associated statistical results are not as sharply defined, perhaps reflecting the larger result variances and the smaller sample size. Nonetheless, there was still a general trend for lower errors when training EMG-force/target models using contralateral feedback, and unacceptably higher errors when training with no feedback—consistent with results from the able-bodied subjects. Also, there were limited distinctions between the wrist DoFs (although Pro-Sup did have better 1-DoF performance than Rad-Uln). Pro-Sup would be the most intuitive if used to control wrist rotation. And, in limb-absent subjects, it is interesting to note that providing mirror visual feedback was not statistically different from providing no feedback.

2.4.5 Train EMG-Force, EMG-Target: Test Using Respective Feedback Signal—All Subjects

Our results found a rather clear performance hierarchy, with dominant limb feedback providing the lowest EMG-force error (as would be expected), followed by feedback based on bilateral tracking (using either the forces from the contralateral side, or mirror visual tracking), followed by no feedback. EMG-force models based on bilateral tracking seemed adequate, but require the use of a load cell and would exclude persons with bilateral limb-absence. EMG-target models formed using no feedback seemed inadequate. In such cases, population-based EMG-force models (as least for EMG-force dynamics; one gain per EMG channel is always needed to scale its contribution) might perform better.

In general, we chose to equate the dominant side of able-bodied subjects to the affected side of limb-absent subjects. We did so because prostheses aspire to be a high quality replacement of limb function (which is best represented by the dominant side in able-bodied subjects) and, thus, we wish to advance prosthesis control towards the performance expectations of the dominant limb. In addition, most prior EMG-force

modeling has been performed on the dominant side of able-bodied subjects. Nevertheless, the sound side of limb-absent subjects becomes used as the dominant side, regardless of natural handedness—due largely to the limited functionality provided by existing prostheses.

We did not find many substantive differences in performance as a function of DoF. Such changes have been found in the literature (e.g., when relating dominant-limb EMG to hand position in the contralateral hand of able-bodied subjects, during bilateral mirror contractions (Muceli and Farina 2012)) and postulated to be consistent with deeper muscle fibers (which are more poorly represented in surface EMG) that are prime torque generators for the poorer performing DoFs (Hahne, Schweisfurth et al. 2018). Perhaps if such differences exist, they are subtle enough to be difficult to find with the small sample sizes common in experimental studies in this field. Also, the use of a large number of electrodes, placed about the full extent of the remnant limb (as was done in our work), may help to mitigate these issues (Muceli and Farina 2012).

The tasks tested in this study were relatively novel to both our able-bodied and limb-absent subjects. In particular, 2-DoF target tracking was both novel and challenging. It would be interesting to determine if more tracking practice (or, repeated experimental sessions) would have led to better 2-DoF tracking (Hahne, Schweisfurth et al. 2018, Tabor, Bateman et al. 2018). Note that our force-varying target trajectories were selected for their system identification properties (uniform distribution gives equal weight to each force level; bandlimited and white gives equal weight to each frequency). If subjects are better able to produce the requested forces, the quality of the identified model is likely to improve.

We separated our statistical analyses of 1-DoF tasks from those of 2-DoF tasks, because these tasks are inherently different. Testing for a statistical difference between inherently distinct tasks is, generally, not of scientific value (Clancy, Martinez-Luna et al. 2017, Dai, Zhu et al. 2019). As shown in Table 2.2, Opn-Cls tracking latencies during 2-DoF tasks trended longer than those from 1-DoF tasks. Similarly, Fig. 2.5 and Fig. 2.8 suggest a trend for larger 2-DoF EMG-force RMSEs compared to 1-DoF. These trends are consistent with our anecdotal observation that subjects had more difficulty tracking in 2-DoFs than 1-DoF. Future work might seek to better understand the decrement in performance, if any, in 2-DoF tracking tasks vs. 1-DoF tracking tasks.

It is always important to recognize that the neuromuscular anatomy of limb-absent subjects is both different from that of able-bodied subjects and highly variable. For example, our able-bodied subjects had a mean ± std. dev. forearm circumference of 25.9 ± 3.2 cm compared to 22.2 ± 2.3 cm for the limb-absent subjects. Remnant muscle tissue typically has more neuromuscular damage and may be more prone to fatigue (e.g., (Hahne, Schweisfurth et al. 2018)). And, the sensation of a phantom hand may be more or less

expressive in different subjects. Anecdotally, phantom limb sensation may have been more of a limitation in 2-DoF tasks than in 1-DoF tasks. Each of these factors may influence EMG-force performance.

Finally, there is some evidence suggesting that an accurate model of the dynamics between muscular activation (inputs) and kinetic/kinematic outputs is not paramount to control of the existing generation of myoelectrically-controlled prostheses, which provide relatively rudimentary function. If the myoelectric control model is repeatable and largely linear, then prosthesis users are hypothesized to adapt/re-learn the necessary inputs (muscular activations) required to achieve the desired output (Jiang, Vujaklija et al. 2014, Hahne, Markovic et al. 2017, Hahne, Schweisfurth et al. 2018) In fact, existing commercial prosthesis users have been doing so for years, albeit at the cost of additional mental workload (among other limiting factors) (Williams III 1990). Of course, the higher the fidelity with which future prosthetic devices reproduce the function of intact limbs, the more apparent will become the benefit of accurately identifying models relating muscular activation to kinetics/kinematics. And, unilateral prosthesis users should benefit from more accurate forward-path activation models during, for example, bilaterally symmetric tasks, wherein the central nervous system nominally matches muscular activation between the affected and the sound side.

2.5 Conclusion

The prime goal of this work was to evaluate distinct options for surrogate supervised output sources in hand-wrist EMG-force models for limb-absent subjects. We did so using novel instrumentation in which hand Opn-Cls forces as well as wrist Rad-Uln force and Pro-Sup moment were simultaneously measured on both sides of our able-bodied subjects. This instrumentation allowed us to report novel quantitative results on the latency between force/moment and our random target (Table 2.2); and on the ability of these subjects to perform random target tracking during our various tasks, contrasting RMSE to cross-correlation coefficient (Fig. 2.4).

For EMG-force modeling, our comparison of different feedback approaches found that use of the phantom limb for bilateral tracking (with or without mirror visual feedback) permitted the limb on the sound side to provide a reasonable substitute force measurement. But, this output source is only available to persons with unilateral limb-absence and still requires use of a load cell. As such, it is primarily of use in a prosthetist's office, and not in the field. We found that use of the tracking target without a feedback source (applicable to limb-absent subjects) resulted in an inadequate EMG-force model. In such cases, use of generic models for EMG-force dynamics, combined with simple gain selection for each EMG channel, would likely provide better performance.

Chapter 3: Normative Force/Moment Tracking Performance During Constant-Pose, Force-Varying, Bilaterally Symmetric, Hand-wrist tasks

This chapter is in development as a journal paper submission. Ziling Zhu, Carlos Martinez-Luna, Jianan Li, Benjamin E. McDonald, Chenyun Dai, Xinming Huang, Todd R. Farrell, Edward A. Clancy.

***Abstract*— Bilateral movement is widely used as rehabilitation therapy for patients with motor impairment, limb-absence, and for athletes to achieve balanced motor control. However, the cerebral intrinsic asymmetry and external conditions reflects the between limb difference, which was examined by two visual guided target tracking in both one degree of freedom (DoF) and 2-DoF tasks: (1) unilateral tracking by dominant limb with/without visual feedback, (2) bilateral tracking with mirror visual feedback provided by dominant/non-dominant limb. The "best-case" unilateral tracking error with visual feedback was ~ 10% of maximum voluntary contraction (MVC) and up to 30% MVC without visual feedback. Bilateral between limb difference averaged ~10% MVC difference and was affected little by visual conditions. The 1-DoF bilateral tracking showed dominant side had statistically lower error than the non-dominant side, while the 2-DoF bilateral tracking showed that the side providing mirror visual feedback (MVF) exhibited lower error than the opposite side. The results provide guidance of normative bilateral hand-wrist target tracking performance in target tracking and between limb difference.**

***Keywords*— Bilateral movement, Target tracking, Visual Feedback, Between limb difference, Symmetric movement.**

3.1 Introduction

Bilateral movement is very common during daily life, and is widely used in rehabilitation therapy. Patients with motor impairment, such as stroke, typically show impaired bilateral force control during recovery (Ramachandran and Altschuler 2009, Lodha, Naik et al. 2010, Coupar, Pollock et al. 2011, Thieme, Mehrholz et al. 2012, Sainburg, Good et al. 2013, Mozaffarian, Benjamin et al. 2016). A prominent rehabilitation technique is bilateral movement training, which activates the motor synergies of neurological interlimb coordination (Whitall, Waller et al. 2000, Kang and Cauraugh 2017). For limb-absent people, mirror therapy plays an important role to help build phantom limb sensation and/or relieve phantom limb pain (Nikolajsen and Jensen 2001, Ramachandran and Altschuler 2009). Furthermore, many athletes seek to achieve balanced motor control between dominant and non-dominant limbs in sports such as swimming, basketball and weightlifting (Hrysomallis 2011, MacDonald, Losier et al. 2014). Thus, research has focused on bilateral movement to improve an athlete's performance. A goal of all of these studies is to explore motor equivalency in bilateral movement by investigating the difference between dominant and non-dominant limbs during different tasks (Schmidt 1975, Todor and Doane 1978, Carson 1989).

Although intrinsic cerebral asymmetry reflects a difference in gain relative to each hemisphere and limb (Triggs, Subramanium et al. 1999, Babiloni, Carducci et al. 2003, Liu, Stufflebeam et al. 2009), some recent literature on upper limb asymmetries shows more distinctions between two limbs—the dominant limb is more specialized for control of movement trajectory, while the non-dominant limb is more reliable in obtaining static arm positions or postures (Schaefer, Haaland et al. 2001, Bagesteiro and Sainburg 2002, Sainburg 2002, Bagesteiro and Sainburg 2003, Haaland, Prestopnik et al. 2004). Another perspective is described as the vision-proprioception mechanism, which is mainly concerned with movement-related sensory feedback—the dominant limb is more reliant on visual feedback during the control of movement, whereas the non-dominant limb is enhanced for proprioceptive feedback processing (Goble and Brown 2008, Goble and Brown 2008). These views provide a direction for experimental design utilizing different visual feedbacks.

To examine bilateral difference and motor control in healthy people, different visual guided tasks have been performed, including: aiming/throwing with an explosive force (Goble and Brown 2008, Sherwood 2014), and pushing or pressing with a static/constant force or slow varying force (Hogan and Mann 1980, Rancourt and Hogan 2001, Kenway, Bisset et al. 2015, Tracy, Hitchcock et al. 2015). Different types of visual feedback conditions were applied to discern how the visuomotor system interacts with motor control (e.g., visual feedback provided vs. hidden). In bilateral tasks for mirror therapy or stroke rehabilitation, the visual feedback was usually generated only from the sound side, with mirror visual feedback (MVF) provided to

guide the affected/recovering side. There is evidence that changing the visual feedback condition affects a task (Chan, Witt et al. 2007, Barbin, Seetha et al. 2016, Jegatheeswaran, Vesia et al. 2018).

In the research reported herein, we focused on bilateral multi-joint wrist-hand contractions. Subjects completed a series of force-varying, random-target tracking tasks under different visual feedback types to examine their tracking performance during bilaterally symmetric tasks. We initially tested tracking using only the dominant limb with or without a visual feedback, with this performance setting a benchmark. Then in bilateral tasks, MVF was provided, sourced from either the dominant or non-dominant limb, and also compared to performance without visual feedback. We tested both one degree of freedom (1-DoF) tasks (wrist or hand motions) and 2-DoF tasks (one wrist motion + hand open-close) to evaluate performance as a function of different task difficulties. Our results provide normative performance data for novel wrist-hand, bilateral, force-varying, tracking tasks.

3.2 Methods

3.2.1 Participants

Twelve healthy (no limb movement or vision deficits), right-handed subjects participated in this study (six males and six females, aged 18–55 years). All subjects provided written informed consent approved by the WPI Institutional Review Board (IRB Protocol # 17-155).

3.2.2 Experiment setup

Subjects were seated in the experimental apparatus (Fig. 3.1). Each hand was secured into a thermo-formable plastic mold, with the posterior aspect bolted to a six-degree of freedom (DoF) load cell (MC3A-

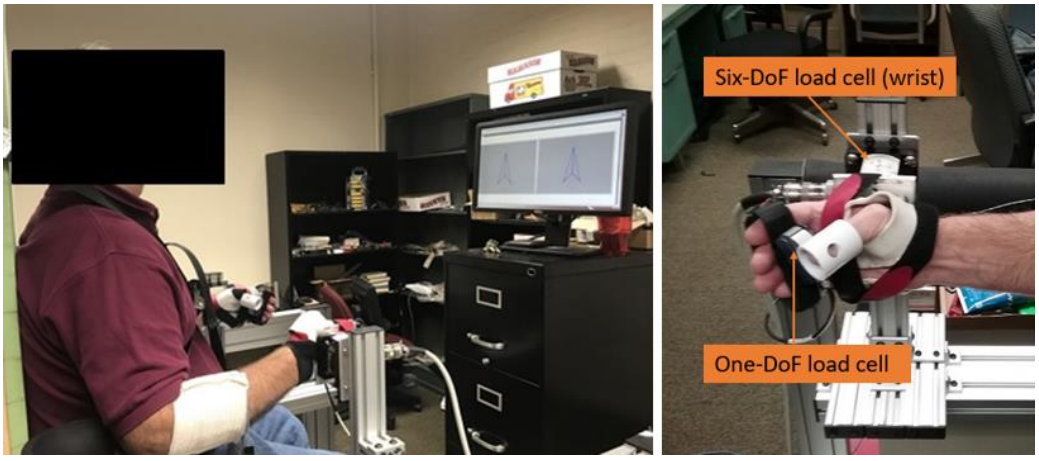

Fig. 3.1. Experimental apparatus. Left: Subject sat in experimental chair with each hand secured into force measurement devices, facing the computer screen which displayed target tracking tasks. Right: force measurement devices at the hand-wrist. Each hand was separately secured via Velcro to a thermo-formable plastic glove that was fixed to a six-axis load cell to measure the moment at the wrist. Fingers were secured to a single-axis load cell to measure hand grip force.

100 transducer, Gen 5 signal conditioner, AMTI, Watertown, MA). Each load cell measured constant-posture wrist radial-ulnar deviation (Rad-Uln) force and wrist pronation-supination (Pro-Sup) moment (Zhu, Martinez-Luna et al. 2020). Additionally, each hand gripped a single-axis load cell (LCR-150 with DMD-465WB amplifier, Omega Engineering, Inc., Stamford, CT) to measure each hand's open-close (Opn-Cls) grip force. The thumb was secured to one side of a load cell via a rigid tube and the other four fingers were secured to the opposite load cell side via Velcro. The palms of the hands were oriented perpendicular to the plane of the floor, facing inwards; the wrists were relaxed in a neutral position; and the shoulders were in the anatomical position.

During unilateral target tracking tasks, a computer-controlled target (blue arrowhead, Fig. 3.2) guided subjects to complete the tasks, while a red arrowhead provided online visual feedback of force/moment (when desired). Arrowhead up-down movement represented Rad-Uln force, rotation represented Pro-Sup moment and size represented Opn-Cls force. During bilateral target tracking tasks, the target and feedback force/moment (when displayed) from one selected side was mirrored in two side-by-side display panels on the screen (Fig. 3).

3.2.3 Experimental Protocol

All trials were constant posture. Subjects rested at least two minutes between trials to reduce the impact from fatigue.

MVC Tasks: Subjects performed bilateral maximum voluntary contraction (MVC) trials for each of Rad-Uln force, Pro-Sup moment and Opn-Cls force. Each trial lasted 6 seconds. Subjects took 2–3 seconds to ramp up to their MVC effort, then maintained that effort for 2–3 seconds. The average force during the maintenance portion of the contraction was measured as their MVC. Lastly, rest trials with all muscles fully relaxed were recorded for EMG noise level evaluation.

Force-varying target tracking trials: For each task listed below, subjects performed force-varying target tracking tasks for 1-DoF Rad-Uln, Pro-Sup and Opn-Cls; and then for 2-DoF combinations of one wrist DoF plus Opn-Cls. The target force/moment was a 0.75 Hz band-limited, white and uniform random process ranging between ±30% MVC (independently) for each DoF. This bandwidth was the widest for which subjects could maintain target tracking for these tasks during preliminary testing. Each trial was 40 s in duration and conducted twice per task, in a randomized order per task. Before each task, subjects could practice until they felt comfortable. Data were recorded from four specific tasks.

Tasks 1 & 2—Unilateral target tracking (Fig. 3.2): Subjects only used their dominant limb to perform target tracking trials. The non-dominant limb was fully at rest during these trials. In Task 1, visual feedback from the dominant limb was provided. In Task 2, no visual feedback was provided.

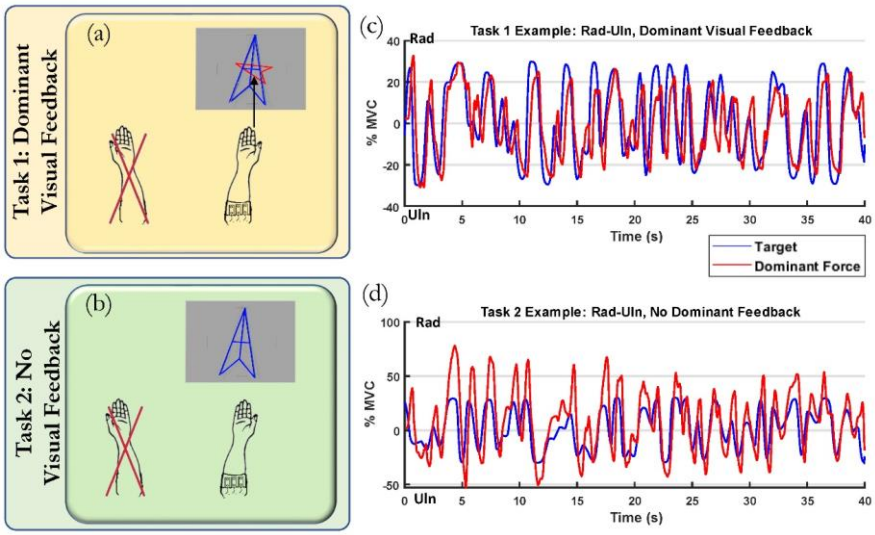

Fig. 3.2. a) Task 1: subjects tracked target with their dominant limb given real-time visual feedback of their dominant limb force. Blue arrowhead is target and red arrowhead is visual feedback. b) Task 2: subjects tracked target with their dominant limb with no visual feedback. c, d) Examples of 1-DoF target-force time-series trials for Tasks 1 and 2

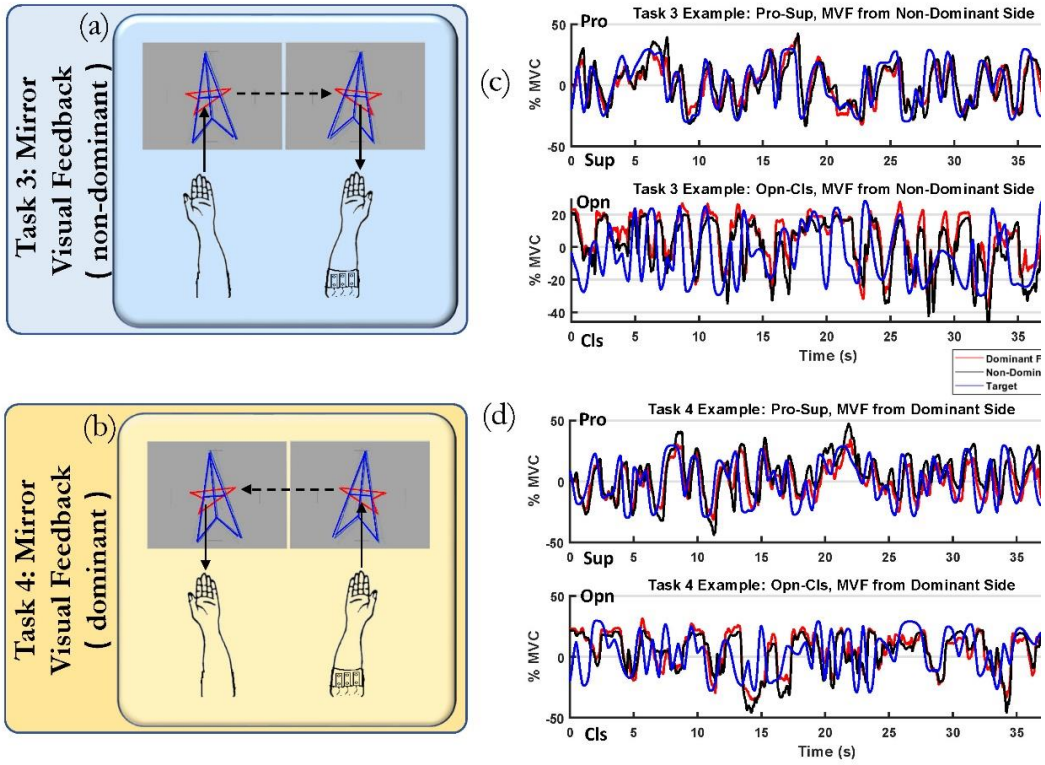

Fig. 3.3. a) Task 3: subjects tracked target with both limbs given real-time mirror visual feedback originating from their non-dominant limb force. Blue arrowhead is target and red arrowhead is visual feedback. b) Task 4: subjects tracked target with both limbs given real-time mirror visual feedback originating from their dominant limb force. c, d) Examples of 2-DoF target-force time-series results for Tasks 3 and 4.

Tasks 3 & 4—Bilateral target tracking (Fig. 3.3): Subjects used both limbs to simultaneously track a bilaterally symmetric target, with visual feedback from one side displayed on both panels—the second panel

displayed a mirrored image of the first. In Task 3, MVF originated from the non-dominant limb (MVF[Non-Dom]). In Task 4, MVF originated from the dominant limb (MVF[Dom]).

3.2.4 Methods of Analysis

Data pre-processing: In total, 40 tracking trials of 40 s duration each were available per subject, comprised of 4 tasks x 5 DoF conditions (three 1-DoF conditions and two 2-DoF conditions) x 2 repetitions. Data were analyzed off-line using MATLAB version 2019b (Mathworks, Inc., Natick, MA). All filters were implemented using the two-pass, zero-phase method. Each force/moment signal and each target trajectory was lowpass filtered (f_c = 8 Hz, Chebyshev Type I filter, ninth-order, 0.05 dB peak-to-peak passband ripple), then downsampled from 2048 Hz to 20.48 Hz. The wrist Rad-Uln data were normalized by $(|MVC_{Rad}| + |MVC_{Uln}|)/2$, and similar normalization was applied to the Pro-Sup and Opn-Cls data.

Latency between forces/moments and the target; RMS error (RMSE): Due to reaction time delays, the force/moment signal lags target movement by approximately 250–350 ms (Luce 1986, p. 209–210, Zhu, Martinez-Luna et al. 2020, Zhu, Martinez-Luna et al. in press). So, we estimated the cross-correlation coefficient function $\rho[m]$ (where m is the decimated sample index) between force and target over each discrete-time delay between 0 to 1 s. The time location corresponding to the maximum value of $\rho[m]$ was denoted ρ_{max}. After adjusting for this latency, RMSE was computed between the force/moment signal and the target. For 2-DoF conditions, each DoF was analyzed separately. When comparing the forces/moments in the dominant side to those of the non-dominant side, latency was allowed to be positive-valued (dominant side led non-dominant side) or negative-valued.

Histogram of forces/moments and target signals in time domain: The normalized force/moment signals from 1-DoF tasks from each of the three DoFs from Task 3 (bilateral MVF from non-dominant side) were separately concatenated from the 12 subjects x 2 repetitions. For each DoF, a normalized histogram (i.e., probability density function, PDF, estimate) was computed to represent the distribution of force/moment data by %MVC. Each histogram used a force resolution of 5 %MVC over a range extending from 100 %MVC extension to 100 %MVC flexion. This process was repeated for Task 4 (bilateral MVF from dominant side) and also for target trajectories. Then, the complete process was repeated for the 2-DoF bilateral tasks. For 2-DoF conditions, each DoF was analyzed separately.

Power spectrum density (PSD) of forces/moments and target signals: We estimated the PSD of each trial using Welch's method (50% overlap, 256-length DFT, Hamming window). Then, for each different DoF condition and feedback, PSD estimates from all 12 subjects and 2 repetitions were ensemble averaged. For 2-DoF conditions, each DoF was analyzed separately.

3.2.5 Statistics

Repeated measures analysis of variance (RANOVA) was computed to evaluate the performance under different conditions with a significant level of $p = 0.05$. The test of sphericity (ε) was used to adjust the degrees of freedom either via the method of Greenhouse-Geisser ($\varepsilon < 0.75$) or Hyunh-Feldt ($0.75 < \varepsilon < 1$) prior to RANOVA. *Post hoc* pairwise comparisons used paired *t*-tests with Bonferroni correction. Only Bonferroni-corrected p-values are listed.

3.3 Results

3.3.1 Unilateral tasks, target tracking

Fig. 3.2 shows example unilateral task time-series trials. Fig. 3.4 shows summary RMSE, ρ_{Max} and time latency results of 1- and 2-DoF unilateral target tracking tasks (Tasks 1 and 2) between dominant force and the target. Overall, tracking with visual feedback had better performance (lower RMSE, higher ρ_{Max}) than tracking without visual feedback among all DoFs. Separate RANOVAs were calculated for each of the two DoF pairs (Rad-Uln & Opn-Cls, Pro-Sup & Opn-Cls) using three factors: DoF (1-DoF or 2-DoF), feedback type (dominant feedback, no feedback) and force/moment (Rad-Uln or Opn-Cls, Pro-Sup or Opn-Cls for different DoF pairs). Thus, the 1-DoF vs. 2-DoF portion of the comparison compared a 1-DoF task to the corresponding force/moment from the 2-DoF task.

For (Rad-Uln & Opn-Cls) and (Pro-Sup & Opn-Cls) RMSE, both three-way RANOVAs found only feedback type was significant ($F(1, 11) > 46$, $p < 10^{-4}$). Both *post hoc* comparisons found that providing dominant feedback had significantly lower error than no feedback ($p < 10^{-4}$).

For (Rad-Uln & Opn-Cls) and (Pro-Sup & Opn-Cls) ρ_{Max}, both three-way RANOVAs found three-way significant interaction among all factors ($F(1, 11) > 7$, $p = 0.005$). *Post hoc* comparisons found that: 1-DoF always had significant higher ρ_{Max} than 2-DoF ($p < 10^{-4}$), except for both wrist force/moments (Rad-Uln, Pro-Sup) with dominant feedback; providing dominant feedback had significantly higher ρ_{Max} than no feedback ($p < 0.001$); Rad-Uln had significantly higher ρ_{Max} than Opn-Cls ($p < 0.04$); and Pro-Sup had significantly higher ρ_{Max} than Opn-Cls ($p < 0.003$).

For Rad-Uln & Opn-Cls time latency, a three-way RANOVA found two-way interactions among all factors. *Post hoc* comparison found 1-DoF had lower latency than 2-DoF ($p < 0.008$), except for Rad-Uln with dominant feedback; and Rad-Uln had lower latency than Opn-Cls ($p < 0.013$) when providing dominant feedback for both 1-DoF and 2-DoF. For Pro-Sup & Opn-Cls time latency, a three-way RANOVA found feedback type was significant ($F(1, 11) = 19.01$, $p = 0.001$), and that DoF and force/moment had significant interaction ($F(1, 11) = 28.265$, $p < 10^{-3}$). *Post hoc* comparison found latency in dominant feedback was

significantly longer than in no feedback ($p = 0.001$); 1-DoF had significantly lower latency than 2-DoF only for Opn-Cls ($p < 10^{-4}$); and Pro-Sup had lower latency than Opn-Cls in 2-DoF tracking ($p < 10^{-3}$).

3.3.2 Bilateral tasks, matching dominant to non-dominant forces/moments

Fig. 3.3 shows example bilateral task time-series trials. Fig. 3.5 shows summary RMSE, ρ_{Max} and time latency results of 1- and 2-DoF bilateral tasks (Tasks 3 and 4), comparing the ability to match dominant to non-dominant forces/moments. As above, separate RANOVAs were calculated for each DoF pair under three factors: DoF (1-DoF, 2-DoF), feedback type (MVF[Non-dom], MVF ([Dom]), force/moment (Rad-Uln or Opn-Cls, Pro-Sup or Opn-Cls for different DoF pairs).

For Rad-Uln & Opn-Cls RMSE, a three-way RANOVA found DoF significantly interacted with feedback type ($F(1, 11) = 5.42$, $p = 0.04$) and force/moment ($F(1, 11) = 6.67$, $p = 0.025$). *Post hoc* comparison showed that 1-DoF had significantly lower error than 2-DoF only for Opn-Cls ($p = 0.02$); and in 1-DoF, Rad-Uln had significantly higher error than Opn-Cls ($p = 0.049$). For Pro-Sup & Opn-Cls RMSE, a three-way RANOVA found only DoF was significant ($F(1, 11) = 10.78$, $p = 0.007$). *Post hoc* comparison showed that 1-DoF had significantly lower error than 2-DoF ($p = 0.007$).

For Rad-Uln & Opn-Cls ρ_{Max}, a three-way RANOVA found no significance for all factors. For Pro-Sup & Opn-Cls, a three-way RANOVA found DoF was significant ($F(1, 11) = 15.08$, $p = 0.003$). *Post hoc* comparison found that 1-DoF had significantly higher ρ_{Max} than 2-DoF ($p = 0.003$).

For Rad-Uln & Opn-Cls time latency, a three-way RANOVA found no significance for all factors. For Pro-Sup & Opn-Cls, a three-way RANOVA found DoF was significant ($F(1, 11) = 7.60$, $p = 0.019$) and feedback type significantly interacted with motion ($F(1, 11) = 6.34$, $p = 0.029$). *Post hoc* comparison found that 1-DoF had significantly lower latency than 2-DoF ($p = 0.019$); and Pro-Sup had longer latency than Opn-Cls only with MVF[Non-Dom] ($p = 0.002$).

3.3.3 Bilateral tasks, target tracking

Fig. 3.6 shows summary RMSE, ρ_{Max} and time latency results of 1- and 2-DoF bilateral target tracking tasks (Tasks 3 and 4) between dominant/non-dominant force and the target. RANOVAs were separately calculated for each DoF pair under four factors: DoF (1-DoF, 2-DoF), feedback type (MVF[Non-Dom], MVF[Dom]), tracking side (measurement side: dominant, non-dominant), motion (Rad-Uln or Opn-Cls, Pro-Sup or Opn-Cls for different DoF pairs).

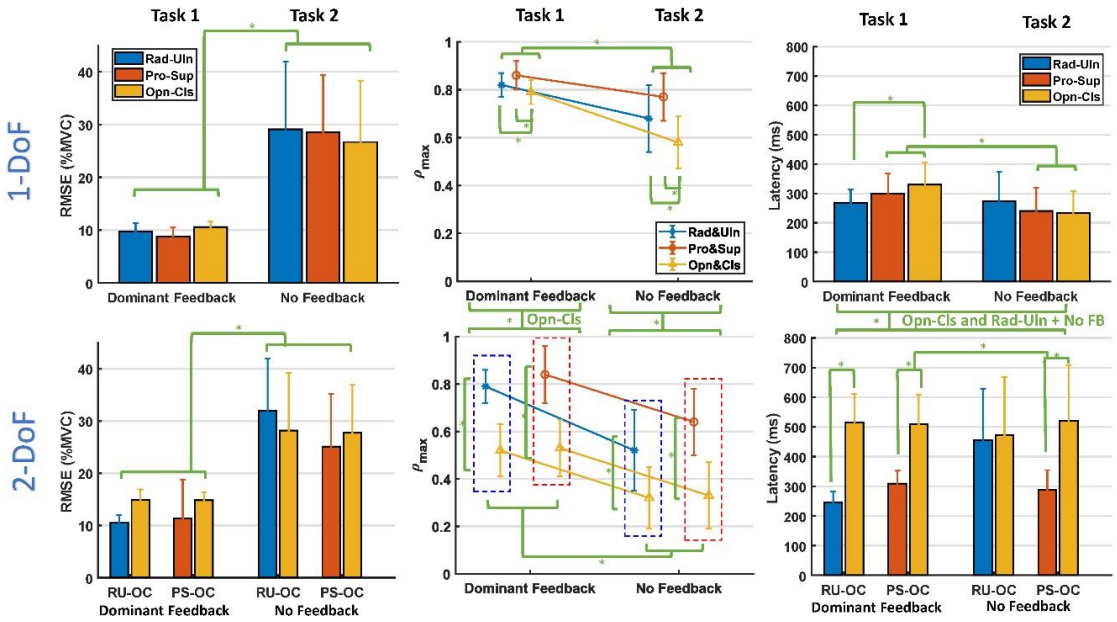

Fig. 3.4. Unilateral (Tasks 1 & 2) tracking summary results. Mean + std. dev. errors between dominant limb force/moment and target, after adjusting for time latency. RMSE (left) with different feedback conditions [dominant (Task 1), none (Task 2)] as a function of DoF for 1-DoF tasks (top) and as a function of DoF pairs for 2-DoF tasks (bottom). Maximum cross-correlation coefficients (ρ_{Max}) shown in the middle (dash-line boxes group DoF pairs) and latency shown at right. Green brackets denote statistically significant differences between groups, green lines denote differences between individual items. Differences between 1- and 2-DoF were too complex to show (see text for details). Supplementary Table S1 lists all plot values.

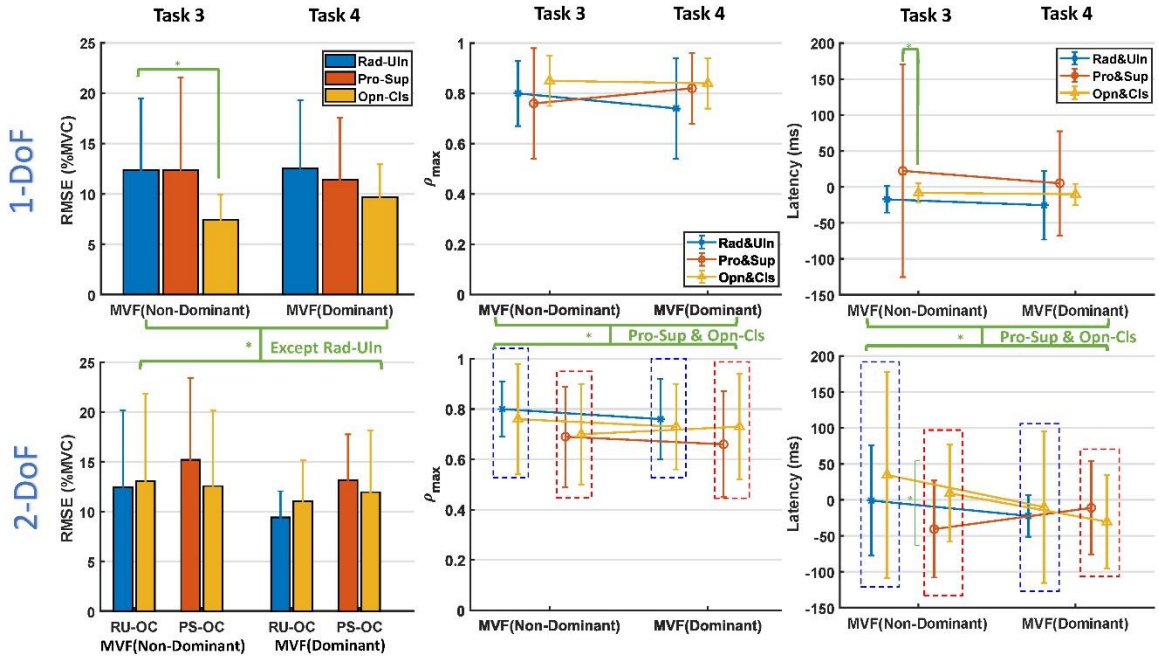

Fig. 3.5. Bilateral (Tasks 3 & 4) tracking summary results, matching dominant to non-dominant forces/moments. Mean + std. dev. errors between dominant and non-dominant limb force/moment after adjusting for latency. RMSE (left) with different feedback conditions [mirror visual feedback originated from non-dominant side (Task 3), dominant side (Task 4)] as a function of DoF for 1-DoF tasks (top) and as a function of DoF pairs for 2-DoF tasks (bottom). Maximum cross-correlation coefficients (ρ_{MAX}) shown in the middle (dash-line boxes group DoF pairs) and latency shown at right. Green brackets denote statistically significant differences between groups, green lines denote differences between individual items. See text for details. Supplementary Table S2 lists all plot values.

For (Rad-Uln & Opn-Cls) and (Pro-Sup & Opn-Cls) RMSE, four-way RANOVAs found interaction

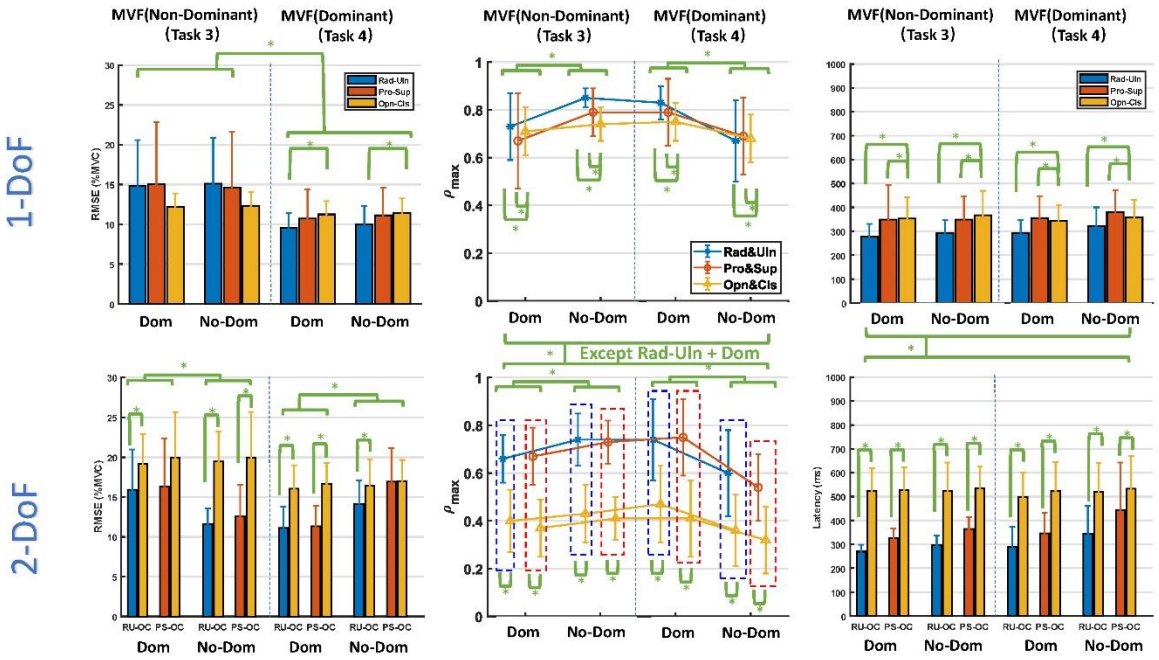

Fig. 3.6. Bilateral (Tasks 3 & 4) tracking summary results, matching forces/moments to target. Mean + std. dev. errors of dominant tracking (dominant force vs. target) and non-dominant tracking (non-dominant force vs. target) after adjusting for latency. RMSE (left) with different feedback conditions [mirror visual feedback (MVF) originated from non-dominant side (Task 3), dominant side (Task 4)] as a function of DoF for 1-DoF tasks (top) and as a function of DoF pairs for 2-DoF tasks (bottom). Maximum cross-correlation coefficients (ρ_{MAX}) shown in the middle (dash-line boxes group DoF pairs) and latency shown at right. Green brackets denote statistically significant differences between groups, green lines denote differences between individual items. Supplementary Table S3 lists all plot values.

among all factors ($F(1, 11) > 14.031, p < 10^{-3}$). *Post hoc* comparison found that: in 1-DoF, MVF[Dom] always had significantly lower error than MVF[Non-Dom] ($p < 0.005$); and in 2-DoF for Rad-Uln or Pro-Sup, if the tracking side was the same side as MVF origination, RMSE was significantly lower than the opposite side (non-dominant side + MVF[dom] vs. dominant side + MVF[Dom], $p < 0.004$; non-dominant side + MVF[Non-Dom] vs. dominant side + MVF[Non-Dom], $p < 0.028$). For hand Opn-Cls, no significance was found with different feedback types. 3). Separately, for Rad-Uln in 1-DoF with Dominant MVF, and 2-DoF with both dominant and non-dominant MVF, Rad-Uln had lower error than Opn-Cls ($p < 0.028$). Also, for Pro-Sup in 2-DoF tracking, when the tracking side was the same side as MVF origination (MVF[Dom] + dominant side or MVF[Non-Dom] + non-dominant side), Pro-Sup had lower error than Opn-Cls ($p < 0.003$).

For (Rad-Uln & Opn-Cls) and (Pro-Sup & Opn-Cls) ρ_{Max}, four-way RANOVAs found multiple interactions. *Post hoc* comparison found that, except for Pro-Sup on the dominant side, 1-DoF always had significantly higher ρ_{Max} than 2-DoF ($p < 0.023$). Separately, forRad-Uln or Pro-Sup, if the tracking side was the same side as MVF origination, ρ_{Max} was significantly higher than the opposite side (dominant side + MVF[Dom] vs. non-dominant side + MVF[Dom], $p < 0.012$; non-dominant side + MVF[Non-Dom] vs. dominant side + MVF[Non-Dom], $p < 10^{-3}$). Also, Rad-Uln or Pro-Sup always had significantly higher ρ_{Max} than hand Opn-Cls ($p < 0.037$).

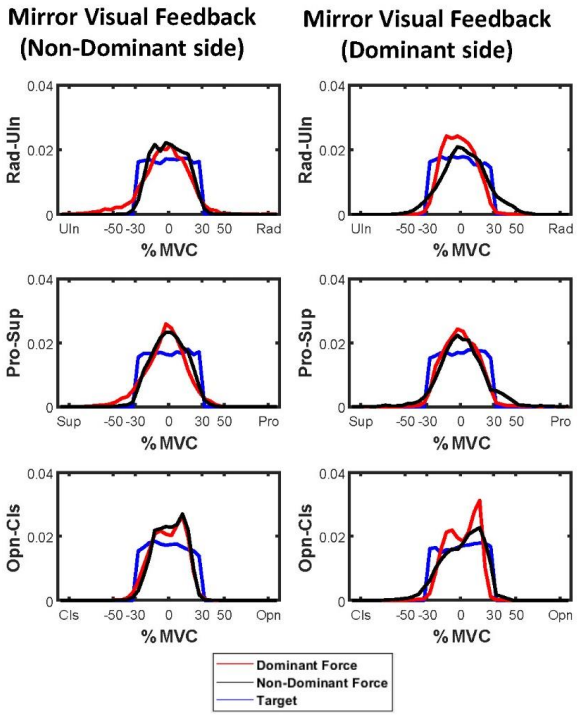

Fig. 3.7. One-DoF probability density function (PDF) estimate (Tasks 3 & 4) summary results. Estimates from dominant force, non-dominant force and target movement are shown with the factors: feedback types (MVF from non-dominant side, MVF from dominant side) and three force/moments (Rad-Uln, Pro-Sup, Opn-Cls). Supplementary Table S4 lists

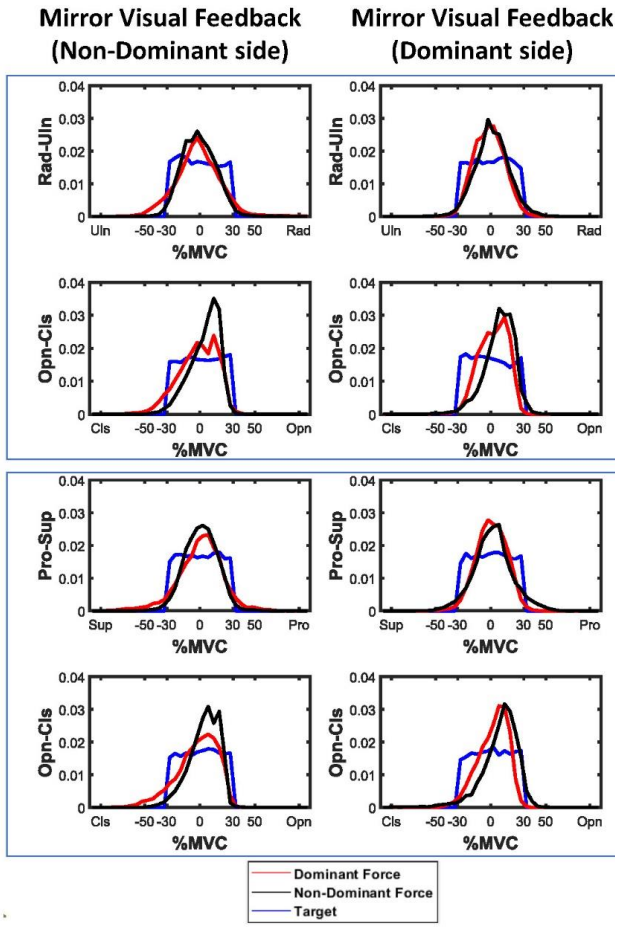

Fig. 3.8. Two-DoF probability density function (PDF) estimate (Tasks 3 & 4) summary results. Estimates from dominant force, non-dominant force and target movement are shown with the factors: feedback types (MVF from non-dominant side, MVF from dominant side) and two force/moments pairs (Rad-Uln & Opn-Cls, Pro-Sup & Opn-Cls). Supplementary Table S5 lists all plot values.

For (Rad-Uln & Opn-Cls) and (Pro-Sup & Opn-Cls) time latency, both four-way RANOVAs found significant interaction between DoF and force/moment ($F(1, 11) > 26.69$, $p < 10^{-3}$). *Post hoc* comparison found that 1-DoF always had lower latency than 2-DoF ($p < 10^{-5}$). and Rad-Uln or Pro-Sup had significantly lower latency than hand Opn-Cls ($p < 10^{-3}$).

3.3.4 Force Histogram Results, Unilateral vs. Bilateral Tasks

Fig. 3.7 shows 1-DoF and Fig. 3.8 shows 2-DoF, respectively, PDF estimates of applied forces (dominant/non-dominant) as well as the actual target, ensemble-averaged across all subjects. For each experimental trial, the area difference between the trial's PDF estimate vs. an ideal uniform distribution ranging from –30% to 30% MVC was calculated. RANOVA comparison considered four factors: DoF (1-

DoF, 2-DoF), feedback type (MVF[Non-Dom], MVF[Dom]), force/moment (Rad-Uln, Pro-Sup, Opn-Cls) and PDF estimate origination (dominant side, non-dominant side, target movement).

For Rad-Uln & Opn-Cls, a four-way RANOVA found multiple interactions. *Post hoc* comparison found that: 1-DoF had significantly lower error than 2-DoF ($p < 0.01$); the target's error was lower than that of dominant force and non-dominant force ($p < 10^{-5}$) for both 1-DoF and 2-DoF; and when the tracking side was the same side as MVF origination, Rad-Uln had lower error than Opn-Cls (MVF[Non-Dom] + non-dominant side, $p = 0.003$; MVF(Dom) + dominant side, $p < 10^{-3}$).

For Pro-Sup & Opn-Cls, a four-way RANOVA found multiple interactions. *Post hoc* comparison found that: 1-DoF had significantly lower error than 2-DoF only for the non-dominant side ($p = 0.001$); the target's error was lower than that of dominant force and non-dominant force ($p < 10^{-5}$) for both 1-DoF and 2-DoF; and Pro-Sup had lower error than Opn-Cls (non-dominant side, $p < 0.001$; dominant-side, $p = 0.005$).

3.4 Discussion

In this study, we focused on describing normative performance of healthy subjects performing bilateral upper limb target tracking tasks in 1-DoF and in 2-DoFs. One of our own interests is in the development of multiple DoF myoelectric control for hand-wrist prostheses. But, this normative performance is of general interest to many applications, ranging from stroke rehabilitation to sport training.

3.4.1 One-DoF vs. Two-DoF, One joint vs. Two joints

While details varied between our experimental tasks, the overall trend was for better performance (lower RMSE and latency, higher correlation) on 1-DoF tasks, as compared to 2-DoF tasks. For example, Fig. 3.5 (results of matching dominant to non-dominant forces/moments) shows average RMSE for Pro-Sup increasing from 12 %MVC during 1-DoF tasks to 14–15 %MVC during 2-DoF tasks; and RMSE for Opn-Cls increasing from 7–10 %MVC during 1-DoF tasks to ~12 %MVC during 2-DoF tasks. Fig. 3.6 (results of bilateral target tracking) shows average RMSE for Opn-Cls increasing from <12.5 %MVC during 1-DoF tasks to nearly 20 %MVC during 2-DoF tasks. Fig. 3.6 also shows average latencies for Opn-Cls increasing from ~350 ms for 1-DoF tasks to >500 ms for 2-DoF tasks. These particular changes are substantial.

Although much research has explored bilateral movement by changing several external conditions like visual feedback, experiment types etc., most of them didn't consider about how task difficulty affected the performance since this kind of "difficulty" was hard to defined precisely. In this experiment, we treated 2-DoF as a relatively harder task since it enrolled two joints of wrist and hand simultaneously, as well as 2-dimensional target movement and visual feedback. From the result, 2-DoF had overall poorer

performance than 1-DoF, and even both wrist and hand motions could achieve the similar performance in 1-DoF, their errors and latencies had great different in 2-DoF. In our experiment, all subjects performed better on wrist rather than hand, which exhibited a preference. This preference could not be explained as subjects paid more attention on wrist, since a lot of external conditions on experimental design would affect the result, such that subjects might felt more comfortable on wrist movement, or got more sensitive on cursors movement (Rad-Uln) or rotation (Pro-Sup) than size change (Opn-Cls). However, This result could be a good instruction that when subjects faced a relatively hard task and not familiar with it (randomly), they preferred to divide the task into different dimension and then gave different priority to deal with.

3.4.2 Between Limb Difference, Dominant vs. Non-Dominant Force/Moment

In this experiment, we explored the difference between dominant and non-dominant force/moment by errors, maximum cross-correlation and latencies. Subjects were enrolled in both 1-DoF and 2-DoF tasks, provided MVF from either dominant side or non-dominant side, but the between limb force/moment error were always around 10% MVC, and hardly affected by external conditions. The mirror movement is mainly decided by intrinsic factors, as movement of one side induce activity patterns within ipsilateral motor cortex that are related to the mirror-symmetric movement of the other side. The little difference mainly reflected on difference in gains. Although the between limb error became larger in 2-DoF than 1-DoF, but this difference would reduce if subjects were more familiar with the tasks.

3.4.3 Bilateral tracking Accuracy, Dominant/Non-Dominant Force/Moment vs. Target movement

The tracking accuracies of dominant and non-dominant limbs were a combination of many factors. Different types of tracking or matching tasks were designed, such as aiming, grasping precision, mirror movement, or keeping static force level, focused on how external conditions (visual feedback) and internal characters (dominance) influenced the performance together. As some review of literatures showed different functions of dominant and non-dominant side, in one-DoF tracking which was relatively easy tasks, subjects could achieve lower error on dominant side no matter what MVF provided. The reason would be dominant limb attracted more visual attention in bilateral movement since people more relied on dominant limb for daily tasks.

Although some research suggested that dominant limb was more effective processing of visual feedback, in this experiment, we still saw that in 2-DoF, the performance of tracking was highly affected by MVF type, and the side where MVF originated from always performed better even without telling subjects which side

they could control the MVF. The MVF was provided to both limbs for guidance, and as showed above, subjects could achieve good symmetric movement under all visual conditions, they could still feel a slight incongruity from the side opposite to MVF origination. So, on the side of MVF origination, the performance was good since the visual feedback was always consistent with the force/moment, but on the opposite side of MVF origination, subjects need to adjust back and forth to matching the target as well as the visual feedback. Therefore, in mirror therapy, or athletes balance training, people continue to overcome this additional sensation to rebuild or strengthen the body's balance mechanism.

3.5 Conclusion

This study evaluated the tracking accuracy in both unilateral and bilateral movement, and between limb difference in wrist-hand random target tracking tasks. We found that visual feedback could help improve the tracking accuracy in both bilateral tracking and unilateral tracking, and the bilateral tracking was affected by both dominance and MVF origination. Between limb difference was hardly affected by visual feedback types, the asymmetry is relatively stable as a result of different functions on dominant and non-dominant side.

3.6 Appendix

Table S1. Plot values for Fig. 3.4, Unilateral (Tasks 1 & 2) tracking summary results (mean ± standard deviation errors).

RMSE （%MVC）		Dominant feedback	No feedback
Rad-Uln		9.77 ± 1.52	29.10 ± 12.85
Pro-Sup		8.75 ± 1.74	28.52 ± 10.94
Opn-Cls		10.58 ± 0.98	26.67 ± 11.57
Rad-Uln & Opn-Cls	Rad-Uln	10.50 ± 1.50	32.02 ± 10.01
	Opn-Cls	14.95 ± 1.96	28.48 ±11.02
Pro-Sup & Opn-Cls	Pro-Sup	11.32 ± 7.50	25.13 ± 10.11
	Opn-Cls	14.83 ±1.51	27.75 ± 9.18

Cross Correlation Max, ρ_{max}		Dominant feedback	No feedback
Rad-Uln		0.82 ± 0.05	0.68 ± 0.14
Pro-Sup		0.85 ± 0.06	0.77 ± 0.10
Opn-Cls		0.83 ± 0.04	0.79 ± 0.11
Rad-Uln & Opn-Cls	Rad-Uln	0.79 ± 0.07	0.52 ± 0.17
	Opn-Cls	0.52 ± 0.11	0.32 ± 0.13
Pro-Sup & Opn-Cls	Pro-Sup	0.84 ± 0.06	0.64 ± 0.12
	Opn-Cls	0.53 ± 0.13	0.33 ± 0.14

Latency （ms）		Dominant feedback	No feedback
Rad-Uln		267.5 ± 46.1	273.6 ± 100.0
Pro-Sup		300.1 ± 68.8	240.1 ± 78.9
Opn-Cls		329.6 ± 75.4	234.0 ± 73.2
Rad-Uln & Opn-Cls	Rad-Uln	245.7 ± 36.1	455.7 ± 174.0
	Opn-Cls	514.7 ± 96.8	472.0 ± 196.8
Pro-Sup & Opn-Cls	Pro-Sup	309.2 ±43.4	286.9 ± 67.6
	Opn-Cls	508.6 ± 100.3	520.8 ± 186.9

Table S2. Plot values for Fig. 5, Bilateral (Tasks 3 & 4) tracking summary results for matching dominant to non-dominant forces/moments (mean ± standard deviation errors).

RMSE （%MVC）		Non-Dominant	Dominant
Rad-Uln		12.38 ± 7.10	12.53 ± 6.80
Pro-Sup		12.39 ± 9.18	11.39 ± 6.21
Opn-Cls		7.43 ± 2.49	9.67 ± 3.27
Rad-Uln & Opn-Cls	Rad-Uln	12.44 ± 7.75	9.42 ± 2.63
	Opn-Cls	13.09 ± 8.77	11.06 ± 4.08
Pro-Sup & Opn-Cls	Pro-Sup	15.20 ± 8.21	13.17 ± 4.60
	Opn-Cls	12.57 ± 7.57	11.96 ± 6.18

Cross Correlation Max, ρ_{max}		Non-Dominant	Dominant
Rad-Uln		0.80 ± 0.13	0.74 ± 0.20
Pro-Sup		0.76 ± 0.22	0.82 ± 0.14
Opn-Cls		0.85 ± 0.10	0.84 ± 0.10
Rad-Uln & Opn-Cls	Rad-Uln	0.80 ± 0.11	0.76 ± 0.16
	Opn-Cls	0.76 ± 0.22	0.73 ± 0.17
Pro-Sup & Opn-Cls	Pro-Sup	0.69 ± 0.16	0.66 ± 0.20
	Opn-Cls	0.70 ± 0.20	0.73 ± 0.21

Latency （ms）		Non-Dominant	Dominant
Rad-Uln		-17.3 ± 18.4	-25.4 ± 47.8
Pro-Sup		22.4 ± 147.9	5.08 ± 72.4
Opn-Cls		-8.1 ± 13.1	-10.2 ± 14.6
Rad-Uln & Opn-Cls	Rad-Uln	-1.0 ± 76.6	-22.4 ± 28.9
	Opn-Cls	34.6 ± 143.4	-10.17 ± 105.4
Pro-Sup & Opn-Cls	Pro-Sup	-40.7 ± 26.7	-11.2 ± 56.7
	Opn-Cls	9.16 ± 67.5	-30.5 ± 64.9

Table S3. Plot values for Fig. 6, Bilateral (Tasks 3 & 4) tracking summary results for matching forces/moments to target (mean ± standard deviation errors).

RMSE （%MVC）		**Non-Dominant MVF**		**Dominant MVF**	
Tracking side		Dominant side	Non-dominant	Dominant	Non-dominant
Rad-Uln		14.80 ± 5.81	15.11 ± 5.74	9.56 ± 1.85	9.96 ± 2.33
Pro-Sup		15.03 ± 7.81	14.66 ± 6.95	10.72 ± 3.65	11.12 ± 3.46
Opn-Cls		12.20 ± 1.68	12.29 ± 1.75	11.25 ± 1.67	11.41 ± 1.84
Rad-Uln	& Rad-Uln	15.92 ± 5.05	11.63 ± 1.95	11.11 ± 2.65	14.15 ± 2.89
Opn-Cls	Opn-Cls	19.15 ± 3.77	19.47 ± 3.77	16.04 ± 2.97	16.43 ± 3.32
Pro-Sup	& Pro-Sup	16.35 ± 6.03	12.54 ± 4.02	11.33 ± 2.58	16.92 ± 4.24
Opn-Cls	Opn-Cls	19.91 ± 5.72	19.98 ± 5.73	16.69 ± 2.54	17.02 ± 2.63

Cross Corr Max, ρ_{max}		**Non-Dominant MVF**		**Dominant MVF**	
Tracking side		Dominant	Non-dominant	Dominant	Non-dominant
Rad-Uln		0.73 ± 0.14	0.85 ± 0.04	0.83 ± 0.07	0.67 ± 0.17
Pro-Sup		0.67 ± 0.20	0.79 ± 0.10	0.79 ± 0.14	0.69 ± 0.16
Opn-Cls		0.71 ± 0.10	0.74 ± 0.07	0.75 ± 0.08	0.68 ± 0.10
Rad-Uln	& Rad-Uln	0.66 ± 0.10	0.74 ± 0.11	0.74 ± 0.17	0.60 ± 0.18
Opn-Cls	Opn-Cls	0.40 ± 0.13	0.43 ± 0.12	0.47 ± 0.16	0.36 ± 0.15
Pro-Sup	& Pro-Sup	0.67 ± 0.15	0.73 ± 0.12	0.75 ± 0.12	0.54 ± 0.17
Opn-Cls	Opn-Cls	0.37 ± 0.12	0.41 ± 0.09	0.41 ± 0.16	0.32 ± 0.14

Latency （ms）		Non-Dominant MVF		Dominant MVF	
Tracking side		Dominant	Non-dominant	Dominant	Non-dominant
Rad-Uln		277.71 ± 52.60	292.97 ± 53.59	291.95 ± 53.71	321.45 ± 78.65
Pro-Sup		348.92 ± 144.10	348.92 ± 98.00	355.02 ± 91.56	381.57 ± 90.92
Opn-Cls		352.99 ± 88.25	367.22 ± 101.66	344.85 ± 66.07	358.07 ± 73.30
Rad-Uln &	Rad-Uln	269.57 ± 29.19	297.04 ± 40.43	289.92 ± 84.75	344.85 ± 115.82
Opn-Cls	Opn-Cls	523.89 ± 94.33	522.87 ± 120.04	498.45 ± 103.56	519.82 ± 120.22
Pro-Sup &	Pro-Sup	324.50 ± 51.12	364.18 ± 49.06	345.87 ± 85.90	442.50 ± 200.39
Opn-Cls	Opn-Cls	527.95 ± 94.14	535.07 ± 92.21	524.90 ± 119.72	533.04 ± 136.56

Table S4. Plot values for Fig. 7, one-DoF probability density function (PDF) estimate summary results for matching dominant/non-dominant forces/moments and target to ideal uniform distribution (mean ± standard deviation errors).

RMSE	Non-Dominant MVF (Error %)			Dominant MVF (Error %)		
Tracking side	Dominant	Non-dominant	Target	Dominant	Non-dominant	Target
Rad-Uln	1.13 ± 0.30	0.85 ± 0.25	0.40 ± 0.05	0.99 ± 0.30	1.17 ± 0.40	0.43 ± 0.09
Pro-Sup	1.23 ± 0.40	0.89 ± 0.25	0.44 ± 0.08	0.95 ± 0.37	1.15 ± 0.28	0.42± 0.06
Opn-Cls	1.18 ± 0.28	1.19 ± 0.30	0.42 ± 0.11	1.30 ± 0.40	1.23 ± 0.47	0.43 ± 0.12

Table S5. Plot values for Fig. 8, two-DoF probability density function (PDF) estimate summary results for matching dominant/non-dominant forces/moments and target to ideal uniform distribution (mean ± standard deviation errors).

RMSE		Non-Dominant MVF (Error %)			Dominant MVF (Error %)		
Tracking side		Dominant	Non-dominant	Target	Dominant	Non-dominant	Target
Rad-Uln & Opn-Cls							
	Rad-Uln	1.22 ± 0.22	1.03 ± 0.28	0.40 ± 0.08	1.12 ± 0.31	1.33 ± 0.59	0.37 ± 0.06
	Opn-Cls	1.10 ± 0.21	1.05 ± 0.31	0.44 ± 0.08	1.10 ± 0.35	1.05 ± 0.55	0.39 ± 0.08
Pro-Sup & Opn-Cls							
	Pro-Sup	1.44 ± 0.45	1.50 ± 0.67	0.41 ± 0.08	1.49 ± 0.34	1.83 ± 0.84	0.40 ± 0.06
	Opn-Cls	1.49 ± 0.64	1.56 ± 0.66	0.41 ± 0.06	1.44 ± 0.37	1.74 ± 0.65	0.40 ± 0.08

Chapter 4: Comparison of EMG-Force Calibration Protocols for Myoelectric Control of Prostheses

This chapter has been published as: Z. Zhu, J. Li, C. Dai, B. McDonald, T. Farrell, X. Huang, E. A. Clancy, "*Comparison of EMG-Force Calibration Protocols for Myoelectric Control of Prostheses*", 2019 *IEEE Signal Processing in Medicine and Biology Symposium (SPMB)*, 7 Dec. 2019. Color Vsersions of one or more of the figures in this paper are available online at https://ieeexplore.ieee.org/abstract/document/09037835.

The surface electromyogram (EMG) is used as a control source for limb prostheses. When developing hand-wrist prostheses control schemes with able-bodied subjects, it is common to relate forearm EMG to hand-wrist forces/moments using supervised models. However, subjects with unilateral limb absence cannot produce such forces. Thus, we contrasted use of "output" alternatives from the force generated by the sound side in "mirror" movements (Muceli, Jiang et al. 2010, Nielsen, Holmgaard et al. 2011), or directly using a target followed with their limb-absent side (Ameri, Kamavuako et al. 2014, Ameri, Scheme et al. 2014).

Data were collected at 2048 Hz from 12 able-bodied subjects (6 male, 6 female). Bipolar EMG electrodes (16) were secured around their dominant distal forearm. Each wrist was secured to a separate three-axis load cell to measure wrist force/moment. Each hand was secured to a separate one-DoF load cell to measure handgrip force. Subjects performed constant-posture, 1-degree-of-freedom (DoF) random force target [0.75 Hz, white, bandlimited, 40 s, –30 to 30% maximum voluntary contraction (MVC)] tracking trials of: a) wrist radial-ulnar deviation (Rad-Uln), b) wrist pronation-supination (Pro-Sup) or c) hand open-close (Opn-Cls). Different modes of real-time visual feedback were studied: 1) subjects tracked the target only using real-time force feedback from their dominant limb (EMG-ForceDom); 2) subjects tracked the target with only their dominant limb, with no feedback provided (EMG-TargetDom); 3) subjects tracked a pair of symmetrical targets (one per side), with force feedback from the non-dominant side shown in both displays (mirror visual feedback: EMG-ForceND); 4) EMG data from the prior mode was re-used off-line and related to the target (EMG-TargetMVF). Each trial combination (a–c vs. 1–3) was repeated twice.

Raw EMG were highpass filtered (5th-order Butterworth, fc=15 Hz) to remove motion artifact, notch filtered at the power-line frequency (2nd-order IIR at 60 Hz, notch bandwidth of 1 Hz) and rectified. Hand/wrist force/moment was normalized to MVC. Then, all signals were decimated (lowpass filter: fc=16 Hz, Chebyshev Type I, 9th-order, 0.05 dB peak-to-peak passband ripple) to 40.96 Hz. Since feedback-based

force tracking incurs a time latency of up to approximately 200–300 ms, this alignment latency (k samples) was estimated by maximum cross-correlation between Force-Force (or Force-Target). Then, EMG-Force/Target was modeled as below, where Q=20 was the order of the linear dynamic model, E=16 was the number of electrodes, m was the decimated sample index, and EMGσ were the processed EMG:

$$Force[m] = \sum_{q=0}^{Q} \sum_{e=1}^{E} c_{e,q} EMG\sigma_e[m-q-k].$$

The first trial trained coefficients via the linear least squares pseudo-inverse method (Tol = 0.1), and the second trial tested RMSE between estimated and measured force/target. Then the two trials were flipped for cross-validation and their average was reported.

A two-way repeated measure analysis of variance (RANOVA) was computed with the factors of feedback (EMG-Force$_{Dom}$, EMG-Force$_{ND}$, EMG-Target$_{Dom}$, EMG-Target$_{MVF}$) and DoF (Rad-Uln, Pro-Sup, Opn-Cls). Only feedback was significant ($F(3,33) = 14.9$, $p < 10^{-3}$), without interaction. Post hoc pairwise comparison t-tests with Bonferroni correction found that conventional EMG-Force$_{Dom}$ had significantly lower RMSE than EMG-Target$_{Dom}$ ($p = 0.008$) and EMG-Target$_{MVF}$ ($p = 0.001$); and EMG-Force$_{ND}$ had significantly lower RMSE than EMG-Target$_{MVF}$ ($p < 10^{-3}$).

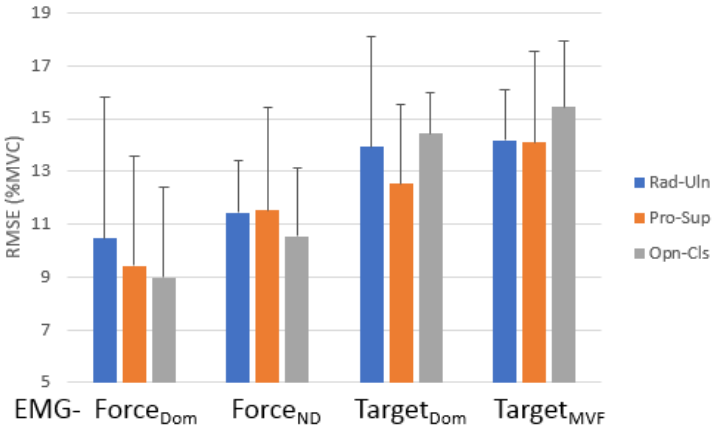

Fig. 2.7. Example 2-DoF EMG-force time-series results, limb-absent subject 21, Rad-Uln & Opn-Cls when using (a) no feedback, (b) contralateral feedback and (c) mirror feedback. EMG acquired from the affected side. Both true force and EMG-estimated force are shown in each plot.

In this experiment, able-bodied subjects simulated limb-absent conditions. Using the contralateral limb for force feedback had similar performance as using conventional ipsilateral limb feedback, and much better performance than using no feedback. Mirror movement did not enhance target estimation. Symmetry is an intrinsic human characteristic (Swinnen 2002), but target tracking is a highly demanding task which needs practice. However, for limb-absent subjects, either congenital or traumatic amputation leads to amyotrophy or neuron damage and may influence the symmetric movement. Thus, further testing on limb-absent subjects is necessary to evaluate the performance of different EMG-force calibration protocols.

Chapter 5: Myoelectric Control Performance of Two Degrees of Freedom Hand-Wrist Prostheses by Able-Bodied and Limb-Absent Subjects

This chapter is in development as a journal paper submission. Ziling Zhu, Jianan Li, William J. Boyd, Carlos Martinez-Luna, Chenyun Dai, Haopeng Wang, He Wang, Xinming Huang, Todd R. Farrell, Edward A. Clancy.

***Abstract*—Recent research has advanced two degree of freedom (DoF), simultaneous, independent and proportional control of hand-wrist prostheses using surface electromyogram signals from remnant muscles as the control input. We evaluated two such controllers, along with conventional, sequential two-site control with co-contraction mode switching (SeqCon), in box-block, refined clothespin and door-knob tasks, on 10 able-bodied and 4 limb-absent subjects. Subjects operated a commercial hand and wrist using a bypass harness. One 2-DoF controller (DirCon) related the intuitive hand actions of open-close and pronation-supination to the associated prosthesis hand-wrist actions, respectively. The other (MapCon) mapped more distinct actions of wrist flexion-extension and ulnar-radial deviation. Both 2-DoF controllers were calibrated from the same 90 s set of calibration contractions. SeqCon performed best in the predominantly 1-DoF box-block task (>20 blocks/minute vs. 8–18 blocks/minute, on average), but only statistically better than MapCon. In this task, SeqCon likely benefited from an ability to easily focus on 1-DoF by not co-contracting mode switching. The remaining two tasks require 2-DoFs, and both 2-DoF controllers each performed better (factor of 2–4) than SeqCon. We also compared the use of 12 vs. 6 EMG electrodes as inputs, finding no statistical difference. Overall, we provide further evidence of the benefits of regression-based EMG prosthesis control of 2-DoFs in the hand-wrist.**

***Index Terms*— Prosthesis control, EMG-force, EMG signal processing, Electromyogram, Myoelectric control.**

5.1 Introduction

More than two million people live with limb absence in the U.S., and this number increases by an average 185,000 each year (Dillingham, Pezzin et al. 2002, McGimpsey and Bradford 2008, Force and Coalition 2012). Trans-radial amputations make up 60% of total wrist and hand amputations, and documented rates of prosthesis use vary from 27–56% for upper-limb amputation (Ziegler-Graham, MacKenzie et al. 2008). The high demand for prostheses, expected to increase by at least 47% by the year 2020, has brought more support from government and growth of the market (Neilson 2002).

While laboratory-based research on electromyogram (EMG) control has generated new strategies based on machine learning algorithms, most commercial prostheses still use simple two-site control schemes that have been available for decades (Sherman 1964). Typical myoelectric prosthetic sockets are designed with two bipolar electrodes, one each located over flexor and extensor muscles, to control one degree-of-freedom (DoF) prosthetic hand open and close (Opn-Cls), respectively. Kestner (Kestner 2006) found need for a prosthetic wrist, as the fixed angle of a prosthetic hand is not compatible with all daily tasks (e.g., holding flatware for eating, a bottle for drinking). Although some advanced prostheses have a wrist rotator and users can co-contract their muscles to switch between hand open-close and wrist pronation-supination (Pro-Sup) (Lovely 2004, Fougner, Stavdahl et al. 2012), users mostly employ their body and arm/shoulder movement for compensation instead (MacPhee 2007, Ross 2007, Bertels, Schmalz et al. 2009). Prosthesis mode switching, a.k.a. sequential 2-DoF control, allows users to rotate the wrist with a complex and time-consuming approach (Muzumdar 2004). Performance of this technique is highly influenced by a user's residual limb condition, since muscle contraction imbalance or neuron damage impede co-contraction; and users need a long period of time to master this skill, but easily fatigue (Popović 2003).

Features extracted from myoelectric signals train models to estimate users' intent. Regression modeling is one learning approach used to realize simultaneous, independent and proportional multi-DoF control (Parker, Englehart et al. 2006, Jiang, Englehart et al. 2009, Clancy, Liu et al. 2012, Hahne, Biessmann et al. 2014, Liu, Liu et al. 2015). Compared with classification models, e.g. linear discriminant analysis (Englehart and Hudgins 2003, Spanias, Perreault et al. 2015), support vector machines (Alkan and Günay 2012, Al-Timemy, Bugmann et al. 2013) or multi-layer perceptrons (Kelly, Parker et al. 1990), regression estimates continuous outputs to more naturally mimic human movement. Regression models have been found to be more robust to some unpredictable small variations in EMG signals, such as fatigue or poor contact of electrodes, and may generate better performance during untrained conditions compared to classification models (Hahne, Markovic et al. 2017).

Most myoelectric control users can easily operate hand open-close via the two-site conventional approach. But for wrist rotation—although most limb-absent users can easily rotate their residual limb repeatedly—the pronator teres (a wrist rotator) is a deep muscle difficult to record using surface EMG (Gilroy, MacPherson et al. 2008, p. 328–336), and electrodes often shift during forearm rotation. These factors challenge the usability of surface EMG signals. As an alternative, researchers assessed offline other wrist motions of extension-flexion (Ext-Flx) and Radial-Ulnar deviation (Rad-Uln), especially since the EMG signal during Rad-Uln has demonstrably distinct patterns compared with the other wrist motions (Rojas-Martínez, Mañanas et al. 2012). These results provide a potential 2-DoF control strategy by a corresponding "motion" mapping/translation.

Some prior lab-based prostheses testing of multiple-DoF control schemes used a large number of electrodes, or matrix electrodes. Such systems are not practical in current commercial prostheses due to cost and issues of electrode shorting/lift-off. Some researchers found that at least 4 electrodes were necessary to realize 2-DoF control, with improvement occurring if the number of electrodes increased (Parker, Englehart et al. 2006, Peerdeman, Boere et al. 2011, Dai, Zhu et al. 2019). A balance can be found between economic benefits and product quality if an optimal number of electrodes and their location were decided (Clancy, Martinez-Luna et al. 2017, Dai, Zhu et al. 2019).

Recent laboratory work studied myoelectric control using a 2-D virtual target tracing task, assessing performance via path efficiency, completion time, and attempt-ratio (Igual, Igual et al. 2019). Others have studied the influence of training protocol (Dyson, Dupan et al. 2020), or of using modeling techniques of myoelectric representation learning (MRL) (Olsson, Malešević et al. 2021), principle component analysis (PCA) (Dyson, Dupan et al. 2020), and frequency division technique (FDT) (Pradhan, Kuruganti et al. 2020). Real 2-DoF prosthesis control during either laboratory or home study found a potential advantage of regression-based controllers (Hahne, Schweisfurth et al. 2018) and classification-based (Amsuess, Goebel et al. 2014, Kuiken, Miller et al. 2016) in multi-DoF control compared with conventional control strategies, but the aggregate sample size available in the literature remains small.

In this paper, we assessed regression-based simultaneous, independent and proportional 2-DoF (hand-wrist) myoelectric prosthesis control on both able-bodied and limb-absent subjects, comparing three control strategies—Opn-Cls & Pro-Sup direct control, a new Ext-Flx & Rad-Uln mapping control with translation, and conventional two-site sequential control. Six or twelve electrodes were tested on a real prosthesis to investigate the minimum number of electrodes feasible on commercial prostheses. Bypass brackets were designed separately for able-bodied and limb-absent subjects to carry a hand-wrist prosthesis adjacent to the forearm/residual limb. These control strategies were tested with different standard physical tasks (box-block,

refined clothespin relocation 2-DoF sequential task and door-knob 2-DoF simultaneous task). Six vs. twelve optimally selected electrodes were tested to explore the minimum number of necessary electrodes for able-bodied subjects. Based on these results, more targeted tasks were conducted on limb-absent subjects.

5.2 Methods

5.2.1 Experimental Apparatus

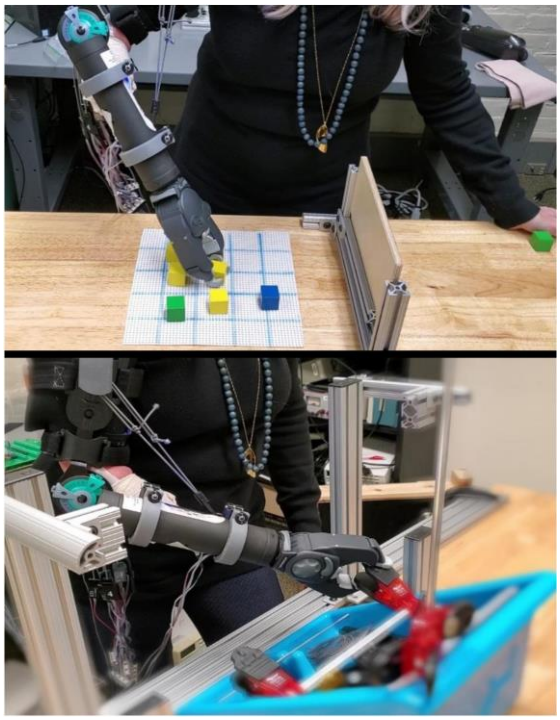

Fig. 5.1. Experimental apparatus for box-block (top) and clothes pin (bottom) tasks, limb-absent subject. The subject was asked to wear a bypass bracket that attached a hand-wrist prosthesis. The forearm could move freely.

Experimental data were collected from 10 able-bodied (5 male, 5 female; aged 18–45 years) and 4 trans-radial limb-absent (3 male, 1 female; aged 39–65 years) subjects at Worcester Polytechnic Institute (WPI), as approved by the WPI Institutional Review Board (IRB Protocol 17-155). Able-bodied subjects had no physical limitations of their dominant forearm muscles. Limb-absent subjects had ≥5 cm residual limb length with functional muscle contraction and prior experience with myoelectrical-controlled prostheses. Subjects provided written informed consent.

Subjects stood at the experimental table, adjusted to hip height (Fig. 5.1). Sixteen bipolar EMG electrodes were secured on the proximal forearm, equally spaced about the forearm's circumference. For able-bodied subjects, electrodes were secured on the dominant side with the midpoint of the bipolar contacts placed 5 cm distal to the elbow crease. For limb-absent subjects, electrodes were secured on the affected side at the level corresponding to that of their own prosthesis. Each bipolar electrode consisted of 5 mm diameter, stainless steel, hemispherical contacts separated 1 cm edge-to-edge, oriented along the forearm's long axis. Each EMG signal was differentially amplified (Liberating Technologies, Inc. BE328 amplifier; 30–500 Hz pass band, CMRR>100 dB over the pass band) and provided selectable gain. All EMG channels were sampled at 2000 Hz (16-bit resolution).

Then a 3D printed bypass bracket was strapped to the shoulder and arm (Fig. 5.1). A wrist rotator (Fillauer Motion Control Standard Wrist Rotator, maximum speed 28 rpm, highest torque 15 in-lb, input: 0–5 V) and hand (Ottobock System Electric Greifer DMC Plus, proportional speed 8–200 mm/sec, proportional gripping force 0–160 N, two inputs: 0–5 V) extended from the bypass, providing wrist Pro-Sup and hand

Opn-Cls, respectively. The electrodes (input) and the prosthesis (output) were connected to a PC-based prosthesis control system programed in MATLAB (The MathWorks, Natick, MA, USA) (Boyd 2018).

5.2.2 Prostheses Control System

1) Control Sources: Subjects compared two regression based 2-DoF simultaneous, independent and proportional velocity control algorithms and conventional two-site velocity control. Limb-absent subjects controlled the prostheses by attempting to move their phantom limb. The control algorithms were as follows. 1) Direct control (DirCon) in which subjects' Opn-Cls controlled Greifer Opn-Cls, and subjects' Pro-Sup controlled prosthetic wrist rotation. 2) Direct control with mapping/translation (MapCon) in which subjects' wrist Ext-Flx controlled Greifer Opn-Cls (Ext corresponded to Opn), and subjects' Rad-Uln controlled prosthetic wrist rotation (Rad corresponded to pronation). Subjects were permitted to invert either/both of these mappings. 3) Sequential control (SeqCon) in which subjects controlled either Opn-Cls or Pro-Sup, then switched between them by triggering a co-contraction EMG signal. Co-contraction was defined as a simultaneous contraction of both forearm EMGσ values above set thresholds for a defined time duration (Kelso 1982, Gribble, Mullin et al. 2003). Each respective threshold was set between the EMG values triggered during a maximum co-contraction and normal hand-wrist tasks, as selected by the subject. The time duration was set between 30–100 ms, again selected by subject preference.

2) Control Calibration and Thresholding: For calibration of DirCon and MapCon (Fig. 5.2), subjects performed a 90 s calibration consisting of 10-s of rest and eight 10-s, contiguous constant-posture constant-force contraction segments (four 1-DoF and four 2-DoF). Subjects were instructed to maintain a contraction target effort of 30% (without feedback). For DirCon, the contraction sequence was: Cls, Opn, Sup, Pro, Cls+Sup, Cls+Pro, Opn+Sup, and Opn+Pro. For MapCon, the contraction sequence was: Flx, Ext, Uln, Rad, Flx+Uln, Flx+Rad, Ext+Uln, and Ext+Rad. Raw EMG signals from all channels were digitally notch filtered (second-order IIR filter at 60 Hz, notch bandwidth of 1 Hz), highpass filtered to attenuate motion artifact (f_c=15 Hz, fifth-order Butterworth filter), rectified, lowpass filtered (f_c=16 Hz; Chebyshev Type I filter, ninth-order, 0.05 dB peak-to-peak passband ripple) and downsampled from 2000 Hz to 100 Hz. Then, a critically

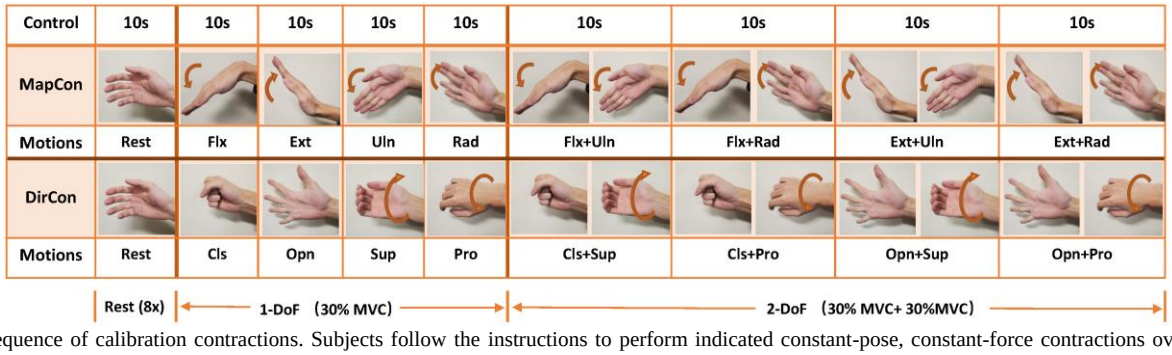

Fig. 5.2. Sequence of calibration contractions. Subjects follow the instructions to perform indicated constant-pose, constant-force contractions over 90 s. The recording was used for coefficient calculation and calibration quality assessment.

damped lowpass filter (f_c=1 Hz, second-order) (Robertson and Dowling 2003) was applied to further smooth the signal and estimate EMG standard deviation (EMGσ). The first and last second of each 10 s segment was removed to avoid filter and movement transients. Then, each EMGσ from the resting segment (weighted eight times) and the eight contraction segments were used as inputs to a regression-based (2-output) static EMGσ-force model (Clancy, Martinez-Luna et al. 2017). A force of zero was assigned as the output target for unused DoFs during each segment. Fit coefficients were estimated via the linear least squares pseudo-inverse method, in which singular values of the design matrix were removed if the ratio of that singular value to the largest was less than a tolerance value ($Tol = 0.01$, based on previous study) (Clancy, Liu et al. 2012, Dai, Bardizbanian et al. 2017). Backward stepwise selection (Clancy, Martinez-Luna et al. 2017, Dai, Zhu et al. 2019) was utilized for optimal selection of either 6 or 12 electrodes. In this manner, only the best channels yielding the lowest RMSE (between EMG-force and target force) were selected and their gains were calculated for prostheses control. In addition, this RMSE provided an assessment of the calibration quality.

During experimental trials using DirCon and MapCon, EMG-force was computed in real-time, then two thresholding methods were applied. First, a resting threshold was applied to each direction of the two individual DoFs (total of four thresholds) to minimize the impact from noise and unintentional EMGσ signals. Second, a fixed-ratio co-activation thresholding method was applied to attenuate the risk of crosstalk from another DoF (Fig. 5.3). When the ratio of the larger force (in %MVC) to the smaller force (from the two DoFs) was less than a threshold, only the DoF with the larger force was actuated. If the two forces are drawn in the *x*-*y* plane, a default threshold angle of α=25 degrees (Fougner, Stavdahl et al. 2014) was used. This angle could be changed during setup as desired by the subject.

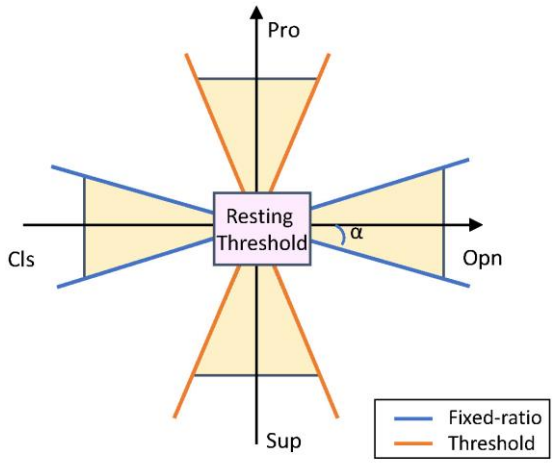

Fig. 5.3. Calibration examples for a) MapCon and b) DirCon. Dashed red line segments show target force level. Wavy blue lines show model-estimated force.

For SeqCon, the two channels which produced the largest EMGσ when subjects performed Ext and Flx calibration, respectively, were chosen. Each channel gain was set to correspond to 30% MVC. For limb-absent subjects, the channel selection was also under the consideration of their own two-site prostheses electrode locations. The estimated force was calculated as the sum of the forces estimated by each channel. A resting threshold was applied to each channel to reduce the influence of noise and small unintentional activation. For switching between the 2 DoFs, a fixed window size (30–100 ms) and a co-contraction

threshold were set to detect a co-contraction. All the channels and coefficients were manually calibrated until subjects could easily control the prostheses and trigger co-contraction.

3) Hardware Control: The estimated hand and wrist force levels, in %MVC, were linearly mapped to hand and wrist velocity (speed and direction), with 50% MVC in each corresponding to maximum speed. Built-in hardware thresholds were essentially disabled by matching the software thresholds to them. Thus, all thresholding was set in our custom software.

5.2.3 Experimental Protocol

All tasks were free posture with the subject standing (Fig. 5.1). To prevent cumulative muscle fatigue, at least two minutes rest after calibration and one minute rest between trials were provided. All limb-absent subjects were offered mirror-box training before the trials to help rebuild their phantom limb control sensation.

To assess controller performance, three tasks were chosen from widely-used outcome measures described in the literature. 1) The box-block task (Mathiowetz, Volland et al. 1985) was a 1-DoF assessment mainly testing hand Opn-Cls. Subjects grasp (hand Cls) a block and then drop it (hand Opn) after traversing over a partition. They return back over the partition and repeat. We did not lock the prostheses into 1-DoF control during this task. The number of transferred blocks in 60 s and number of drops were measured in each trial. 2) A refined clothespin relocation task (Hussaini and Kyberd 2017) was a sequential 2-DoF assessment. Subjects performed hand Cls to grasp a clothespin (2 lbs. resistance) from a horizontal rod, rotate the clothespin 90º (wrist Pro or Sup), then place and release (hand Opn) the clothespin onto a vertical rod. Once complete, subjects rotated their wrist back to its original orientation and attempted to relocate another clothespin. Subjects were allowed to use arm or body movement for compensation. If the clothespin dropped, subjects moved on to the next clothespin. The time required to complete three successful moves (maximum of 120 s) and number of drops were measured in each trial. 3) A doorknob task was a simultaneous 2-DoF assessment. Opening a door is a common but important task that most people face every day. Compared with the SHAP door-handle test (Light, Chappell et al. 2002), our task used a round knob which requires cooperation of both the wrist and hand—more appropriate for 2-DoF assessment. During each task cycle, subjects grasped the round knob of the door (hand Cls), rotated the knob (wrist Pro or Sup) while maintaining hand Cls, pulled the door open, and then released the knob (hand Opn). Subjects then shut to door to ready for the next trial. The time required to complete three successful door openings (maximum of 120 s) was measured in each trial.

Three control strategies (DirCon, MapCon, SeqCon) were tested on all subjects. Subjects initially performed calibration, then used all 16 electrodes to test all motions and their combinations. Thresholds were adjusted, based on their feedback, to enhance control robustness and accuracy. If it was still hard to control

the prostheses, subjects were offered at most three calibrations and chose the best one for the tasks. Then for control tasks, able-bodied subjects used DirCon and MapCon with either 6 or 12 electrodes. Limb-absent subjects only used 6 electrodes for DirCon and MapCon, to shorten the experiment length to prevent fatigue. All subjects used SeqCon with 2 electrodes. The three control strategies, number of electrodes used (only varied for able-bodied subjects) and three tasks were randomized during the experiment. Subjects were blinded to the number of electrodes in use. Three trials of data were collected for each condition.

5.2.4 Statistics

For able-bodied subjects, we separately averaged the number of box-block transfers, time per clothespin transfer, and time per door open and close cycle across the three trials. Since these data satisfied the normality assumption, a repeated measures analysis of variance (RANOVA) and *post hoc* paired t-tests with Bonferroni correction (significance level $p = 0.05$) were used to test performance differences. Prior to RANOVA, the degree of sphericity (ε) was used to adjust the degrees of freedom by either the method of Greenhouse-Geisser ($\varepsilon < 0.75$) or Hyunh-Feldt ($0.75 < \varepsilon < 1$). For limb-absent subjects, we separately conducted ANOVA and *post hoc* t-tests with Bonferroni correction for each subject without the averaging (three trials per condition), due to the limited number of subjects. For the number of drops per trial in box-block and clothespin tasks, if the data did not satisfy the normality assumption, a non-parametric Friedman test was used to test performance differences, rather than a RANOVA.

5.3 Results

5.3.1 Calibration Quality Assessment

Fig. 5.4 shows example target force levels and EMG-estimated forces for a set of calibration trials. Fig. 5.5 summarizes across subjects the RMSE between the target %MVC and that estimated from EMGσ of each calibration segment, separately for able-bodied and limb-absent subjects, and number of electrodes retained

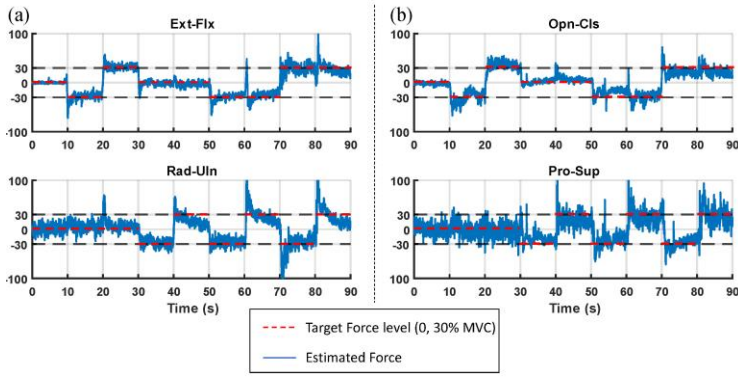

Fig. 5.4. Thresholding methods for 2-DoF control including resting (inner square) and fixed-ratio thresholding (blue and red lines emanating from inner square). Based on method of Fougner *et al.* (Fougner, Stavdahl et al. 2014).

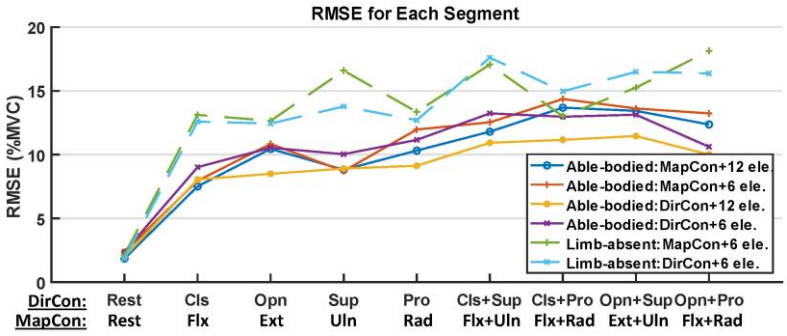

Fig. 5.5. Results of calibration quality assessment. The RMSE for each segment under different control methods (MapCon, DirCon) and number of electrodes (6 or 12) for both able-bodied and limb-absent subjects.

after backward stepwise selection. Both hand and wrist errors always contributed to the RMSE, even during 1-DoF tasks. This assessment describes how well subjects can produce the desired calibration contraction, which forms the basis of the 2-DoF control algorithms. For able-bodied subjects, a three-way RANOVA was computed with factors: control strategy (DirCon, MapCon), number of electr odes (6, 12) and calibration segment (9 options). A significant interaction was found between control strategy and number of electrodes [$\mathrm{F}(1,9) = 16.0, p = 0.002$], while calibration segment was significant [$\mathrm{F}(8,72) = 43.2, p < 10^{-6}$]. *Post hoc* comparison for the interaction found that for both DirCon and MapCon, 12 electrodes had lower RMSE than 6 electrodes ($p \leq 10^{-4}$). For segments, rest always had lower RMSE than all other segments ($p < 10^{-4}$), Cls / Flx exhibited lower RMSE than Pro / Rad ($p = 0.005$), Cls+Sup/ Flx+Uln ($p = 0.003$), Cls+Pro /Flx+Rad ($p = 0.006$) and Opn+Sup / Ext+Rad ($p = 10^{-4}$); Opn /Ext had lower RMSE than Opn+Sup /Ext+Rad ($p = 0.004$); and Sup / Uln had lower RMSE than Cls+Pro / Flx+Rad ($p = 0.012$) and Opn+Sup / Ext+Rad ($p = 0.026$).

For limb-absent subjects, a two-way RANOVA with factors control strategy and segment found only segments was significant [$F(1.5,4.5) = 19.1,\ p_{GG} = 0.007$]. Post hoc comparison only found rest motion had lower RMSE than all others ($p < 0.04$).

5.3.2 Box-block Task

For able-bodied subjects (summary results shown in Fig. 5.6), the number of transfers in one minute was compared between five different control strategies (MapCon+12 electrodes, MapCon+6 electrodes, DirCon+12 electrodes, DirCon+6 electrodes, SeqCon), where more transfers represented better performance. A one-way RANOVA found significance [$\mathrm{F}(4,36) = 9.8, p = 10^{-5}$]. *Post hoc* comparison only found that SeqCon transferred significantly more blocks than MapCon (a 30–68% improvement, on average) with both 12 and 6 electrodes ($p < 0.023$). Note that while using SeqCon on this task, mode switching was not disabled. Nonetheless, the task was completed predominantly using only the hand DoF, and body/shoulder movement. Furthermore, a Friedman test on number of drops per trial found no significant difference between the five control strategies.

For limb-absent subjects (summary results for each subject shown in Fig. 5.7, and for the ensemble in Fig. 5.6), the number of transfers in one minute was compared between three different control strategies

(MapCon+6 electrodes, DirCon+6 electrodes, SeqCon). A one-way RANOVA was calculated for each subject, with *post hoc* comparison made when a significant difference was found. For three of the four subjects, the RANOVA was significant $[F(2,6) > 27, p \leq 0.001]$, with *post hoc* comparison showing that SeqCon transferred more blocks (by a factor of 2–4) than either of MapCon or DirCon ($p < 0.038$). For two of the associated *post hoc* evaluations, DirCon also transferred more blocks than MapCon ($p < 0.038$). Furthermore, a Friedman test on number of drops per trial among all subjects found no significant difference between the three control strategies.

Additionally, we compared able-bodied to limb-absent results via a one-way RANOVA using three control strategies as the factor (MapCon+6 electrodes, DirCon+6 electrodes, SeqCon). This comparison found no statistical difference $[F(1,12) = 3.3, p = 0.095]$.

5.3.3 Refined Clothespin Relocation Task

For able-bodied subjects (Fig. 5.6), the time per move was compared between the five different control strategies, where shorter time represented better performance. A one-way RANOVA found significance $[F(2.2, 35.6) = 7.2,\ p_{GG} = 0.004]$. *Post hoc* comparison only found that SeqCon took significantly longer time (factor of 2) than MapCon with 12 electrodes ($p = 0.0002$) and DirCon with 6 electrodes ($p = 10^{-5}$). Furthermore, a Friedman test on number of drops per successful move found no significant difference between the five different control strategies.

For limb-absent subjects (Fig. 5.7), a one-way RANOVA was computed between the three different control strategies, with *post hoc* comparison made when a significant difference was found. For two of the four subjects, the RANOVA was significant $[F(2,6) = 11, p \leq 0.009]$, with *post hoc* comparison in both showing that SeqCon required more time (poor performance) than DirCon ($p \leq 0.01$). For one of these subjects, SeqCon also required more time than MapCon ($p = 0.001$). Furthermore, a Friedman test on number of drops per successful move also found no significant difference.

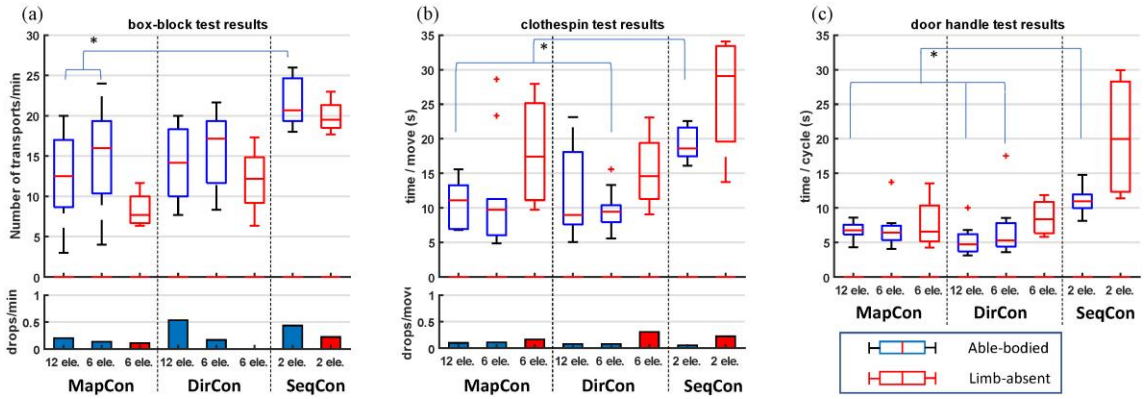

Fig. 5.6. Boxplot results for a) box-block task (number of transfers per minute, drops per minute), b) clothespin task (time per move, drops per successful move), c) door-knob task (time per open/close cycle).

Additionally, we compared able-bodied to limb-absent results via a one-way RANOVA using three control strategies as the factor (MapCon+6 electrodes, DirCon+6 electrodes, SeqCon). This comparison was significant $[\mathrm{F}(1,12) = 6.1, p = 0.03]$ and *post hoc* comparison found that limb-absent subjects used significantly more time to complete the tasks than able-bodied subjects ($p = 0.03$).

5.3.4 Door-Knob Task

For able-bodied subjects (Fig. 5.6), the time per door-open-close cycle was compared between the five different control strategies, where shorter time represented better performance. A one-way RANOVA found significance $[\mathrm{F}(2.0, 18.4) = 10.4,\ p_{GG} = 0.001]$. *Post hoc* comparison found that SeqCon took significantly longer time (factor of 2–4) than each of DirCon with 12/6 electrodes and MapCon with 12 electrodes ($p < 0.011$).

For limb-absent subjects (Fig. 5.7), a one-way RANOVA was computed between the three different control strategies for each subject, with *post hoc* comparison made when a significant difference was found. For two of the four subjects, the RANOVA was significant $[\mathrm{F}(2,6) > 24, p \leq 0.001]$, with *post hoc* comparison finding that SeqCon required more time than either of MapCon ($p \leq 0.003$) or DirCon ($p \leq 0.003$). For one other subject, the RANOVA was significant $[\mathrm{F}(2,6) = 20.72, p = 0.002]$, with *post hoc* comparison only finding that SeqCon and DirCon each required more time than MapCon ($p \leq 0.009$).

Additionally, we compared able-bodied to limb-absent results via a one-way RANOVA using three control strategies as the factor (MapCon+6 electrodes, DirCon+6 electrodes, SeqCon), finding a significant two-way interaction $[\mathrm{F}(2,24) = 3.8, p = 0.037]$. *Post hoc* comparison found that limb-absent subject used significantly more time to complete the tasks than able-bodied subjects only using SeqCon ($p = 0.008$).

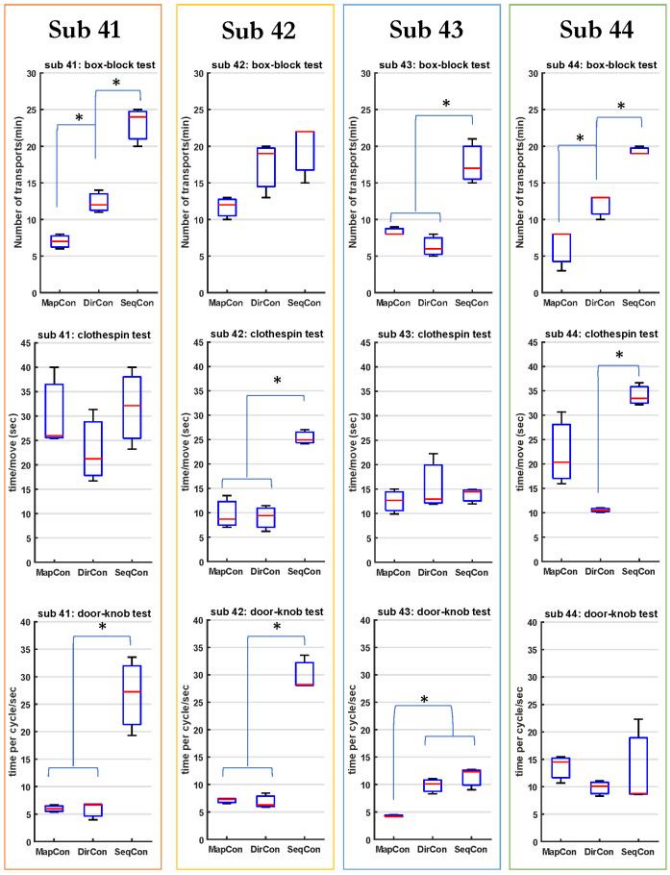

Fig. 5.7. Boxplot results for each limb-absent subject for the box-block task (top row), clothespin task (middle row), and door-knob task (bottom row).

5.4 Discussion

This research assessed the performance of regression-based 2-DoF simultaneous, independent and proportional myoelectric prosthesis control with different control strategies (DirCon, MapCon) and number of electrodes (6, 12), as compared to conventional sequential control. Evaluation was tested on standard box-block task (1-DoF assessment), refined clothespin relocation task (sequential 2-DoF assessment) and a door-knob task (simultaneous 2-DoF assessment). The overall results showed no significant difference between 6 and 12 electrodes. When tested on limb-absent subjects with only 6 electrodes, all subjects successfully controlled the prostheses to complete the tasks. Both DirCon and MapCon exhibited good performance, indicating they could be potential approaches for 2-DoF control.

5.4.1 Calibration Quality Assessment

In this study, subjects were offered up to three calibration trials, and could self-select the "best" trial after briefly controlling the prosthesis. We presumed that a calibration with low EMG-force RMSE facilitates successful 2-DoF control, and vice versa. Hence, we assessed EMG-force performance of the accepted trial. The principal findings were that RMSE was lower during rest contractions and that 12 electrodes provided better EMG-force estimation than 6. The rest result is likely due to the fact that subjects can easily maintain a reproducible rest contraction, even in the absence of force feedback. But, it is difficult to accurately maintain a fixed active force level in the absence of feedback (Johansen-Berg and Matthews 2002, Noble, Eng et al. 2013), leading to poor tracking of the target force. One possible future solution is to feedback EMGσ in real time, which still avoids the need for measurement of force.

The finding that EMG-force improved with 12 electrodes vs. 6 has been noted previously (Clancy, Martinez-Luna et al. 2017, Dai, Zhu et al. 2019). Anecdotally, however, we found that subjects were not necessarily choosing the calibration trial with the lowest RMSE. In fact, some low RMSE calibration trials produced control models in which subjects could not actuate in one of the directions (i.e., no movement achievable). These calibrations were not selected. Nonetheless, a better metric might be the worst-case error out of the various control directions within a calibration trial, or some other metric that insures robust performance in all movement directions. In any case, further investigation is warranted to develop a self-assessment of calibration quality.

We calibrated using 10 s contractions at 30% MVC effort. It is likely that shorter durations would yield similar EMG-force performance, and thus be more convenient (Clancy and Hogan 1997, Bardizbanian, Zhu et al. 2020). Other effort levels might also be more appropriate, and could be investigated in the future. In fact, it is not clear that the same effort level should be prescribed for each movement direction. What is most important seems to be controllability. Additional gain (or gain reduction) could be applied to each movement

direction by the controller. Further, selection of the various noise floor thresholds also could strongly influence controller performance.

5.4.2 Sequential Control with Co-Contraction Trended Better for 1-DoF Task

Compared with regression-based 2-DoF MapCon, sequential control clearly performed better on the 1-DoF box-block task. And, SeqCon had higher number of transports per minute than 2-DoF DirCon, but this difference was not statistically significant. Because we didn't lock wrist rotation during this task, 2-DoF control had the risk of unwanted wrist rotation, after which subjects lost time realigning the wrist to grasp the next block. This problem didn't occur during 2-site SeqCon with limb-absent subjects, since all were familiar with this control and seldom triggered co-contraction inadvertently. Subjects reliably contracted flexor muscles, then extensor muscles to grasp and release blocks, respectively. Therefore, 2-site control still may be necessary in advanced prostheses controllers as an alternative scheme when only Opn-Cls (1-DoF) contractions are required.

5.4.3 Two-DoF Control was Best for 2-DoF Task

Sequential control is a complicated approach for 2-DoF control. None of our able-bodied subjects had prior experience using co-contraction for mode switching, thus required a long training time. One limb-absent subject had used a prosthesis with EMG co-contraction mode switching for several years, so achieved complete calibration in less than 5 minutes. The remaining limb-absent subjects struggled to learn the skill. Their imbalanced contraction between flexion and extension muscles made co-contraction difficult. EMGσ from one channel often increased faster than the another, thus the difference between the two channels caused prosthesis movement prior to triggering the desired co-contraction. Furthermore, frequent co-contraction is likely to cause fatigue.

Multi-DoF control is the trend for future prostheses development. Several virtual studies utilizing classification tests (Soares, Andrade et al. 2003, Xing, Yang et al. 2014) and/or target tracking (Igual, Igual et al. 2019, Zhu, Martinez-Luna et al. 2020) have shown that limb-absent subjects can control a 2-dimensional movement task with high precision. Using a physical prosthesis, all our limb-absent subjects had no difficulty realizing simultaneous, independent and proportional 2-DoF control, without prior experience doing so. Some prior research has found poorer performance when using Pro-Sup inputs, perhaps due to electrode shift over muscle during Pro-Sup rotation or because key active muscles (e.g., pronator teres) are found deeper within the forearm and may not have EMG that is as identifiable at the skin surface. In contrast, our results found that DirCon (Pro-Sup queued wrist rotation) was more often the best control strategy for both able-bodied and limb-absent subjects. MapCon, which used muscle actions from muscles that are physically more

distinct (Rad-Uln queued wrist rotation), also performed noticeably better than SeqCon and nearly as well as MapCon (summarizing across the 2-DoF task results).

To realize 2-DoF control, four distinct patterns/dimensions of EMG signals should be generated and then distinguished by the controller. For MapCon, which utilized more distinct wrist actions (Ext-Flx and Rad-Uln), subjects found little difficulty in separately controlling prosthesis open, close, pronate, supinate, or their combinations. But for DirCon, which utilized less distinct wrist actions (Opn-Cls and Pro-Sup), some subjects inadvertently produced wrist supination when attempting to trigger hand open. We largely mitigated this problem by setting higher Sup thresholds, reducing the sensitivity of rotation. Subjects seemed to prefer this higher threshold, since they seemed to prioritize hand performance, achieving small hand rotations through body posture and shoulder movement. Another principal to realize 2-DoF control is the ability of subjects to reproduce the same EMG patterns as during calibration. For able-bodied subjects, reproducibility is facilitated by feedback from their real hand and wrist to produce the same motions. Limb-absent subjects do not have this advantage. In fact, congenital limb-absent subjects will never have experienced these feedback sensations. These differences may explain, in part, why the able-bodied subjects performed better than the limb-absent subjects on both 2-DoF tasks (clothespin relocation and door-knob). Accordingly, congenital limb-absent subjects may be more amenable to MapCon, since they would be mapping "motions" which they have never experienced in the first place. If novel motor patterns are to be learned, selection of patterns that are likely more distinguishable from surface EMG might be beneficial.

5.4.4 Number of Electrodes and Channel Selections

For able-bodied subjects, 6 or 12 electrodes demonstrated no significant difference when subjects controlled the prostheses. The tasks and conditions were randomized and subjects were blinded to the number of active EMG channels in use. Most subjects could recognize the difference between 12 vs. 6 channels due to different channel selection and different coefficients, but they could not tell which option provided better control. Six electrodes are reasonable to apply on a commercial prostheses considering cost, complexity and required microcontroller computation speed. When 6 electrodes were applied on limb-absent subjects, they could easily control the prosthesis after practice. Since adjacent EMG signals are highly correlated, a further increase in EMG channels introduces more redundant information, along with increased risk of electrode shorting, lift-off, etc. (Clancy and Hogan 1995). We used backward stepwise selection from 16 candidate electrodes to gradually reduce the number of electrodes to 12 or 6. In practice, this selection step would be part of the prosthesis fitting operation completed by a prosthetist and, thereafter, the electrode sites would be fixed in to their socket. Though different subjects had their own best electrode locations, the selected electrodes were always spread around the limb, not concentrated in one muscle region.

5.4.5 Limb-Absent Subject Performance

Due to time constraints during an experimental session, subjects necessarily limited their practice time before the tasks. Nonetheless, we anecdotally observed that subjects became more skilled in the use of the prosthesis trial by trial. Hahne *et al.* (Hahne, Schweisfurth et al. 2018) compared 2-DoF, regression-based hand-wrist prosthesis control performance in five limb-absent subjects across two days, and found some improvement on the second day. They postulated that prosthesis control might benefit from interactive learning; the algorithm learns the EMG signal patterns from the user and generates corresponding coefficients, then the users learn how to use the prosthesis, etc.

The tests of within-subjects effects for limb-absent subjects variously found significance for the box-block, clothespin and door-knob tasks (two of three tasks produced significantly different results per subject, but the significantly different tasks varied per subject), suggesting that different subjects exhibited unique differences in performance. Numerous pre-existing factors—such as muscle contraction ability, length of prosthesis use, limb-loss type and learning ability—should greatly influence task performance. Hence, prosthesis controller implementation for different users must consider their unique needs and characteristics. Of note, all limb-absent subjects used 2-DoF control for the first time in this study, and with only 20–30 minutes of practice. Yet, each subject performed better on at least one of the 2-DoF tasks using a 2-DoF controller. Also of note was that limb-absent subjects performed poorer than able-bodied subjects on aspects of each 2-DoF task. But, it is unclear if such differences would remain after more practice.

5.4.6 Two-DoF Controller Limitations and Challenges

Though each subject could complete each of the three tasks using the 2-DoF controllers, significant challenges remain. It was obvious that the quality of calibration was essential to a subject's performance. For some subjects, the first calibration did not result in effective prosthesis control, perhaps because these subjects may have focused more on achieving the instructed calibration contraction profile and not on contraction efforts that would be easy for them to reproduce during real tasks. For these subjects, the second or third calibration usually led to a dramatic improvement in control. A more objective measure of calibration "success" is desired to inform the user if they need to re-calibrate for better control. Assessment of overall RMSE between target force and EMG-estimated force may be dubious. Analyzing the error from each individual motion direction after calibration might better help the user gradually develop the best patterns for everyday calibration.

Another issue was unintentional movement from another DoF. We manually applied two thresholding methods to reduce the impact from unintentional movement. However, a more reproducible, automated method for threshold selection should be developed. The unintentional movement usually happened in two

cases. First, it occurred when subjects had a fast change from one motion to another. In this situation, EMG in most channels would spike, producing EMGσ values much higher than normal contraction. These contractions usually triggered a correct movement of the desired DoF, but also generated unexpected movement from another DoF. Second, unintentional movement was sometimes produced when subjects used very high force levels to control the prostheses, likely due to antagonist muscle co-contraction. In both of these cases, the contraction patterns are not present in the calibration data. It is hard to completely avoid unintentional movement during control, but effective threshold selection and lower muscular efforts can reduce the sensitivity. In this way, users can focus on one DoF with accurate and robust control and use an addition DoF when needed.

5.5 Conclusion

This laboratory study evaluated two regression-based 2-DoF prosthesis control methods, compared with conventional co-contraction sequential control in box-block, refined clothespin and door-knob tasks on both able-bodied and limb-absent subjects. We found that in tasks focused on 1-DoF performance, SeqCon perform best (on average), but this difference was not statistically significant when compared to DirCon. In 2-DoF tasks (clothespin, door-knob), both MapCon and DirCon performed better than SeqCon, with faster and more robust performance. Six electrodes had overall similar performance with 12 electrodes and are more feasible for commercial prosthesis applications. More algorithm and hardware design to improve control comfort and robustness are appropriate next steps.

Chapter 6: Two Degree of Freedom Dynamic EMG-Force at the Wrist Using a Minimum Number of Electrodes

This chapter is published as: Ziling Zhu, Chenyun Dai, Carlos Martinez-Luna, Marek Waterberg, Todd R. Farrell, Edward A. Cla*ncy, "Two Degree of Freedom Dynamic EMG-Force at the Wrist Using a Minimum Number of Electrodes," 2017 IEEE Signal Processing in Medicine and Biology Symposium (SPMB), 2 Dec. 2017.* Color Versions of one or more of the figures in this paper are available online at https://ieeexplore.ieee.org/abstract/document/8257052.

***Abstract*—Myoelectric upper-limb prostheses are generally limited to control of one degree of freedom (DoF) at a time when proportionally actuating two upper-limb devices (e.g., hand-wrist). Mode switching is then used between the two devices. Users would greatly prefer an ability to control both DoFs simultaneously, independently and proportionally (SIP control). Researchers have previously studied 2-DoF SIP control via EMG-force tasks in able-bodied subjects (as well as limb-absent), showing feasibility using high density EMG electrode systems. These high-density systems are not practical for fielded prosthetic devices, thus recent research has studied 2-DoF EMG-force using a small number of commercial electrodes. We previously reported 2-DoF EMG-force results at the wrist using a minimum number of electrodes and static contractions - constant-posture, slowly force varying. Herein, we report pilot results from five able-bodied subjects with the experimental conditions expanded to constant-posture force-varying (dynamic) conditions. We found that the minimum number of electrodes for 2-DoF EMG-force at the wrist was four, when selected using backward stepwise selection from a pool of 16 electrodes. The average RMS errors ranged from 6.0-16.3% maximum voluntary contraction, depending on the attempted motions and the training-testing strategy used. This technique is promising. Evaluation in a larger sample and by limb-absent subjects in a prosthesis control task is suggested as necessary future work.**

***Index Terms*—EMG-force, EMG signal processing, electromyogram, myoelectric control, prosthesis control**

6.1 Introduction

Many patients with transradial upper-limb absence use electromyogram (EMG) signals from residual forearm muscles to control the functions of a powered prosthetic wrist and/or hand (Mann and Reimers 1970, Parker, Englehart et al. 2006, Farina, Jiang et al. 2014). Current commercial EMG-controlled prostheses that proportionally control motor speed are limited to control of one degree of freedom (DoF) at a time (Parker, Englehart et al. 2006), which is considered a substantial limitation (Atkins, Heard et al. 1996). To provide advanced control, pattern recognition techniques have been introduced to select between a small set of pre-programmed hand (or hand-wrist) actions (Coapt , Graupe and Cline 1975, Hudgins, Parker et al. 1993, Boostani and Moradi 2003, Englehart and Hudgins 2003, Powell, Kaliki et al. 2014). Multi-joint movement can be programmed, but the action is still only 1-DoF in nature. Kuiken and colleagues have used targeted muscle reinnervation surgery to realize simultaneous, independent and proportional (SIP) control of multiple upper limb prosthetic devices (Kuiken, Dumanian et al. 2004, Kuiken, Li et al. 2009). However, the high cost, invasiveness of the surgery and extended recovery period (3–6) months are a barrier to more general use.

Researchers have studied upper-limb prosthesis SIP control using high density electrode arrays as the sensor input (Muceli and Farina 2012, Liu, Brown et al. 2013, Muceli, Jiang et al. 2014). While showing scientific feasibility, it is understood that such arrays are not practical for use with commercial prosthetic devices. Nonetheless, this research has given way to studies in which progressively fewer conventional surface EMG electrodes were applied (Jiang, Englehart et al. 2009, Nielsen, Holmgaard et al. 2011, Jiang, Vest-Nielsen et al. 2012, Ameri, Kamavuako et al. 2014, Fougner, Stavdahl et al. 2014, Amsuess, Vujaklija et al. 2016). (See a thorough review in (Clancy, Martinez-Luna et al. 2017)).

Recently, we furthered this vein of research by investigating the minimum number of electrodes necessary for EMG-force models of two wrist DoFs, studying ten able-bodied and three limb-absent subjects (Clancy, Martinez-Luna et al. 2017). This initial investigation was necessarily limited in scope, but was intended as a starting point to progress to 2-DoF EMG-based SIP control in a hand-wrist prosthesis. We studied fixed-posture contractions that were essentially static (slowly force-varying), to avoid the complexity of EMG-force dynamics. For the able-bodied subjects, four backward-selected electrodes provided performance that was statistically indistinguishable from the full 16 electrodes. In the research described herein, we extend this prior work to fixed-posture force-varying contractions, and extend our EMG-force models accordingly.

6.2 Methods

6.2.1 Experimental Methods

Five abled-bodied subjects provided written informed consent for an experiment approved by New England IRB (Newton, MA). Data were acquired at Liberating Technologies, Inc. (Holliston, MA).

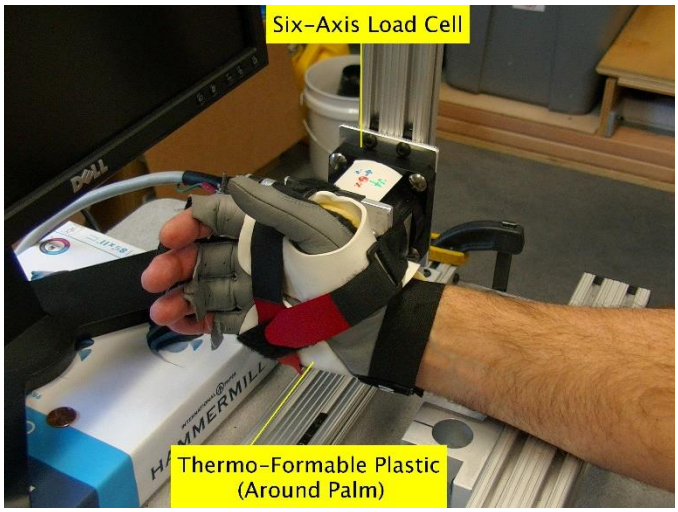

Fig. 6.1. Experimental apparatus. Dominant hand was tightly secured via thermo-formable plastic and Velcro to six-axis load cell. Sixteen electrodes (not visible) were secured about the distal aspect of the dominant forearm.

The experimental apparatus mainly consisted of three parts. Firstly, a six DoF load cell (MC3A-100 transducer with Gen 5 signal conditioner, AMTI, Watertown, MA) measured extension-flexion (Ext-Flx), radial-ulnar deviation (Rad-Uln) and pronation-supination (Pro-Sup) force/moment of the wrist, with a hand-shaped thermo-formable plastic splint attached to the load cell to fix the pose of the dominant hand (Fig. 6.1). Secondly, 16-channel bipolar surface EMG electrodes were placed around the forearm to measure EMG signals. Each electrode pair consisted of 5 mm diameter, stainless steel hemispherical contacts with 1 cm edge-to-edge separation. An amplifier (Liberating Technologies, Inc. BE328; 30–500 Hz pass band, CMRR>100 dB over the pass band) processed the differential EMG signal and selectable gain was applied. The average ratio of resting RMS EMG to the RMS EMG at 50% maximum voluntary contraction (MVC), expressed as a percentage, was 8.1 ± 5.4%. Thirdly, two arrowheads were displayed on a computer screen. One arrowhead displayed the load cell measurements, with *x*-axis location corresponding to Ext-Flx force, *y*-axis location to Rad-Uln force and rotation to Pro-Sup moment. The other arrowhead used a different color to display a computer-controlled target to guide the subject to perform each task. The three load cell signals and 16 EMG signals were sampled at 2048 Hz with 16-bit resolution.

Experimental Preparation: The dominant forearm skin surface of a subject was wiped using alcohol prep pads and electrode gel was applied. EMG electrodes were placed on a row transversely about the forearm at equal inter-electrode distances, with the mid-point of each electrode 5 cm distal from the crease of the elbow. Each electrode was oriented with the bipolar contacts along the long axis of the forearm. A reference electrode was gelled and secured on the ventral forearm, just distal to the row of active electrodes. Then the subject sat on the apparatus with the dominant hand cuffed to the load cell by a thermo-formable plastic splint (hand was vertical to the floor) to maintain a constant posture. The wrist was in a neutral position with respect to the hand and the elbow was supported at the olecranon process. The shoulder was flexed 45° forward from the anatomical position along the sagittal plane.

MVC Trials: Subjects were provided warm-up preparation before the contraction trials and 2–3 minutes rest between each contraction to prevent muscle fatigue. MVC was measured for each DoF (Ext-Flx, Rad-Uln and Pro-Sup). Subjects progressively increased contraction for 2–3 seconds and the plateau level of their force/moment maximum was their MVC. Signal noise levels were also evaluated by rest trials.

One-DoF Dynamic Tracking Trials: Each of the four DoFs was investigated separately. For Ext-Flx, the target arrowhead randomly moved between ± (|30%MVC Ext|+|30%MVC Flx|)/2. The movement of the arrowhead was a white, uniform process with a band-limit of 0.75 Hz; an arrowhead speed of movement that could be tracked by subjects. The other arrowhead displayed as feedback the load cell force/moment of the active DoF only. The 16 EMG channels and all load cell data were recorded for 4 trials of 40s duration. Identical trials were conducted for the other DoFs. The order of presentation of the DoFs was randomized between subjects.

Two-DoF Dynamic Tracking Trials: All three combinations of DoF pairs (Ext-Flx & Rad-Uln, Ext-Flx & Pro-Sup, and Rad-Uln & Pro-Sup) were tracked for tests. Each trial involved two different DoFs simultaneously—the target arrowhead moved with two independent random instances, and the feedback arrowhead tracked both DoFs simultaneously. (The third DoF was suppressed.) Each of the three combinations had four trials of 40s duration.

6.2.2 Methods of Analysis

Pre-Processing: All data processing was computed offline by MATLAB (The MathWorks, Inc., Natick, MA). MATLAB function "filtfilt()" (non-casual, zero-phase, forward and reverse filtering technique) was used for all filtering. Each EMG channel was firstly highpass filtered (5^{th} order Butterworth, cut-off at 15 Hz) to attenuate motion artifacts, notch filtered at 60 Hz with 1 Hz bandwidth to cancel the power line interference, and then rectified. Secondly, each rectified signal was lowpass filtered at 16 Hz (Chebyshev Type 1 filter, 9^{th} order, 0.05 dB peak to peak passband ripple) and downsampled from 2048 Hz to 40.96 Hz. This smoothed EMG standard deviation estimate (EMGσ) made the signal suitable for system identification of EMGσ-force dynamic models. Each of the force/moment signals (Ext-Flx, Rad-Uln and Pro-Sup) was normalized by (|MVC of one direction|+|MVC of opposite direction|)/2 and then similarly decimated.

One-DoF Dynamic Models: For Ext-Flx, a linear least squares method used two training trials to fit the EMGσ-force/moment dynamic linear model:

$$T_{E-F}[m] = \sum_{q=0}^{Q} \sum_{e=1}^{E} c_{e,q}\, EMG\sigma_e[m-q]$$

where $T_{E\text{-}F}[m]$ was Ext-Flx force at decimated sample index m, q was the order of the linear dynamic model, e was the EMG channel index, $c_{e,q}$ were the fit coefficients, and EMGσ_e was the EMG standard deviation estimate for channel e. The analogous model was utilized for the other two DoFs. The maximum lag of the model was selected as Q=20 (Clancy, Liu et al. 2012). The pseudo-inverse technique was used to regularize the least squares fit, in which singular values were removed if the ratio of that singular value to the largest singular value in the design matrix was less than a tolerance value (Press, Flannery et al. 1994). A tolerance value of 0.01 was selected based on prior works (Clancy, Liu et al. 2012, Clancy, Martinez-Luna et al. 2017). The remaining two testing trials were used for testing, computing the RMS error between the measured force and EMG-estimated force (using the coefficients fit from the training trials). Then the training and testing sets were switched for two-fold cross-validation, which was selected for computational efficiency because of the model correlations of the four remaining cross validation folds. The average RMS error from the two cross-validation folds is reported. The backward stepwise technique was applied for electrode selection. Initially from 16 electrodes, the channel was excluded when its absence resulted in the lowest RMS error step by step until only one electrode remained. Only training data were used for backward stepwise selection decisions. For comparison, we additionally computed the multivariate R^2 index (Jiang, Englehart et al. 2009), which is also commonly used to assess model error. Identical analysis was performed on the other two DoFs.

Two-DoF Dynamic Models: Two-DoF dynamic models were separately estimated and evaluated for all three combinations of two simultaneous DoFs, using a model that was an extension of (1). The same pseudo inverse tolerance value and maximum lag were used, as was backward stepwise selection of electrodes. Three different training paradigms (training with 1-DoF trials, with 2-DoF trials, or with both 1- and 2-DoF trials) and two testing paradigms (testing on 1-DoF trials or on 2-DoF trials) were applied to estimate the performance, as different training strategies represented different methods by which real prostheses might be trained, and different testing strategies evaluate if 2-DoF models retain good performance when encountering 1-DoF tasks.

Statistics: Repeated measures analysis of variance (RANOVA) was applied to test differences of the factors and levels, using SPSS 22 (IBM, New York). If data violated the assumption of sphericity, the degrees of freedom for the effect was adjusted: for $\varepsilon < 0.75$ with the method of Greenhouse-Geisser, for $\varepsilon > 0.75$ with the method of Huynh-Feldt (Girden 1992, p. 21). *Post hoc* pair-wise comparisons used paired *t*-tests with Bonferroni correction (to control for multiple comparisons). A significance level of $p = 0.05$ was used for all tests.

6.3 Results

6.3.1 One-DoF Models

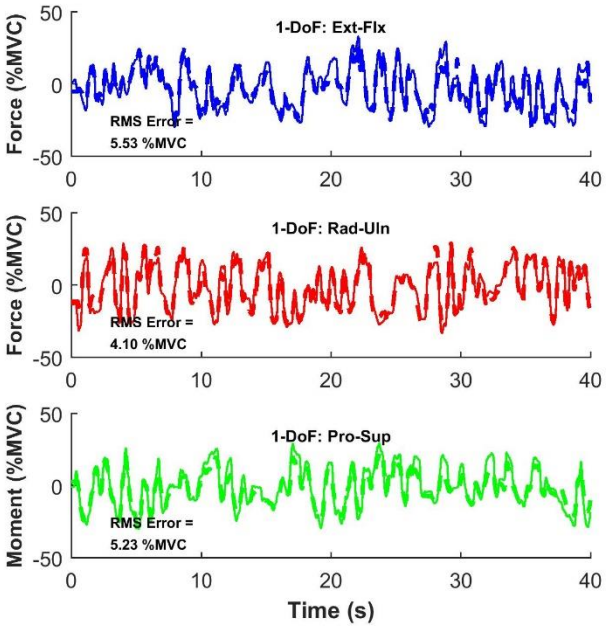

Fig. 6.2. Example time-series plots of 1-degree-of-freedom models, two electrodes (Subject 05, Trials 71, 74, 77). Solid lines are actual forces/moment, dashed lines are EMG-estimated.

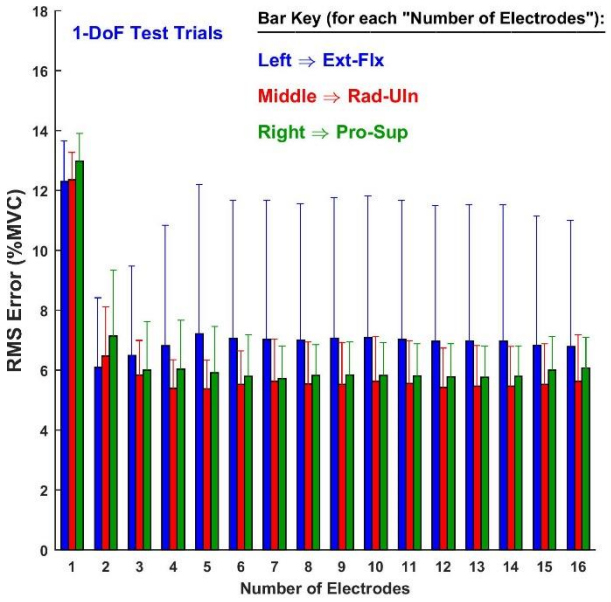

Fig. 6.3. Summary RMS error results: 1-degree-of-freedom models, five subjects. Error lines show one standard deviation above the mean.

Fig. 6.2 shows sample time-series EMG-force test results for the 1-DoF models. Fig. 6.3 shows summary RMS error results as a function of number of electrodes selected. Performance was calculated for 1–16 numbers of electrodes, separately for each of the 3 DoFs. Using all the RMS error results of 1-DoF models, a two-way RANOVA (factors: DoF, number of electrodes) indicated that only number of electrodes had a significant effect on performance [$F(1.5, 6.0) = 67$, $p_{GG} < 10^{-4}$], without interaction. Post hoc comparison found that only one electrode had higher error than 2–4, 6–8 and 12–15 electrodes ($p < 0.048$), and there were no differences in performance when comparing 2 or more electrodes. Table 6.1 shows the RMS errors for 2 backward-selected electrodes (typical in a commercial 1-DoF prosthesis controller) and the R^2 index values corresponding to these RMS errors, for each DoF.

6.3.2 Two-DoF Models

Two-DoF models separately estimated 2 DoFs models for Ext-Flx & Rad-Uln, Ext-Flx & Pro-Sup, or Rad-Uln & Pro-Sup. Fig. 6.4 shows sample time-series EMG-force test results during 2-DoF trials and Fig. 6.5 shows summary RMS error results. Table 6.1 (except for the top row) shows RMS errors and the R^2 index values for the different training/testing strategies.

Two-DoF Models Assessed on **1-DoF** trials: A three-way RANOVA (factors: DoF, number of electrodes, training conditions) was computed and all three factors were significant, but training condition interacted with number of electrodes: [F(1.7, 6.7) = 6.2, $p_{GG} = 0.034$]. As training condition had the lowest degrees of freedom, separate two-way RANOVAs were conducted with each of the three training conditions fixed.

When training with only 1-DoF trials, only number of electrodes was significant [F(1.7, 6.9) = 76, $p_{GG} < 10^{-4}$], with no interaction. *Post hoc* comparison found that 1 electrode always had higher errors than 3, 7–10, 12–14 and 16 electrodes ($p < 0.05$), and there was no difference when comparing 2 and more electrodes.

Results when training with only 2-DoF trails only found a significant difference for DoF [F(2, 8) = 5.8, $p = 0.027$], without interaction. *Post hoc* comparison found no differences.

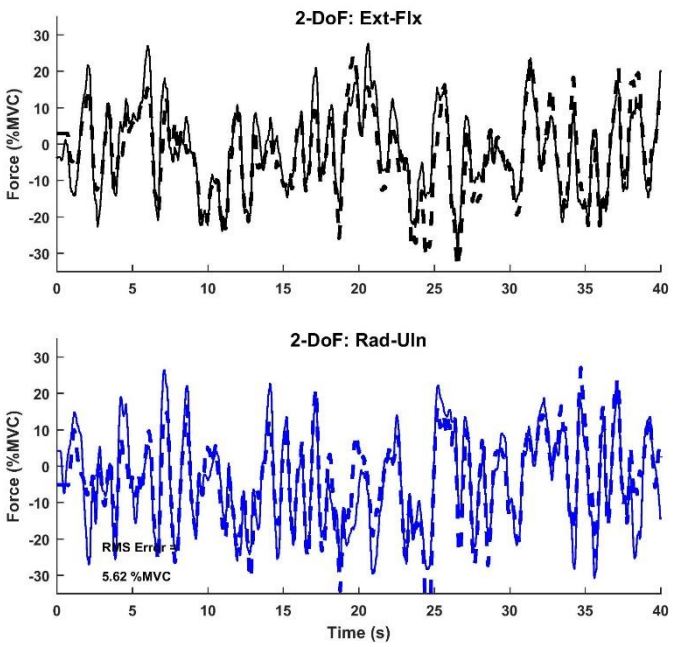

Fig. 6.4. Example time-series plots of 2-degree-of-freedom models from subject 05, trial 81 (four electrodes). Key: solid lines=actual forces, dashed=estimated; black=Ext-Flx, blue=Rad-Uln. Four EMG channels and training from both 1- and 2-DoF trials.

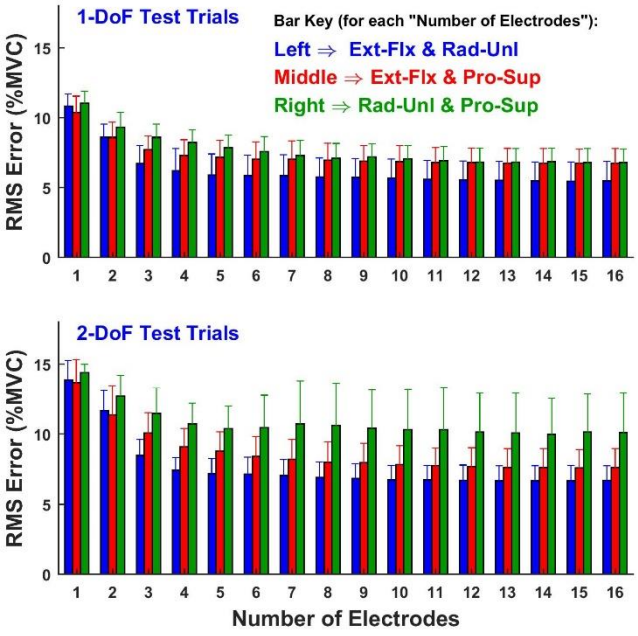

Fig. 6.5. Summary results: 2-degree-of-freedom (DoF) models, five subjects. Models trained from both 1- and 2-DoF trials, Top: testing on 1-DoF trials. Bottom: testing on 2-DoF trials. Error lines show one standard deviation above the mean.

The two-way RANOVA when training with both 1- and 2-DoF trials found that only number of electrodes was significant [F(1.9, 7.6) = 117, $p_{GG} < 10^{-5}$], without interaction. *Post hoc* comparison found that 1 electrode exhibited higher error than 6 and more ($p < 0.04$); 2 electrodes higher than 7 and more ($p < 0.045$); and 3 electrodes higher than 9 and 10 ($p < 0.04$). There were no differences when comparing 4 or more electrodes.

As the RMS error vs. number of electrodes trended to a steady state above 4–5 electrodes, the number of electrodes was fixed at 4 and a two-way RANOVA was computed with factors of DoF and training condition. Both the DoF [F(2, 8) = 9.9, $p = 0.007$] and training condition [F(1.0, 4.1) = 62, $p_{GG} < 10^{-3}$] were significantly different, without interaction. *Post hoc* analysis only found that Ext-Flx & Rad-Uln always

exhibited lower errors than Rad-Uln & Pro-Sup ($p = 0.046$) and the performance of training with only 2-DoF trials exhibited higher error than the other two conditions ($p < 0.005$).

Two-DoF Models Assessed on **2-DoF** trials: A three way RANOVA showed that all three factors were significant, but number of electrodes and training condition interacted [$F(2.2, 9.0) = 4.9$, $p_{GG} = 0.034$]. Thus, three two-way RANOVAs were computed with each of training conditions fixed, similar to above.

When training with only 1-DoF trials, there was no significant difference found, without interaction.

Results when training with only 2-DoF trials found that only number of electrodes was significant [$F(1.2, 5.0) = 25$, $p_{GG} = 0.003$], without interaction. *Post hoc* comparison found no significant differences between each level of number of electrodes.

TABLE 6.1

MEAN ± STD. DEV. RMS ERRORS (%MVC, LEFT) AND CORRESPONDING R^2 INDEX (RIGHT), FIVE SUBJECTS, BACKWARD SELECTED ELECTRODES

. Condition	DoF(s), RMS Error (%MVC)			DoFs, R^2 Index (%)		
1-DoF Models (2 electrodes)	**Ext-Flx**	**Rad-Uln**	**Pro-Sup**	**Ext-Flx**	**Rad-Uln**	**Pro-Sup**
Assessed on 1-DoF trials	6.1 ± 2.3	6.5 ± 1.6	7.1 ± 2.2	81 ± 11	79 ± 9	71 ± 21
2-DoF Models (4 electrodes)	**Ext-Flx & Rad-Uln**	**Ext-Flx & Pro-Sup**	**Rad-Uln & Pro-Sup**	**Ext-Flx & Rad-Uln**	**Ext-Flx & Pro-Sup**	**Rad-Uln & Pro-Sup**
Assessed on 1-DoF trials:						
Train with 1-DoF trials	6.0 ± 1.6	7.1 ± 1.2	7.6 ± 1.6	69 ± 13	57 ± 8	50 ± 17
Train with 2- DoF trials	9.0 ± 2.5	10.7 ± 1.1	12.8 ± 1.6	38 ± 20	25 ± 13	10 ± 8
Train with 1-, 2- DoF trials	6.2 ± 1.6	7.4 ± 1.1	8.1 ± 1.5	66 ± 13	52 ± 9	44 ± 15
Assessed on 2-DoF trials:						
Train with 1-DoF trials	9.8 ± 2.6	11.3 ± 2.2	16.3 ± 6.7	53 ± 15	41 ± 23	19 ± 21
Train with 2-DoF trials	6.7 ± 0.7	7.8 ± 1.4	10.8 ± 1.6	78 ± 2	72 ± 10	45 ± 14
Train with 1-, 2-DoF trials	7.3 ± 1.1	9.1 ± 1.5	11.4 ± 1.5	74 ± 4	62 ± 12	42 ± 14

Lastly, we also computed a two-way RANOVA (factors: DoF, training condition) fixing the number of backward-selected electrodes to four. We selected four electrodes for this comparison (even though the statistical comparisons found no differences for 2 and more electrodes) because Fig. 6.5 shows a trend that suggests improvements out to at least four electrodes, the low sample size likely contributed to a difficulty in finding statistical significance for more than 2 electrodes related to this trend, our prior work with a larger sample size suggests a statistical significance is supported with four electrodes (Clancy, Martinez-Luna et al. 2017), and this number of electrodes is preferred in a 2-DoF commercial prosthesis controller. Both DoF [$F(2, 8) = 7.9$, $p = 0.013$] and training condition [$F(1.0,4.1) = 12$, $p_{GG} < 0.024$] were significant, without interaction. *Post hoc* pairwise comparison for DoFs found that all three combinations had no significant difference. Training with only 2-DoF trials always exhibited lower errors than with both 1- and 2-DoF trials ($p = 0.026$).

6.4 Discussion

We evaluated 1-DoF models primarily as a basis of comparison to existing proportional controllers and to our own 2-DoF results. For 1-DoF models, our results showed that the RMS error was much higher when only one electrode was retained[†]. The main reason is that EMGσ is a unipolar (non-negative) measurement, while any wrist force/moment has two contraction directions (e.g., extension and flexion), which means the force/moment is a bipolar quantity. Therefore, poor performance can be expected when a linear model is used. This conclusion is consistent with our previous study (Clancy, Martinez-Luna et al. 2017). Furthermore, our results established the findings that no significant improvement was achieved when using more than two electrodes. We found no significant differences as a function of DoF. However, Table 6.1 shows a trend for higher Pro-Sup RMS error. Some previous studies have found that EMG-force using the Pro-Sup DoF was more challenging (Jiang, Englehart et al. 2009, Nielsen, Holmgaard et al. 2011, Jiang, Vest-Nielsen et al. 2012). One possible reason is that the muscles producing Pro-Sup contraction reside deeper within the forearm, thus being less accessible to surface EMG recordings (Jiang, Vest-Nielsen et al. 2012). A larger sample size might substantiate this relationship with our protocol, although it is unclear if such differences would have a clinically significant impact on prosthesis performance.

For 2-DoF models, the suggested minimum requirement of conventional electrodes increased to four, compared with 1-DoF models (although summary plots in Fig. 6.3 and Fig. 6.5 show more gradual performance changes as a function of the number of electrodes). This conclusion was intuitive that more electrodes were required to represent the relationship between EMGσ and force/moment, due to the increased complexity when one more DoF was involved. There were no substantive differences as a function of DoF, perhaps due to the limited statistical power (N=5 subjects). The RMS errors of 2-DoF models varied from 6.0% to 16.3% according to different DoF combinations and training-testing strategies. For different training-testing strategies, the performance of 1-DoF tasks were initially evaluated since a 2-DoF prosthesis controller still needs to be operated for 1-DoF tasks. When assessed on 1-DoF trials, the performance of training with 2-DoF trials and using four electrodes was *poorer* than the other two strategies. On the other hand, when assessed on 2-DoF trials, the performance of training with 2-DoF trials and using four electrodes was *better* than the other two strategies. Therefore, training with both 1- and 2-DoF trials is recommended since both 1-DoF and 2-DoF tasks would be performed when a 2-DoF prosthesis controller is operated. Of course, the interplay between these EMG-force errors due to training might not be entirely indicative of performance in a fielded prosthesis, for which simpler (and less time consuming) calibration tasks are desired.

[†] Note that the use of even one electrode *does* perform better in estimating force than ignoring the EMG altogether—an average RMS error of 17.3% would result if the 1-DoF target was compared to a fixed estimate of 0 %MVC.

A prime limitation of this work is its small sample size (N=5 subjects). With this small sample, our statistical results are biased towards non-significance due to the lack of statistical power. For example, a few of our significant ANOVA results produced *post hoc* paired comparisons (with Bonferroni correction) in which none of the comparisons was significant. Multiple comparisons with Bonferroni correction are easy to apply and can reduce the risk of a Type I error. However, the disadvantages of this procedure are that the statistical power to reject an individual hypothesis is too low, and controlling Type I error leads to the increasing of Type II error, making it hard to find significant results (particularly with small sample sizes) (Howell p. 366, 2010). Other limitations include: laboratory performance of an EMG-force task does not fully represent performance of an algorithm in a fielded prosthesis, low EMG-force errors do not easily translate into predictive performance of a prosthetic controller, we only studied able-bodied subjects, we limited our contractions to those at a fixed pose and conducted during a single experimental session, and that our backward selection technique might not find a unique (or global) minimum (Clancy, Martinez-Luna et al. 2017).

In spite of these limitations, these methods and results contribute towards the feasibility of a practical 2-DoF SIP controller. Of course, the various algorithms implemented offline in this work will need to be translated into appropriate online equivalents. Note that we studied three candidate DoF pairs—in practice, the best performing of these pairs would be selected by a prosthetist for use by each specific prosthesis user. Our results showed little preference as to which pair might be best, on average; the only significant *post hoc* result for DoF was that Ext-Flx & Rad-Uln exhibited lower errors than Rad-Uln & Pro-Sup when 2-DoF models were assessed on 1-DoF tasks with the number of electrodes fixed at four.

6.5 Conclusion

This pilot study has investigated both 1- and 2-DoF *dynamic* EMGσ-force at the wrist using as few conventional electrodes as possible. Our results showed that the minimum requirement of conventional electrodes was two for 1-DoF and four for 2-DoFs. For 1-DoF, the average ± std. dev. RMS errors were 6.1 ± 2.3%, 6.5 ± 1.6% and 7.1 ± 2.2% for Ext-Flx, Rad-Uln and Pro-Sup, respectively, using two electrodes. For 2-DoFs, the average RMS error of the three possible pairs of 2-DoF contractions ranged from 6.0% to 16.3% MVC, depending on different training-testing strategies using four electrodes. Our findings revealed that 2-DoF simultaneous EMGσ-force at the wrist may be feasible by utilizing a very small number of conventional electrodes. The technique is promising for 2-DoF wrist prosthesis control.

Chapter 7: Two Degree of Freedom, Dynamic, Hand-Wrist EMG-Force Using a Minimum Number of Electrodes

This chapter is published as: Chenyun Dai, Ziling Zhu, Carlos Martinez-Luna, Than R. Hunt, Todd R. Farrell, Edward A. Clancy,"*Two Degree of Freedom, Dynamic, Hand-Wrist EMG-Force Using a Minimum Number of Electrodes," Journal of Electromyography and Kinesiology,* 2019, 47: 10-18. Color Versions of one or more of the figures in this paper are available online at: https://www.sciencedirect.com/science/article/pii/S1050641119300379?casa_token=1fzQsrOR_VYAAAAA:9kG2zc1HbObcsGt1sXcC5RLASA2mb-QPiH4TefL9Ky-DKOxZcREqdw1se5HxREIKalhhOXhegA.

***Abstract*— Relating the surface electromyogram (EMG) of forearm muscles in able-bodied subjects to hand-wrist forces has frequently been used to screen candidate myoelectric prosthesis control algorithms. Traditional prostheses only control one degree of freedom (DoF) at a time, regulating the hand or wrist sequentially. Hence, we researched the feasibility of simultaneously controlling two DoFs—hand open-close paired with one wrist DoF—using as few as four commercial electrodes. Experimental data from nine able-bodied subjects were analyzed. Subjects produced 1-DoF and 2-DoF uniformly distributed random forces (bandlimited to 0.75 Hz) up to 30% maximum voluntary contraction (MVC). EMG standard deviation (EMGσ) was related to force using linear dynamic models via linear least squares regression. For 1-DoF forces, the average RMS errors ranged from 8.3–9.0 %MVC, depending on the DoF, and indicated that two electrodes were required. For 2-DoFs, overall performance was best when training from both 1- and 2-DoF trials. When doing so, average RMS errors were 9.2 %MVC for each DoF pair (hand open-close paired with one wrist DoF), using four electrodes. For each model, more electrodes showed no statistical improvement. The results suggest that 2-DoF SIP hand-wrist control with a small number of electrodes may be feasible.**

***Keywords*— EMG-force · EMG signal processing · Electromyogram · Myoelectric control · Prosthesis control**

7.1 Introduction

It is estimated that 41,000 people in the U.S. were living with upper-limb loss in 2005 (Ziegler-Graham, MacKenzie et al. 2008) and that 95% of traumatic upper-limb extremity amputations are transradial or more distal (Dillingham, Pezzin et al. 2002). For several decades, commercial myoelectric prostheses have used surface electromyogram (EMG) activity from residual muscles to control prosthesis movement, thereby realizing partial replacement of function (Mann and Reimers 1970, Parker, Englehart et al. 2006, Farina, Jiang et al. 2014). However, substantial issues exist for prosthesis control. A fundamental challenge is that only one degree of freedom (DoF) is typically controlled at a time, with mode switching used between them (Parker, Englehart et al. 2006). Prosthesis users recognize this limitation (Atkins, Heard et al. 1996), since even simple daily tasks can require simultaneous use of multiple DoFs—e.g. opening a door requires hand grip of the door knob with simultaneous wrist rotation. Another related issue is that most EMG-based laboratory studies of multi–DoF control have utilized a large quantity of specialized electrodes (upwards of 32–64). High density electrode arrays can extract more information and decrease the error in EMG-force/kinematics estimation (Muceli and Farina 2012, Liu, Brown et al. 2013, Muceli, Jiang et al. 2014), but they are not practical for commercial prostheses.

To improve multi-DoF control of prostheses, Kuiken and colleagues (Kuiken, Dumanian et al. 2004, Kuiken, Li et al. 2009) developed targeted muscle reinnervation surgery. Surface EMG electrodes sense the actual muscle contractions of reinnervated residual muscle regions to provide simultaneous, independent and proportional (SIP) control of multiple prosthesis joints (e.g., hand, wrist, elbow). The high cost, invasive surgery and long recovery period (3–6 months) likely limit its acceptability. Another improvement technique is based on the multifunction pattern recognition approach to select desired movements of the hand and/or wrist via EMG signals from the forearm (Graupe and Cline 1975, Hudgins, Parker et al. 1993, Boostani and Moradi 2003, Englehart and Hudgins 2003, Powell, Kaliki et al. 2014) (recently commercialized (Coapt)). Multi-joint control is facilitated, but still only 1-DoF is operated at a time. The performance of this method degrades with the number of functions selected and increases with the number of electrodes applied.

Recent studies have explored EMG-based multiple DoF EMG-force/kinematics (a.k.a. direct prosthesis control) using 7–8 conventional electrodes, equally-spaced transversely about the forearm (Jiang, Englehart et al. 2009, Nielsen, Holmgaard et al. 2011, Jiang, Vest-Nielsen et al. 2012, Ameri, Kamavuako et al. 2014, Amsuess, Vujaklija et al. 2016); and one study has placed 5 electrodes over anatomically-selected locations in able-bodied subjects (Fougner, Stavdahl et al. 2014). However, none of these works explored the influence or feasibility of reducing the quantity of conventional EMG channels to its minimum number. Further, very little work has studied 2-DoF SIP hand-wrist EMG-force [i.e., hand open-close (Opn-Cls) combined with

one wrist DoF]. Limiting the number of applied electrodes is an important goal, since electrode site selection and cabling remain difficult tasks faced by prosthetists who must custom fit each prosthetic device to its user. This problem grows with the number of electrodes used. In addition, when more electrodes are used in a preparation, the odds of a failure increase, with a single failing electrode channel potentially degrading the entire system (Clancy and Hogan 1995). Combining hand Opn-Cls with one wrist DoF could be immediately mapped to existing hand-wrist prostheses (with the one wrist DoF being mapped to rotation of the prosthetic wrist). Improvement to 2-DoF control would then be available immediately to a wide range of existing commercial prosthetic devices. Although low EMG-force error in a laboratory setting has not necessarily reflected improved performance in a prosthesis (Jiang, Dosen et al. 2012), laboratory studies represent an established and inexpensive initial step in the development of new technologies—a method that is particularly adept at screening out unsuccessful approaches and refining algorithms before undertaking expensive applied/field evaluations.

Hence, our laboratory work studied the feasibility of estimating 2 DoFs—hand Opn-Cls force in conjunction with one wrist DoF—using as few conventional electrodes as possible. In particular, each 2-DoF contraction trial, which produced random forces queued by a computer-generated target, incorporated hand Opn-Cls force with one of either extension-flexion (Ext-Flx), radial-ulnar deviation (Rad-Uln) or pronation-supination (Pro-Sup). In a prosthesis controller, the one best performing of these wrist DoFs would be utilized. Backward stepwise selection was utilized to progressively reduce the number of EMG channels. In practice, selection of optimal electrode sites and the best performing wrist DoF would occur in the fitting stage by a prosthetist, with these EMG locations then used to produce the final prosthetic socket. The electrode sites would then be fixed in the definitive prosthesis. Our results show that 2-DoF control had similar error levels when compared to 1-DoF control (which represents the current state of the art) and required as few as four electrodes.

7.2 Methods

7.2.1 Experimental Data and Apparatus

Experimental data from nine able-bodied subjects (five males, four females; aged 27±9.7 years) were acquired at Liberating Technologies, Inc. (Holliston, MA) and approved by the New England Independent Review Board (Newton, MA). All subjects provided written informed consent. Data from one additional subject were excluded from analysis due to erroneous EMG values.

7.2.1.1 Data Collection Setup

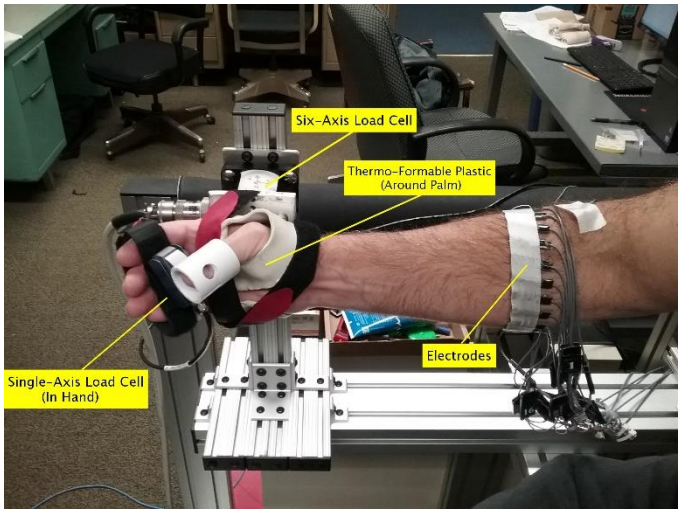

Fig. 7.1. Experimental apparatus. Dominant hand was tightly secured via thermo-formable plastic and Velcro to six-axis load cell. Fingers were secured to a single-axis load cell (thumb on one side, remaining four on the other). Sixteen electrodes were secured about the distal aspect of the dominant forearm.

Subjects sat at the experimental apparatus. The back of the dominant hand was tightly cuffed to a six-DoF load cell (MC3A-100 transducer with Gen 5 signal conditioner, AMTI, Watertown, MA) using a thermo-formable plastic mold, to measure force/torque generated at the wrist. A single-axis load cell (LCR-150 with DMD-465WB amplifier, Omega Engineering, Inc., Stamford, CT) was secured around the distal thumb via a rigid tube and, separately on the opposing side of the cell, Velcro-secured to the proximal aspects of the four fingers to measure grip force during attempted hand Opn-Cls (see Fig. 7.1). The palm of the hand was perpendicular with the plane of the floor, the wrist was relaxed in a neutral position with respect to the hand and the shoulder was flexed 45º forward from the anatomical position along the sagittal plane. The elbow was supported just distal to the olecranon process. The skin surface about the forearm was scrubbed with an alcohol wipe and electrode gel was applied. Sixteen bipolar EMG electrodes were equidistantly placed in a row, circumferentially around the forearm (one electrode aligned at the most dorsal aspect) with the mid-point between bipolar contacts situated 5 cm distal to the elbow crease; and then held in place with bandaging. Each electrode pair consisted of 5 mm diameter, stainless steel, hemispherical contacts separated 1 cm edge-to-edge, oriented along the long axis of the forearm. A reference electrode was gelled and secured on the ventral forearm, just distal to the row of active electrodes. Each bipolar EMG signal was wired to a differential amplifier circuit (Liberating Technologies, Inc. BE328 amplifier; 30–500 Hz pass band, CMRR > 100 dB over the pass band) and then selectable gain was applied. The average ratio of resting RMS EMG to the RMS EMG at 50% maximum voluntary contraction (MVC) was 8.1 ± 5.4% (median of 7.2%). A real-time feedback signal from the load cells was shown via an arrowhead on the computer screen in front of the subject. The arrowhead displayed four different DoFs—*x*-axis location for Ext-Flx force, *y*-axis location for Rad-Uln force, rotation for Pro-Sup moment, and size for hand Opn-Cls. A second arrowhead displayed in another color was a computer-controlled target that guided the subject to complete different experimental tasks. Four load cell signals and 16 EMG channels were each sampled at 2048 Hz with 16-bit resolution.

7.2.1.2 Data Collection Contractions

All contractions were constant-posture. A minimum two-minute rest interval was provided between contractions to prevent muscle fatigue. After a warm-up period, MVC was measured separately for both directions (e.g., open vs. close) for each of the four DoFs. A subject took 2–3 seconds to ramp up their effort to MVC, maintaining that effort for two seconds. The plateau level of this force/ moment was measured as the MVC. Lastly, rest trials were recorded for noise level evaluation.

Next, subjects proceeded to 1-DoF dynamic tracking trials. Each of the four DoFs was tested separately. Subject feedback only modified the arrowhead according to changes in the specified DoF. For Ext-Flx, the guide arrowhead generated a random target moving between ±(|30 %MVC Flx| + |30 %MVC Ext|)/2 on the screen, and subjects were asked to track the movement of the target by controlling the load cell force. The random target was a 0.75 Hz band-limited, white and uniform random process. Preliminary testing was used to select this bandwidth as the widest in which subjects could maintain target tracking for these tasks. Four trials of 40 s duration each were collected. The equivalent experiment was applied for the three remaining DoFs (16 total trials); except that the force maximum was reduced to 15 %MVC for Opn-Cls due to excessive fatigue experienced in preliminary testing of the protocol (particularly during hand open). The order of presentation of the DoFs was randomized.

Lastly, 2-DoF trials were conducted in which two different DoFs were tracked simultaneously. We only considered three combinations: hand Opn-Cls combined with one of the three wrist DOFs (Ext-Flx, Rad-Uln or Pro-Sup)—targeting control of a prosthetic hand/terminal device with a wrist rotator. The same random target style was used, but with two independent random instances (one per DoF). Four trials of 40 s duration were collected for each hand-wrist combination (12 total trials).

7.2.2 Methods of Analysis

7.2.2.1 Pre-Processing

Data analysis was performed offline in MATLAB (The MathWorks, Inc., Natick, MA). Once designed, all filters were implemented using MATLAB function “filtfilt()”, which applied filters in the forward and reverse time directions to achieve a noncausal, zero-phase and magnitude squared response. An estimate of EMG standard deviation (EMGσ) was computed for each EMG channel. Raw EMG was highpass filtered to avoid motion artifact (fifth-order Butterworth, cut-off at 15 Hz), notch filtered to attenuate power-line interference with little loss of signal power (second-order IIR filter at 60 Hz, notch bandwidth of 1Hz), rectified and downsampled (after lowpass filtering at 16 Hz; Chebyshev Type 1 filter, ninth-order, 0.05 dB peak-to-peak passband ripple) from 2048 Hz to 40.96 Hz. This resulting frequency is suitable for system

identification of EMG-force dynamic models (Ljung 1999, Clancy, Bida et al. 2006). The lowpass filter can be regarded as a smoothing window, with additional smoothing (Koirala, Dasog et al. 2015) provided by the dynamic EMG-force model (described below). Each force/moment signal (Opn-Cls, Ext-Flx, Rad-Uln and Pro-Sup) was normalized by its corresponding MVC level pair. For example, Ext-Flx was normalized by: $\left(\left|MVC_{Ext}\right|+\left|MVC_{Flx}\right|\right)/2$.

7.2.2.2 One-DoF Dynamic Models

The processed extension and flexion EMGσ values were related to Ext-Flx wrist force via a 1-DoF linear dynamic model as:

$$T_{E-F}[m]=\sum_{q=0}^{Q}\sum_{e=1}^{E}c_{e,q}\,EMG\sigma_e[m-q]$$

where $T_{E\text{-}F}$ was wrist Ext-Flx force, m was the decimated discrete-time sample index, Q was the order of the linear dynamic model (set to 20 based on (Clancy, Liu et al. 2012) and preliminary evaluation of these data), E was the number of electrodes used in the fit (initially set to 16), and $c_{e,q}$ were the fit coefficients. A linear model was chosen in this initial study to limit the total number of free parameters and, thus, reduce the risk of overfitting (Ljung 1999). Two of four trials were used for coefficient training, using the known EMGσ values and force. The linear least squares pseudo-inverse method (Press, Flannery et al. 1994) was performed for model training, in which singular values of the design matrix were removed if the ratio of that singular value to the largest was less than a tolerance value, *Tol* (set to 0.01 based on (Clancy, Liu et al. 2012) and preliminary evaluation of these data). The remaining two trials were used for testing (RMS error between the estimated and measured torques). The training and testing sets were flipped for two-fold cross-validation, and the average of these two results reported. Two-fold cross validation was selected for computational efficiency, and because the remaining four folds would necessarily yield correlated results (which are statistically less efficient). Since the mechanical signals were normalized by MVC, the final RMS error was in %MVC. The backward stepwise method was utilized for electrode selection. All 16 EMG channels were entered initially. Then, the channel whose absence resulted in the lowest RMS error was excluded for each step. Stepping continued until only one electrode remained. For comparison, a subset of the models additionally reported their performance using the multivariate R^2 index (Jiang, Englehart et al. 2009), assessing each trial between $0\% \le R^2 \le 100\%$, i.e. as a percent of total signal variance of the known force. Identical modeling was separately performed for the other three DoFs (Opn-Cls, Rad-Uln and Pro-Sup).

7.2.2.3 Two-DoF Dynamic Models

Similar 2-DoF EMG-force models were evaluated (including backward stepwise selection of EMG channels based on RMS error, and two-fold cross-validation) for each of the three pairs of dimensions tested (Opn-Cls paired with one wrist DoF), except these models always estimated two DoFs simultaneously. Thus, each EMG channel contributed to each DoF. All six combinations of three different training paradigms and two testing paradigms were performed to evaluate the best modeling strategy. The training paradigms were: training with 1-DoF trials, with 2-DoF trials, or with both 1- and 2-DoF trials. The testing paradigms were: testing on 1-DoF trials or on 2-DoF trials. When testing on 1-DoF trials for these 2-DoF models, the non-used dimension would be expected to remain near a zero value throughout the trial. These 1-DoF tests were intended to determine if 2-DoF models could still perform well when encountering 1-DoF tasks (common to prosthesis use). Again, multivariate R^2 index was also reported on a subset of the models.

7.2.2.4 Statistics

Performance differences were tested statistically with SPSS 22 using multivariate repeated measures analysis of variance (RANOVA), assessing all possible interactions. When ε was <0.75, degrees of freedom was adjusted by the method of Greenhouse-Geisser; and when 0.75≤ε<1, it was adjusted by the method of Huynh-Feldt (Girden 1992, p. 21). *Post hoc* pair-wise comparisons were conducted using paired *t*-tests with Bonferroni correction for multiple comparisons. A significance level of $p = 0.05$ was used.

7.3 Results

7.3.1 One-DoF Models

Fig. 7.2 shows sample time-series EMG-force test results for the 1-DoF models (i.e., separate models formed for each DoF from trials that only examined each respective DoF). Fig. 7.3 shows summary RMS error results as a function of number of electrodes selected. Using all the RMS error results of one-DoF models, a two-way RANOVA was computed (factors: DoF; and number of electrodes, *E*). Number of electrodes was significant [$F(1.8, 14.7) = 99$, $p_{GG} < 0.001$], but DoF was not [$F(3, 24) = 0.54$, $p = 0.66$]. *Post hoc* comparisons for number of electrodes only found that 1 backward-selected electrode exhibited higher error than more than 1 electrode ($p \leq 0.001$); and 10 electrodes exhibited lower error than 13 electrodes ($p = 0.006$). Table 7.1 (top row, left-most four result columns) shows the RMS errors for 2 backward-selected electrodes (typical in a commercial 1-DoF prosthesis controller), for each DoF. The right-most four columns of Table 1 (top row), for comparison, show the R^2 index values corresponding to these RMS errors.

7.3.2 Two-DoF Models

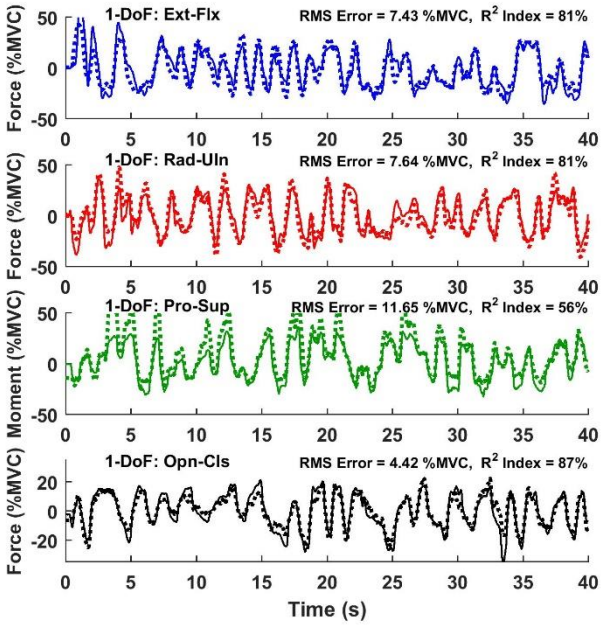

Fig. 7.2. Example time-series plots of 1-degree-of-freedom models, two electrodes (Subject 46, Trials 31, 35, 39 and 43). Solid lines are actual forces/moment, dashed lines are EMG-estimated. Note the difference in *y*-axis scales.

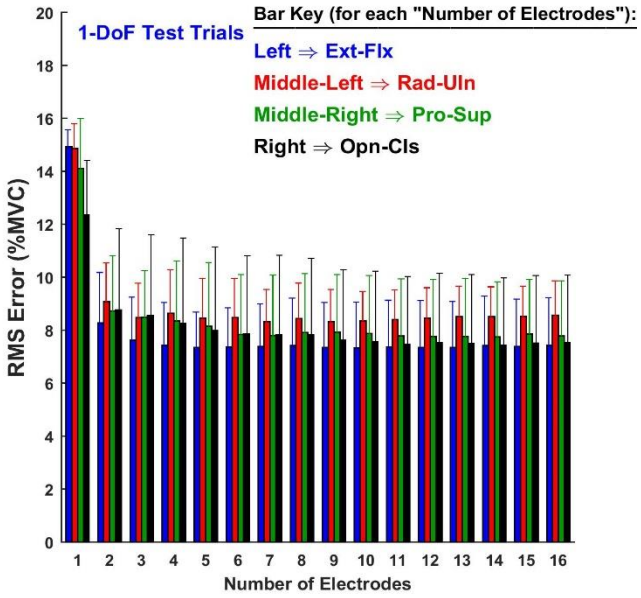

Fig. 7.3. Summary RMS error results: 1-degree-of-freedom models, nine subjects. Error lines show one standard deviation above the mean.

Two-DoF models always estimated Opn-Cls with one other DoF (Ext-Flx, Rad-Uln or Pro-Sup) simultaneously. Fig. 7.4 shows sample time-series EMG-force test results during 2-DoF trials. Table 7.1 (middle three and lower three rows) and Fig. 7.5 show a set of RMS error summary results. For comparison, Table 7.1 (right) shows the corresponding R^2 index values.

7.3.2.1 Two-DoF Models Assessed on 1-DoF Trials

For 2-DoF models assessed on the 1-DoF trials, a three-way RANOVA of RMS errors (factors: DoF, number of electrodes and training condition—either 1-DoF trials, 2-DoF trials or both) found an interaction between number of electrodes and training condition; the main effect of DoF was not significant [$F(2, 16) = 0.74$, $p = 0.5$]. Thus, separate two-way RANOVAs were computed with each of the training conditions fixed. We fixed the training condition because it had the smallest number of degrees of freedom and represented different variants on how a prosthetist might perform electrode site selection. There were no interactions in each of these two-way RANOVAs.

Results when training with 1-DoF trials were significant for the main effect of number of electrodes [$F(1.3, 10.6) = 37$, $p_{GG} = 10^{-4}$], but not for DoF [$F(2, 16) = 2.7$, $p = 0.1$]. *Post hoc* analysis of number of electrodes only found that 1 electrode exhibited higher error than more than 1 electrode ($p < 0.03$), 2 electrodes higher than 6–9 or 16 electrodes ($p < 0.04$), 3 electrodes higher than 6 and 9 electrodes ($p < 0.05$),

4 electrodes higher than 6, 7, 9 or 16 electrodes ($p < 0.05$), and 5 electrodes higher than 7 or 9 electrodes ($p < 0.03$).

Differences in RMS error results when training with 2-DoF trials were not significant for either the main effect of number of electrodes [$F(2.2, 17.9) = 0.5$, $p_{GG} = 0.6$] or DoF [$F(2, 16) = 0.5$, $p = 0.6$].

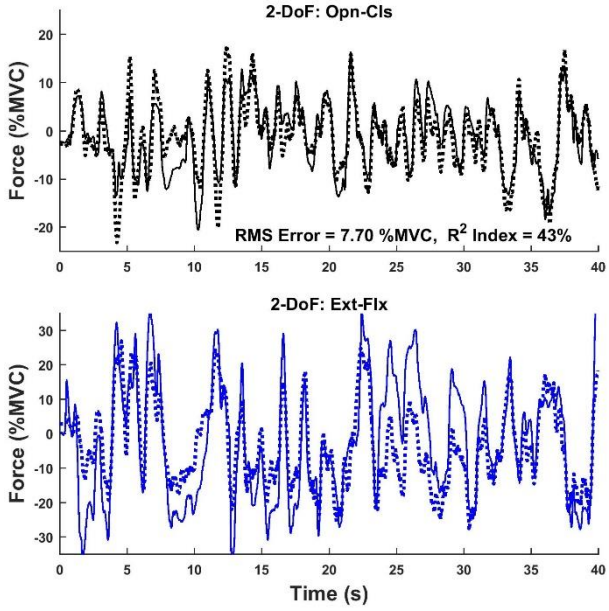

Fig. 7.4. Example time-series plots of 2-degree-of-freedom models applied to co-contraction trials from subject 46, trial 51 (four electrodes). Key: solid lines=actual forces, dashed=estimated; black=Opn-Cls, blue=Ext-Flx. Four EMG channels and training from both 1- and 2-DoF trials. Note the difference in *y*-axis scales

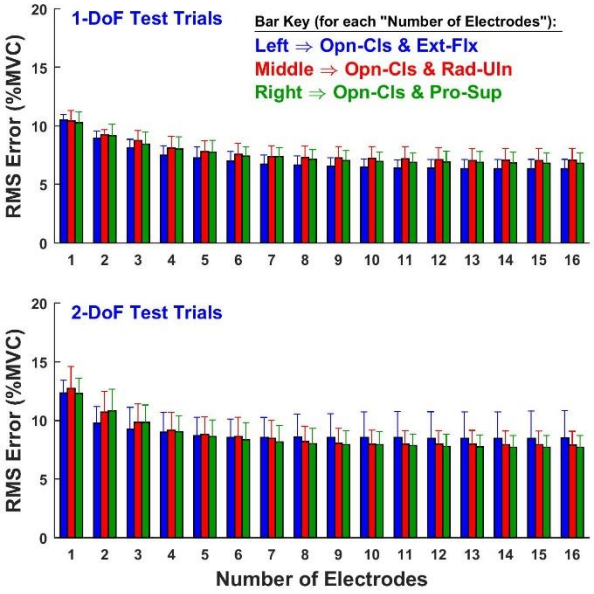

Fig. 7.4. Example time-series plots of 2-degree-of-freedom models applied to co-contraction trials from subject 46, trial 51 (four electrodes). Key: solid lines=actual forces, dashed=estimated; black=Opn-Cls, blue=Ext-Flx. Four EMG channels and training from both 1- and 2-DoF trials. Note the difference in *y*-axis scales

Results when training with both 1- and 2-DoF trials (Fig. 7.5, top) were significant for both main effects of number of electrodes [$F(1.5, 11.9) = 53$, $p_{GG} = 10^{-5}$] and DoF [$F(2, 16) = 6.7$, $p = 0.008$]. *Post hoc* analysis of number of electrodes only found that 1 electrode exhibited higher error than more than 2 electrodes ($p < 0.03$), 2 electrodes higher than more than 3 electrodes ($p < 0.03$), 3 electrodes higher than more than 5 electrodes ($p < 0.05$), and 4 electrodes higher than 12 or 13 electrodes ($p < 0.04$). *Post hoc* analysis of DoF only found that Opn-Cls with Ext-Flx had lower error than Opn-Cls with Rad-Uln ($p = 0.02$).

Table 7.1 (middle rows) shows the RMS errors (and corresponding R^2 indexes) for 4 backward-selected electrodes. This number of electrodes is displayed since it is, arguably, the expected minimum for a commercial prosthesis controller (see Discussion). Lastly, we also computed a two-way RANOVA of RMS errors with number of electrodes fixed at the preferred value of four (factors: DoF, training condition). The main effect of DoF was not significant [$F(2, 16) = 0.2$, $p = 0.8$], but training condition was significant [$F(1.1, 8.8) = 90$, $p = 0.8$], without interaction. *Post hoc* analysis only found that training with only 2-DoF trials had higher errors than each of the other two training conditions $\left(p < 10^{-4}\right)$.

7.3.2.2 Two-DoF Models Assessed on 2-DoF Trials

For 2-DoF models assessed on the 2-DoF trials, a three-way RANOVA of RMS errors (factors: DoF, number of electrodes and training condition) found an interaction between number of electrodes and training condition; the main effect of DoF was not significant [$F(2, 16) = 0.3$, $p = 0.7$]. As justified above, separate two-way RANOVAs were computed with each of the training conditions fixed. There were no interactions in each of these two-way RANOVAs.

Results when training with 1-DoF trials were not significant for either the main effect of DoF [$F(2, 16) = 1.4$, $p = 0.3$] or number of electrodes [$F(1.5, 12.0) = 0.7$, $p_{GG} = 0.5$).

Results when training with 2-DoF trials were significant for the main effect of number of electrodes [$F(2.0, 15.8) = 66$, $p_{GG} = 10^{-6}$), but not for DoF [$F(2, 16) = 0.6$, $p = 0.5$]. *Post hoc* analysis of number of electrodes only found that 1 electrode exhibited higher error than more than 1 electrode ($p \leq 0.01$), and 2 electrodes higher than more than 3 electrodes ($p \leq 0.02$).

Table 7.1 Mean ± std. dev. RMS errors (%MVC, left) and corresponding R^2 indexes (right), nine subjects, backward selected electrodes

Condition	**DoF(s), RMS Errors (%MVC)**				**DoFs, R^2 Indexes (%)**			
1-DoF Models (2 electrodes)	**Ext-Flx**	**Rad-Uln**	**Pro-Sup**	**Opn-Cls**	**Ext-Flx**	**Rad-Uln**	**Pro-Sup**	**Opn-Cls**
Assessed on 1-DoF trials	8.3 ± 2.0	9.0 ± 1.6	8.7 ± 2.2	8.8 ± 3.3	74 ± 11	68 ± 8	66 ± 15	52 ± 23
2-DoF Models (4 electrodes)	**Ext-Flx & Opn-Cls**	**Rad-Uln & Opn-Cls**	**Pro-Sup & Opn-Cls**		**Ext-Flx & Opn-Cls**	**Rad-Uln & Opn-Cls**	**Pro-Sup & Opn-Cls**	
Assessed on 1-DoF trials:								
Train with 1-DoF trials	7.3 ± 1.4	8.0 ± 1.2	7.9 ± 1.0		48 ± 15	40 ± 16	41 ± 10	
Train with 2- DoF trials	11.9 ± 3.2	11.5 ± 3.2	12.0 ± 2.8		20 ± 10	22 ± 11	17 ± 13	
Train with 1-, 2- DoF trials	7.4 ± 0.8	8.0 ± 1.0	7.9 ± 1.0		45 ± 12	39 ± 14	40 ± 13	
Assessed on 2-DoF trials:								
Train with 1-DoF trials	11.6 ± 2.7	11.7 ± 2.0	13.0 ± 3.7		25 ± 22	26 ± 10	6 ± 15	
Train with 2-DoF trials	9.0 ± 3.0	8.6 ± 2.3	7.8 ± 1.2		53 ± 18	57 ± 14	59 ± 7	
Train with 1-, 2-DoF trials	9.2 ± 2.0	9.2 ± 1.6	9.2 ± 1.4		46 ± 19	50 ± 10	43 ± 10	

Results when training with both 1- and 2-DoF trials were significant for the main effect of number of electrodes [$F(1.6, 12.9) = 99$, $p_{GG} = 10^{-6}$], but not for DoF [$F(2, 16) = 0.07$, $p = 0.9$]. *Post hoc* analysis of number of electrodes only found that 1 electrode exhibited higher error than more than 1 ($p < 0.003$), 2 electrodes higher than more than 3 electrodes ($p < 0.003$), 3 electrodes higher than more than 5 electrodes ($p < 0.02$), 4 electrodes higher than more than 5 electrodes ($p < 0.03$), and 5 electrodes higher than 6 or 10–13 electrodes ($p < 0.05$).

Table 7.1 (lower rows) shows the RMS errors (and corresponding R^2 indexes) for 4 electrodes. Lastly, we also computed a two-way RANOVA of RMS errors with number of backward-selected electrodes fixed at the preferred value of four (factors: DoF, training condition). The main effect of DoF was not significant [$F(2, 16) = 0.03$, $p = 1.0$], but training condition was significant [$F(1.1, 8.8) = 23$, $p_{GG} = 0.001$], without interaction. *Post hoc* analysis found that training with only 1-DoF trials had higher errors than each of the other two training conditions ($p < 0.01$), and training with only 2-DoF trials had marginally lower error than training with 1- and 2-DoF trials ($p = 0.045$).

7.3.3 Electrodes Selected

It is helpful to summarize the extent to which the selected electrode locations were distributed about the forearm. When selecting to two electrodes in 1-DoF models, there exist two interposing electrode distances. The average distance must equal 8 electrodes (out of 16 total). An interposing distance of 1 electrode denotes adjacent electrodes. Fig. 7. 6-left shows the distribution of the *minimum* interposing distance, aggregating the results across four DoFs, two cross-validations and nine subjects. The mean ± std. distance was 31 ± 12% of forearm circumference. When selecting to four electrodes in 2-DoF models, there exist four interposing distances (with an average distance of 4 electrodes). Fig. 7. 6-right shows the distribution of *each* interposing distance (same aggregation), when training with both 1- and 2-DoF trials. The mean ± std. distance was 25 ± 17% of forearm circumference. Overall, the selected electrodes were rarely adjacent, but not necessarily spaced equally about the forearm.

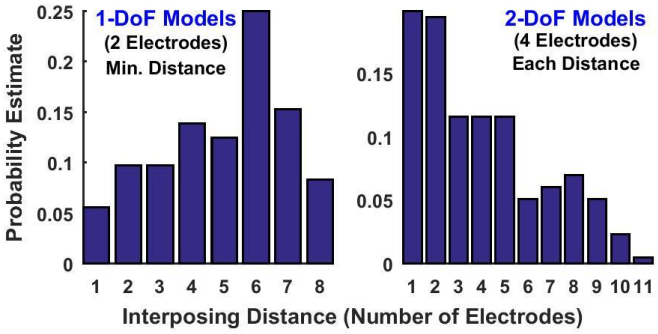

Fig. 7.6. Distribution of interposing electrode distances aggregated across all DoFs, two cross-validations and nine subjects. Left shows proportion of *minimum* distances for the 1-DoF models with two electrodes. Right shows proportion of *each* of distance for the 2-DoF models, trained with 1- and 2-DoF trials, with four electrodes. Total of 16 electrodes per subject.

A more detailed representation of electrode site selection for each subject is shown in Fig. 7 for 2-DoF, four-channel models, trained using both 1- and 2-DoF trials, for Ext-Flx & Opn-Cls. Similar results were found for the other DoF pairs. Fig. 7.7 shows, for each subject, the order in which electrodes were removed, as well as the four retained electrodes. This information is provided for the two distinct training folds used in our cross validation approach. Overall, the four selected sites were spread rather evenly around the circumference of the forearm. Comparing the four selected sites between the two (cross validated) training sets, on average 2.9 ± 0.60 sites were identically selected by both cross validation folds, 3.3 ± 0.50 selected sites were within one electrode distance of each other, and 3.9 ± 0.33 of the four selected sites were within

two electrode distances of each other. Thus, there was substantial consistency between selected electrodes when comparing between training sets.

7.4 Discussion

7.4.1 Electrodes Selected

One-DoF models were studied to quantify the existing state of the art in 1-DoF EMG-force, at least as assessed on these tasks and with this protocol. Fig. 7.3 and its associated statistical results show, as expected, rather poor performance when only one electrode is retained in the models. EMGσ is a non-negative (unipolar) quantity, yet 1-DoF wrist force/moment is bipolar; thus, one would not expect one EMG channel to accurately relate to these outputs when using linear models. It is for this reason that common 1-DoF proportional EMG controllers utilize the difference between agonist and antagonist EMGσ values (Mann 1981, Parker, Englehart et al. 2006), forming a bipolar signal from two unipolar signals. Our results herein confirm the need for two EMG channels (Cavanaugh, Clancy et al. 1983), and show statistically that additional channels (beyond two) provide no benefit. (Considering the overall error trends vs. number of electrodes, the statistical difference found between 10 and 13 electrodes is arguably a statistical anomaly.) Our results found no RMS error differences vs. DoF. However, the smaller range of forces in Opn-Cls suggests higher relative errors in this DoF. With two backward-selected electrodes, the mean errors ranged from 8.3–9.0 %MVC, depending on the DoF.

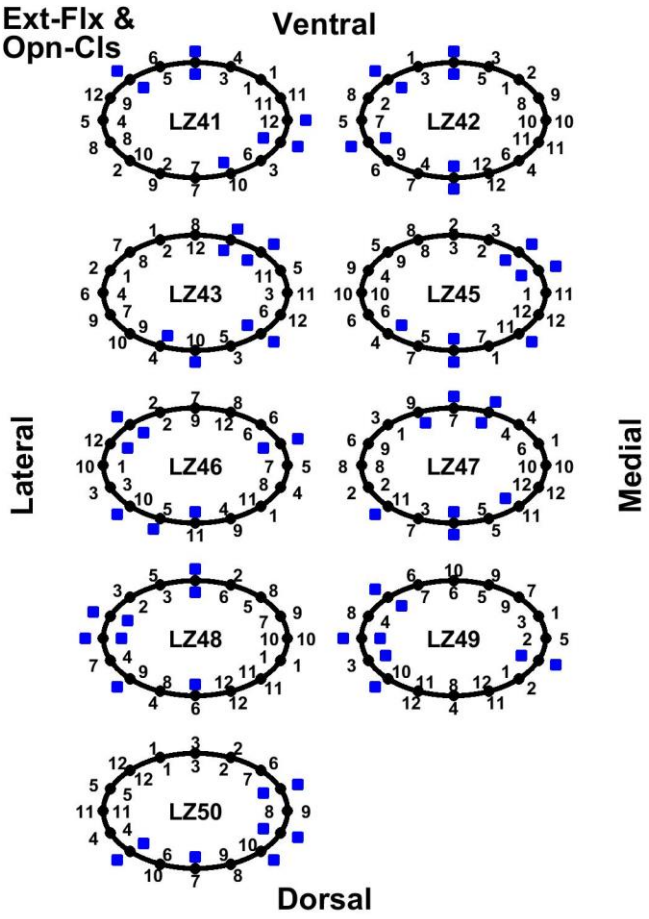

Fig. 7.7. Electrodes selected for 2-DoF, four-channel models, trained using both 1- and 2-DoF trials, for Opn-Cls & Ext-Flx. Results shown for each subject, with subject code shown at the center of each result "circle." Numbers along circle exteriors list the order of electrode elimination for the first cross validation set (e.g., "1" corresponds to first electrode eliminated); while numbers along circle interiors list elimination order for the second cross validation set. Twelve of 16 electrode sites were eliminated for each model. Number locations correspond to electrode locations, as labeled (i.e., lateral, medial, dorsal, ventral forearm). Blue boxes denote the four selected electrodes.

7.4.2 Two-DoF Models

We initially assessed our 2-DoF models on 1-DoF tasks, since 2-DoF prosthesis controllers would still be operated for use in 1-DoF tasks. When training with 1-DoF trials, or both 1- and 2-DoF trials, error was reduced as the selected number of electrodes increased from one until approximately four–five. And, there was preference for *lower* errors when combining Opn-Cls with Ext-Flx, but only when training with both 1- and 2-DoF trials. When the number of electrodes was fixed at four, training with only 2-DoF trials produced higher errors. Hence, the finding of no significant difference vs. number of electrodes when training with only 2-DoF trials would seem moot—this training condition performs poorly and, thus, would not be used.

We next assessed our 2-DoF models on 2-DoF tasks—the prime goal of this work. In general, Table 1 (lower rows) shows that higher average errors were found, compared to assessment on 1-DoF tasks. However, direct comparison between 1-DoF assessment and 2-DoF assessment is not appropriate. In 1-DoF assessment of 2-DoF models, errors in the second DoF were assessed, but their truth values were near zero (as the second DoF was not active). Hence, higher errors are expected in the 2-DoF assessments, since the average %MVC level (across both DoFs) is much higher (Clancy, Martinez-Luna et al. 2017). (Both DoFs were active, and higher effort levels produce higher errors, in general.) When training with 2-DoF trials or both 1- and 2-DoF trials, error was reduced as the selected number of electrodes increased from two until 4–6. Fig. 7.5 (bottom) suggests that most of the improvement happened when the number of electrodes was less than 4–5. And, there was no error dependence vs. DoF. When the number of electrodes was fixed at four, training with only 1-DoF trials produced higher errors. Hence, the finding of no significant difference vs. number of electrodes when training with only 1-DoF trials would seem moot—this training condition performs poorly and, thus, would not be used.

For model training, a single training procedure is required, after which the model is used on both 1-DoF and 2-DoF tasks. The summary of results in the prior paragraph shows that the clearly advantageous training technique is to use both 1- and 2-DoF trials, because this technique produced the lowest errors when assessing 1-DoF and also 2-DoF tasks. This result is undesired, since training would be simpler if only 1-DoF trials were required. Substantial concentration is required to track a random target in two dimensions; simpler tracking is found with only 1-DoF targets. It is, however, not overly surprising that training on both 1- and 2-DoF trials provides the best performance when assessing across both 1- and 2-DoF tasks (Ljung 1999). And, as mentioned previously, training trials of sufficiently long duration so as to permit electrode site selection are only required during the prosthesis fitting task.

For number of backward selected electrodes, there was generally no statistical advantage in the 2-DoF models to having more than approximately four electrodes. Fig. 7.5 shows a trend for some (limited)

improvement due to more than four electrodes. A larger sample size might have borne out this trend statistically, although the likely strength of the error reduction seems small (once the number of electrodes exceeds four). Again, since two bipolar DoFs are being estimated, it is not surprising that at least four unipolar EMGσ channels are appropriate.

Our goal was to facilitate 2-DoF EMG-force, which could be mapped to 2-DoF SIP control of a hand-wrist prosthesis. However, which pair of DoFs to utilize was not assumed *a priori*. We required hand Opn-Cls to be one of the DoFs, but examined pairings with Ext-Flx or Rad-Uln or Pro-Sup. Some previous literature has found higher errors when including the Pro-Sup DoF (Jiang, Englehart et al. 2009, Jiang, Vest-Nielsen et al. 2012). In our work, no preferred DoF pair seemed to emerge with regard to accuracy. This result suggests that the most intuitive wrist contraction for the prosthetic motion that is being controlled can be selected. Currently, only powered wrist pronation-supination mechanisms are commercially available in the U.S. However, other devices are available outside of the U.S. and more are under development.

7.4.3 Comparison of RMS error to R^2 index

Average RMS errors are compared to their corresponding R^2 indexes in Table 1, for 2-channel 1-DoF models and 4-channel 2-DoF models—the preferred number of EMG channels for these respective models. Additional comparisons are provided within the examples shown in Fig. 7.2 and Fig. 7.4. RMS error measures (typically normalized to %MVC) are common in EMG-force studies (Staudenmann, Kingma et al. 2006, Hashemi, Morin et al. 2015, Clancy, Martinez-Luna et al. 2017, Dai, Bardizbanian et al. in press); while correlation-based measures (R^2 index, variance accounted for) have also been used (Kearney, Stein et al. 1997), particularly in recent EMG-based prosthesis control studies (Jiang, Englehart et al. 2009, Nielsen, Holmgaard et al. 2011, Jiang, Vest-Nielsen et al. 2012, Ameri, Kamavuako et al. 2014). Table 1 shows that the RMS and R^2 measures have extremely tight *relative* correspondence *within* a given task (i.e., within a given row of Table 1). That is, the respective performances rise and fall in unison (albeit using inverted and distinct scaling) and show very similar rank order performance. The only apparent exception to this trend within Table 1 is the row 1 Opn-Cls R^2 index value (52 ± 23%), which is noticeably lower than the other 1-DoF values, although its corresponding RMS value is not. However, the Opn-Cls DoF used a smaller MVC range (15%) than the other DoFs (30%), representing a distinct task.

The lower rows of Table 1 show R^2 index values for the 2-DoF models which, at first glance, appear quite low (best average values between 40% and 50%). However, the example in Fig. 7.4 shows a 2-DoF model in which the RMS error of 7.70 %MVC corresponds to an R^2 index of 43%. Visually, the actual and estimated forces track reasonably well in this example. In addition, each of the 2-DoF models included Opn-Cln, which produced lower R^2 index values for 1-DoF models. Hence, it is likely that the R^2 index for our 2-

DoF tasks produces values between 40–50% that reflect good performance. This observation of a tight *relative* correspondence between both measures within a task, but different *absolute* measure scales across distinct tasks—both within and between these two measures—is consistent with prior studies (Clancy, Bida et al. 2006, Clancy, Martinez-Luna et al. 2017). Thus, it can be ill-advised to blindly compare either quantitative measure *across* distinct tasks.

For this class of studies, the better measure of performance is not clear. RMS error is more intuitive (expressed in physical units or normalized to MVC), while correlation-based measures tend to be better at normalizing error from distinct tasks based on effort level. But, both measures also have their own drawbacks. We have previously argued that either measure is likely acceptable, since they both accomplish the primary assessment goal of distinguishing between the relative merits of various EMG-force options. The better performing algorithms are then the best candidates for future testing with an actual prosthesis controller. Further discussion and examples of distinctions between these two error measures as a function of task is available in (Clancy, Martinez-Luna et al. 2017).

7.4.4 Limitations

This study was an initial examination into using the backward stepwise selection method to site a minimum number of electrodes for simultaneous estimation of *force-varying* hand grip (Opn-Cls) and one wrist DoF. The target application was SIP control of a conventional hand-wrist prosthesis, although results can be helpful to the general 2-DoF EMG-force problem. Several limitations are evident.

First, laboratory results with able-bodied subjects must be interpreted cautiously, and ideally are primarily used to refine signal processing techniques, screen out unsuccessful approaches and help plan for studies with limb-absent subjects. For example, the results of the work herein recommend the use of both 1- and 2-DoF trials for training and the use of a minimum of four backward-selected electrodes. Future work should explore how these results translate to limb-absent subjects performing clinically relevant tasks, such as activities of daily living assessed through functional outcomes measures. Such evaluations are important because, while statistical differences were observed in our tests, it is necessary to confirm that these statistical differences translate into changes in clinical performance.

Second, this EMG-force training technique was only studied in able-bodied subjects during a single session. Evaluation in limb-absent subjects should follow; including multi-session training, which has been shown to produce better performance (Powell, Kaliki et al. 2014, Hahne, Dahne et al. 2015). Additionally, session-to-session performance should be studied to evaluate how often EMG-force (re-)calibration should be conducted.

Third, we studied fixed-posture, dynamic contraction with a bandwidth of 0.75 Hz. Varying posture can alter the interpretation of EMG intent (Jiang, Muceli et al. 2013), and the re-donning of a prosthesis can produce subtle shifts in EMG sites and channel gains which may confound prosthesis control (Simon, Lock et al. 2012, Muceli, Jiang et al. 2014).

Fourth, our backward selection method for choosing electrodes (as a subset of the available 16) may not be unique or represent the only successful method. In limb-absent subjects, additional distal sites along the residual limb might prove advantageous. Further, the two distinct folds (from cross-validation) did not necessarily select the same electrodes. When choosing 4 electrodes from 16 total, there are 1820 combinations. Thus, a non-exhaustive search method seems advantageous. But, alternatives to backward selection exist, including selection based on anatomical locations (Fougner, Stavdahl et al. 2014) (appropriate for able-bodied subjects but perhaps problematic for limb-absent subjects who may have altered remnant anatomy), forward stepwise selection and backward-forward stepwise combinations.

Fifth, direct comparison of our *absolute* performance results to those of other studies is quite difficult, as performance is a function of many factors, including: contractions used for training/testing (wider bandwidth contractions and more forceful contractions should each lead to higher average errors, at least as measured in %MVC or physical units), the subject population (young vs. aged able-bodied subjects, vs. limb-absent subjects), the experimental conditions and tasks (ADLs (Light, Chappell et al. 2002, Lipschutz, Kuiken et al. 2006, Simon, Hargrove et al. 2011, Smith, Kuiken et al. 2014) vs. EMG-force measures), and the manner by which error is measured. Regardless, *relative* performance should be more interpretable across studies. In particular, our relative results suggest that: two electrodes are the minimum number for EMG-force estimation of our 1-DoF hand-wrist tasks, and additional electrodes do not reduce error; four electrodes are the minimum number for our 2-DoF tasks, with a few additional electrodes perhaps providing some limited accuracy improvement (which may not be clinically relevant); training for a 2-DoF model should include both 1-DoF and 2-DoF trials; and that we found no substantial evidence—based on accuracy—to either prefer or dissuade the pairing of the hand grip DoF with any of the three wrist DoFs when forming a 2-DoF hand-wrist EMG-force estimator. Therefore, the most intuitive wrist contraction to control the available powered prosthetic component can be used.

7.4.5 Implications for Prosthesis Control

The long-term implications for prosthetic control may best be understood via prosthesis testing in limb-absent subjects. But, the implication from able-bodied subjects is that as few as four backward-selected electrodes—trained from both 1- and 2-DoF trials—may provide 2-DoF EMG-force estimates that are as good (or nearly so) as those from 16 electrodes placed equidistant about the circumference of the forearm.

The automated backward selection algorithm is not biased towards *a priori* site locations, thus the altered anatomy of many limb-absent subjects may not adversely influence this site selection method, so long as the necessary information is available in the surface EMG—an assumption that will require evaluation.

Although we have evaluated site selection, training techniques and DoF pairing with an EMG-force/moment task, many prosthesis controllers map EMGσ to joint velocity (rather than joint torque). And, controllers routinely maintain a "dead zone" at EMGσ values near zero, so that the prosthesis does not actuate in response to EMG measurement noise at rest (Fougner, Stavdahl et al. 2014). These distinctions will need to be added to a controller that is based on our calibration method.

Our modeling techniques require measurement of an output force/moment. No such signal is available from limb-absent subjects. As a surrogate measure, unilateral limb-absent subjects can produce force/moment on the sound side and relate it to EMG produced on the limb-absent side during mirrored contractions (Nielsen, Holmgaard et al. 2011, Jiang, Vest-Nielsen et al. 2012, Muceli and Farina 2012, Ameri, Scheme et al. 2014, Hahne, Biebmann et al. 2014). Alternatively, all limb-absent subjects can directly activate their phantom limb to track a desired target effort pattern, and then relate EMGσ from the affected limb directly to this target (without feedback) (Ameri, Kamavuako et al. 2014, Ameri, Scheme et al. 2014). In either case, one disadvantage is the lack of proprioceptive feedback from the phantom limb.

Training duration is an important issue for prosthesis users. As noted previously, we envision a protocol in which site selection of the preferred number of electrodes (e.g., four of 16 candidate electrode sites) is performed by a prosthetist when fitting a permanent socket. During such a fitting, the several minutes of training time (or more) required when using our data collection protocol would not seem problematic, as the current process of manually siting two electrodes within a socket is already time consuming. Thereafter, a fielded prosthesis would only need an ability to calibrate the permanent (e.g., four) electrode channels. Further, it is also possible that the shape of the EMGσ-force frequency response of each channel might be fixed during fitting (e.g., by normalizing the DC gain to 1), leaving only the channel gains for field calibration—similar to existing prostheses that fix the lowpass filter applied to the rectified EMG, only permitting gain adjustments of each EMG channel. In either case, such a small number of free parameters might be trained in only a few seconds (Ljung 1999, Clancy, Liu et al. 2012). Reasonable field recalibration might be facilitated.

While we limited ourselves to hand grip in combination with one wrist DoF, the long-term goal is the development of upper-limb prostheses that also control individual finger actuation. Limited efforts have been made to do so based on surface EMG from the forearm (Huang and Chen 1999, Cipriani, Zaccone et al. 2008,

Smith, Tenore et al. 2008, Smith, Huberdeau et al. 2009, Cipriani, Antfolk et al. 2011, Khushaba, Kodagoda et al. 2012, Liu, Brown et al. 2013).

7.5 Conclusion

This laboratory study provided evidence that 2-DoF EMG-force estimation in the hand-wrist of able-bodied subjects can be successfully accomplished with the use of four electrodes, which are selected from 16 electrodes via backward stepwise selection. These models should be calibrated using both 1- and 2-DoF trials and there did not seem to be a preference as to which wrist DoF to pair with hand grip. With this training, Table 1 (lower rows) shows that 2-DoF estimation had average RMS testing errors of 9.2 %MVC for each DoF pair. Transition of these techniques to testing in hand-wrist prosthesis users is an appropriate next step.

Acknowledgements Supported by the Eunice Kennedy Shriver National Institute of Child Health & Human Development, U.S. National Institutes of Health (NIH) under award R43HD076519. The content is solely the responsibility of the authors and does not necessarily represent the official views of the NIH.

Conflict of Interest Authors Martinez-Luna, Hunt, Farrell and Clancy are/have been employed by Liberating Technologies, Inc., which has a potential financial benefit from the results of this research.

Chapter 8: Efficiently Training Two-DoF Hand-Wrist EMG-Force Models

This chapter is published as: Berj Bardizbanian, Ziling Zhu, Jianan Li, Xinming Huang, Chenyun Dai, Carlos Martinez-Luna, Benjamin E. McDonald, Todd R. Farrell, Edward A. Clancy, "Efficiently Training Two-DoF Hand-Wirst, EMG-Force Models," *2020 42nd Annual International Conference of IEEE Engineering in Medicine & Biology Society (EMBC)*, 20–24 July, 2020. Color Versions of one or more of the figures in this paper are available online at: https://ieeexplore.ieee.org/abstract/document/9175675.

***Abstract*— Single-use EMG-force models (i.e., a new model is trained each time the electrodes are donned) are used in various areas, including ergonomics assessment, clinical biomechanics, and motor control research. For one degree of freedom (1-DoF) tasks, input-output (black box) models are common. Recently, black box models have expanded to 2-DoF tasks. To facilitate efficient training, we examined parameters of black box model training methods in 2-DoF force-varying, constant-posture tasks consisting of hand open-close combined with one wrist DoF. We found that approximately 40–60 s of training data is best, with progressively higher EMG-force errors occurring for progressively shorter training durations. Surprisingly, 2-DoF models in which the dynamics were universal across all subjects (only channel gain was trained to each subject) generally performed 15–21% better than models in which the complete dynamics were trained to each subject. In summary, lower error EMG-force models can be formed through diligent attention to optimization of these factors.**

8.1 Introduction

Over the past several decades, numerous investigators have studied the dynamic system relationship between the conventional surface electromyogram (EMG) and muscle force/joint torque (Buchanan, Lloyd et al. 2004, Staudenmann, Roeleveld et al. 2010). Much of this modeling trains an EMG-force model for single-use (i.e., a new model is trained each time the electrodes are applied), applicable to areas such as ergonomics assessment, clinical biomechanics, scientific studies relating EMG to joint mechanical impedance, and motor control research. Single-use EMG-force calibration is appropriate, as there is evidence of inter-day decrements in performance when an EMG-force model is not re-calibrated (Oskouei, Paulin et al. 2013). Some emerging studies have introduced the use of large, high-density surface EMG arrays (Muceli and Farina 2012, Liu, Brown et al. 2013, Hahne, Biessmann et al. 2014). But, these arrays generally remain rather complex and expensive for biomechanics investigations, and are presently impractical for most commercial applications of EMG.

In one modeling paradigm, EMG-force dynamics are assumed (e.g., length-tension and force-velocity relationships) and only the gains of each EMG channel are optimized (Hof and Van den Berg 1981, Buchanan, Lloyd et al. 2004). This "Hill-style" paradigm is simpler and of particular benefit in multi-joint studies for which training of system dynamics would be a daunting task. Alternatively, the "black box" system identification paradigm trains subject- and muscle-specific EMG-force models (Hof and Van den Berg 1981, Doheny, Lowery et al. 2008, Clancy, Liu et al. 2012, Hashemi, Morin et al. 2012, Hashemi, Morin et al. 2013, Hashemi, Morin et al. 2015, Liu, Liu et al. 2015). Because these models adapt to the specific subject and/or muscle, they would generally be hypothesized to be more accurate than Hill-style models, but require longer training trials (Ljung 1999) and more effort to program. For simplicity, most early work in this area focused on linear models of single-joint systems. Non-linear models, however, have been shown to improve the relationship (Vredenbregt and Rau 1973, Hashemi, Morin et al. 2012, Dai, Bardizbanian et al. 2017).

Recently, there has been increased interest in expanding these black box models to multi-joint applications, for example to two degree of freedom (DoF) systems in the upper limb (Hahne, Biessmann et al. 2014, Clancy, Martinez-Luna et al. 2017, Hahne, Schweisfurth et al. 2018, Dai, Zhu et al. 2019). In doing so, several technical questions related to system identification are encountered. Previously (Dai, Zhu et al. 2019), we studied 2-DoF EMG-force in the hand-wrist, finding lower errors when training sets included both 1-DoF and 2-DoF trials. Further, we studied the required number of conventional electrodes, when placed eqidistant about the circumference of the proximal forearm. Using backward stepwise selection of 16 electrodes, we found that error was optimized with 6 electrodes. Of course, backward selection of electrode sites may have limited utility in single-use EMG-force studies, since all 16 electrodes must still be applied.

These insights narrow the range of system identification methods that need be considered when conducting single-use EMG-force studies. However, other modeling questions remain: determining the necessary duration of training data used to form the EMG-force relationship and choosing the specificity of the model (subject-specific vs. DoF-specific models of dynamics vs. a "universal" Hill-style model of dynamics used for all subjects and muscles). Herein, we examine these questions when relating forearm surface EMG to hand open-close (Opn-Cls) combined with one of three wrist DoFs—either extension-flexion (Ext-Flx) force, radial-ulnar (Rad-Uln) force, or pronation-supination (Pro-Sup) moment.

8.2 Methods

8.2.1 Experimental Data and Apparatus

Data Collection—Setup: The WPI IRB approved reprocessing of previously acquired data from able-bodied subjects (5 males, 4 females; aged 27±9.7 years) (Dai, Zhu et al. 2019). Subjects sat at the experimental apparatus (see (Dai, Zhu et al. 2019), Figs. 1–3) with their dominant hand cuffed to a 6-DoF load cell, to measure wrist force/torque. Separately, Opn-Cls grip force was measured by a single-axis load cell by securing to the thumb on one side and the distal aspects of the four fingers on the opposite side. The shoulder was flexed 45º forward from the anatomical position along the sagittal plane, the wrist was in a neutral position and the palm of the hand was perpendicular with the plane of the floor. The elbow was supported.

Skin about the forearm was scrubbed with an alcohol wipe and electrode gel was applied. Sixteen bipolar EMG electrodes were applied equidistant and circumferentially about the forearm: their mid-point was located 5 cm distal to the elbow crease. Bipolar electrodes were 5 mm diameter, stainless steel, hemispherical contacts separated 1 cm edge-to-edge, oriented along the forearm's long axis. A gelled reference electrode was secured on the ventral forearm. Each EMG signal was differentially amplified (30–500 Hz pass band, CMRR > 100 dB over the pass band). Load cell force/moment was displayed in real-time as a blue arrowhead on a computer screen. The arrowhead displayed 4 DoFs: x-axis location for Ext-Flx force, y-axis location for Rad-Uln force, rotation for Pro-Sup moment, and size for hand Opn-Cls force. A second red arrowhead displayed a computer-controlled target. Four load cell signals and 16 EMG channels were each sampled at 2048 Hz with 16-bit resolution.

Data Collection—Contractions: All contractions were constant-posture, with a two-minute rest interval between each. After warm-up, maximum voluntary contraction (MVC) was measured separately for both directions of each of the 4 DoFs. Next, subjects produced 5 s constant-force 50% MVC contractions for each direction within a DoF.

Then, subjects completed 1-DoF *dynamic* tracking trials, separately for each DoF (randomized order). Feedback only displayed the specified DoF. For Rad-Uln, the target moved randomly between ±(|30 %MVC Rad| + |30 %MVC Uln|)/2. The random target movement was a 0.75 Hz band-limited, white and uniform random process. Four trials of 40 s duration each were completed. The equivalent trials were completed for the three remaining DoFs (16 trials total); except that the maximum force was reduced to 15 %MVC for Opn-Cls due to excessive hand open fatigue found during preliminary testing.

Lastly, subjects tracked *dynamic* 2-DoF targets: hand Opn-Cls paired with one wrist DOF (Ext-Flx, Rad-Uln or Pro-Sup). The same random target style was used, with independent random instances per DoF. Four trials of 40 s duration were completed for each DoF combination (12 trials total).

8.2.2 Analysis: Signal Pre-Processing

Data analysis was performed offline in MATLAB. Time-varying EMG standard deviation (EMGσ[n], for discrete-time sample n) was estimated for each channel. Raw EMG were highpass filtered (5th-order Butterworth, f_c=15 Hz), notch filtered to attenuate power-line interference (2nd-order IIR filter at 60 Hz, notch bandwidth of 1 Hz), rectified, lowpass filtered at 16 Hz (Chebyshev Type 1 filter, 9th-order, 0.05 dB peak-to-peak passband ripple), and downsampled to 40.96 Hz (Ljung 1999, Clancy, Bida et al. 2006). Each force/moment signal was normalized by its corresponding MVC level pair. For example, Rad-Uln was normalized by: $(|MVC_{Rad}| + |MVC_{Uln}|)/2$.

8.2.3 Analysis: One-DoF Models

1) Subject-Specific, Full-Duration Model: One-DoF modeling only utilized 1-DoF trials. EMGσ values were related to force/moment—separately for each DoF—via regression (20^{th}- order linear dynamic model (Clancy, Liu et al. 2012, Dai, Zhu et al. 2019); 2 or 16 electrodes used in the fit, where values less than 16 were arrived at using backward stepwise selection (Clancy, Martinez-Luna et al. 2017, Dai, Zhu et al. 2019)). Model training used the least squares pseudo-inverse method (Press, Flannery et al. 1994), with singular values of the design matrix removed if the ratio of their magnitude to that of the largest singular value was less than 0.01 (Clancy, Liu et al. 2012). Note that backward selection down to 2 electrodes has previously been shown to perform as well as 16 electrodes for these 1-DoF tasks (Clancy, Martinez-Luna et al. 2017, Dai, Zhu et al. 2019). Two trials were used for training, and two for testing (RMS error between the estimated and measured torques, expressed in %MVC, after discarding the first 2 s of each trial). Training and testing trials were then exchanged (two-fold cross-validation), with the average of these two folds reported.

2) Subject-Specific, Reduced-Duration Model: The above procedure was repeated while utilizing less than the full available training time, thus varying the time duration used for training. In this manner, we could

evaluate model performance vs. training duration. For training durations of 14, 22, 30 and 38 s, only the necessary initial portion of the first training trial was used, and the second training trial was ignored. For training durations of 44, 52, 60, 68 and 76 s, equal durations of both training trials were used (half of the training duration derived from each trial). As above, model testing used both full testing trials, with the two-fold cross-validation results averaged.

3) DoF-Specific Model: General dynamic models, one per DoF, were next constructed, using data from 1-DoF trials. Two trials were used to train subject-specific models for each subject. After backward selecting down to the channels preferred for EMG-force estimation, the fit coefficients define a FIR filter, which is inherently lowpass in shape (Inman, Ralston et al. 1952, Hof and Van den Berg 1981, Winter and Yack 1987, Winter 2005, Koirala, Dasog et al. 2015, Clancy, Negro et al. 2016). These filters were each normalized to a gain of one at 0 Hz—expressing the EMGσ-force dynamics, absent of the gains for each EMG channel. A total of 36 gain-normalized filters were formed per DoF (nine subjects, two EMG channels per subject, two cross-validations). The ensemble mean coefficient values of these filters (one filter per DoF) were computed.

This DoF-specific filter was used, in place of the dynamics provided by subject-specific filters by appending them to the EMG pre-processing (after the decimation step). This evaluation assessed if subject-specific, EMG channel-specific calibration of dynamics could be replaced with one dynamic filter per DoF. Once the DoF-specific filters were formed, the training trials were used to calibrate *only* the gains of each EMG channel. Testing was performed on the remaining two trials. Backward stepwise selection from 16 down to 2 electrodes was performed, with only results for 2 and 16 EMG channels reported (with cross-validation). This analysis was completed for each of the DoFs and training durations.

4) Universal Model: This analysis was similar to the prior analysis, except that the 36 DoF-specific filter coefficients were ensemble averaged into one "universal" filter (Fig. 8.1) to assess if one filter shape could

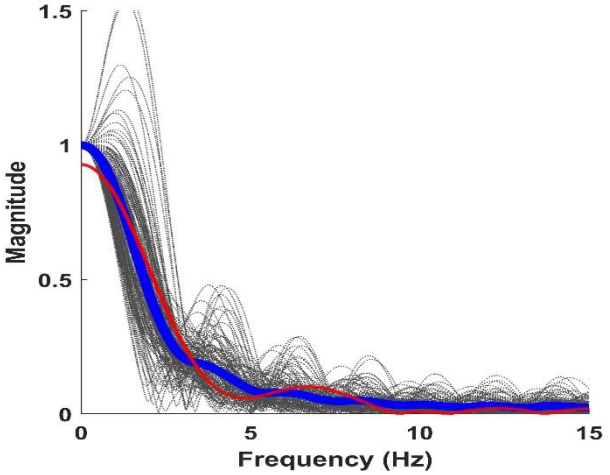

Fig. 8.1. Each of 144 magnitude responses of the 1-DoF models is shown in grey (nine subjects, two EMG channels per subject, two cross-validations, 4 DoFs). Thick blue line is the average and thin red line is the universal FIR filter fit to these responses.

capture all dynamics for all DoFs. Again, analysis was completed for all training durations and only the results for 2 and 16 EMG channels are reported.

8.2.4 Analysis: Two-DoF Models

Similar 2-DoF EMG-force models were evaluated (with backward stepwise selection to 6 EMG channels and two-fold cross-validation) for each of Opn-Cls paired with one wrist DoF, always estimating 2 DoFs simultaneously. Each EMG channel contributed to both DoFs. Model training always combined both 1-DoF trails and the corresponding 2-DoF trial. Model testing was performed only using the 2-DoF trials. Note that backward selection down to 4–6 electrodes has previously been shown to perform nearly as well as 16 electrodes for these 1-DoF tasks (Clancy, Martinez-Luna et al. 2017, Dai, Zhu et al. 2019).

8.2.5 Statistics

Performance differences were tested statistically with SPSS 25 using multivariate RANOVA. Interactions were not significant, unless noted. When degree of sphericity ε was <0.75, degrees of freedom was adjusted by the method of Greenhouse-Geisser; and when $0.75 \leq \varepsilon < 1$, by the method of Huynh-Feldt (Girden 1992). When multiple comparisons are summarized, degrees of freedom are reported without adjustment. Tukey *post hoc* comparisons were conducted using Fisher's least significant difference (LSD). A significance level of $p = 0.05$ was used.

8.3 Results

8.3.1 One-DoF Models

Fig. 8.2 shows summary test error results vs. training duration for the 1-DoF models using 2 electrodes. All models experienced lower mean error as training duration increased from 14 s, with less improvement as training duration grew. Using all the results of 1-DoF models, a four-way RANOVA was computed [factors: model (subject-specific, DoF-specific, universal), number of electrodes (2, 16), duration (14, 22, 30, 38, 44, 52, 60, 68, 76 s) and DoF (Flx-Ext, Rad-Uln, Pro-Sup, Opn-Cls)]. Since there was a significant two way interaction term involving model and DoF [$F(2.5, 20.0) = 6.1$, $p_{GG} = 0.006$], three way RANOVA's were implemented fixing each DoF. The main effects were significant for model [$F(2,16)>77$, $p \leq 0.03$], except for Rad-Uln [$F(2,16)=3.5$, $p = 0.06$]; significant for duration [$F(8,64)>5$, $p \leq 0.04$]; but not significant for number of electrodes [$F(1,8)<6$, $p \geq 0.05$].

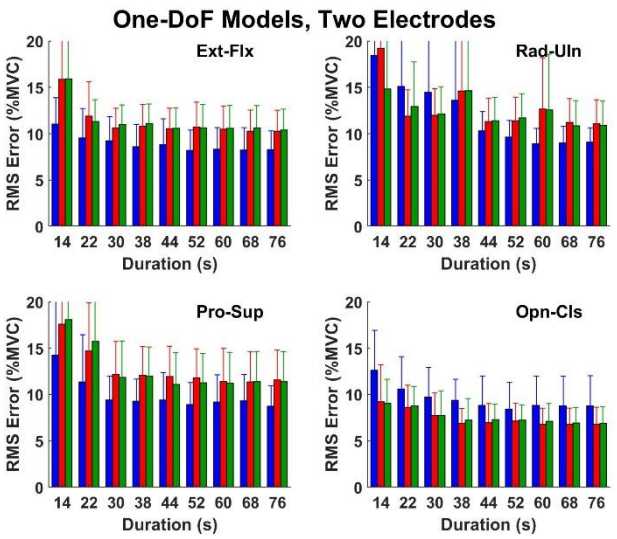

Fig. 8.2. One-DoF summary results for each DoF vs. training duration. Mean error plus one standard deviation shown for 2-electrode models. (Some error bars cropped by *y*-axis scaling.) Subject-specific models in blue, DoF-specific models in red, universal models in green.

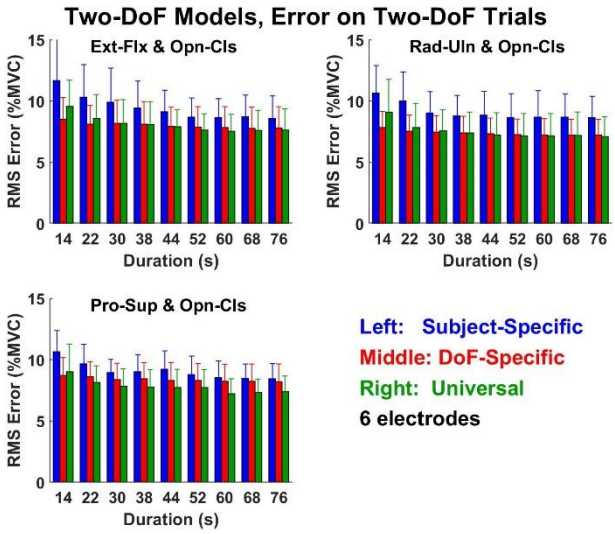

Fig. 8.3. Two-DoF summary results for each DoF pair vs. training duration, when assessing on 2-DoF trials. Mean error plus one standard deviation shown for 6-electrode models.

Tukey *post hoc* comparisons were computed for all significant differences. In summary, when comparing the 1-DoF models, the subject-specific model generally had the lowest errors. There was a clear trend for higher %MVC errors at shorter training durations versus longer durations. For example, training with 14 s always exhibited higher error than ≥ 30s and training with 22 s always exhibited higher error than ≥ 68s. Performance improvement plateaued at longer durations (e.g. there was no statistically significant improvement for durations beyond 30 s for Rad-Uln and Opn-Cls, or beyond 60 s for Ext-Flx and Pro-Sup). With two backward selected electrodes, a training duration of 60 s and subject specific modeling, average ± standard deviation errors (% MVC) were: 8.34 ± 2.32 for Ext-Flx, 8.92 ± 9.65 for Rad-Uln, 9.2 ± 2.93 for Pro-Sup and 8.81 ± 3.18 for Opn-Cls.

8.3.2 Two-DoF Models Assessed on Two-DoF Trials

Fig. 8.3 shows summary test error results vs. training duration for the 2-DoF models using 6 electrodes. All models experienced clearly lower error as training duration increased from 14 s, with less improvement as training duration grew. Using all the results of 2-DoF models, a four-way RANOVA was computed [factors: model (subject-specific, DoF-specific, universal), number of electrodes (6, 16), duration (14, 22, 30, 38, 44, 52, 60, 68, 76 s) and DoF pair (Opn-Cls with Flx-Ext, Opn-Cls with Rad-Uln, Opn-Cls with Pro-Sup). There were significant interactions involving model and duration [$F(16,128)=17$, $p=0.0001$]. Unfortunately, fixing a second factor did not eliminate interactions. Thus, we continued to pursue the non-interacting factors within this four-way RANOVA. These other main effects were significant for number of electrodes [$F(1,8)=16$, $p=0.004$] and not significant for DoF pair [$F(2,16)=0.6$, $p=0.6$]. Tukey *post hoc* comparisons found that using 6 electrodes had a significantly higher mean error than using 16 electrodes.

To examine the model and duration factors, we next performed Tukey pair-wise comparisons for each combination of these factors (with Bonferroni correction). Considering duration: subject-specific models with durations below 38 s always had higher errors than those with durations above 68 s; and DoF-specific and universal models with durations below 30 s always had higher errors than respective models with durations above 68 s. Considering model: subject-specific models always had 15–21% *higher* error than the other two models (except at a duration of 60 s—likely an anomaly), and DOF-specific models did not differ from universal models.

8.4 Discussion

8.4.1 Parameter Selection for Efficient EMG-Force Training

This research focused on two technical details related to forming 2-DoF EMG-force models at the hand-wrist. An ability to time-efficiently and accurately calibrate EMG-force models is of value to several application areas, including ergonomics assessment, clinical biomechanics, scientific studies of muscle tension and joint impedance. First, we examined the duration of training used to form the EMG-force relationship. For single-use applications, it is most useful to be able to train models quickly. With all 1-DoF models, error decreased in an exponential fashion as training duration

increased. These changes were consistently statistically significant at the shorter durations (where the slope of error vs. duration was largest), but less so at the longer training durations (where more statistical power would be required in order to identify the smaller presumed differences). Most of the error reduction occurred with durations up to 40–60 s. These hand-wrist results are consistent with 1-DoF EMG-force results in the elbow (Clancy, Liu et al. 2012), wherein 52 s of training data for similar dynamic models were found to reduce error compared to 26 s. For our 2-DoF models, a similar exponential trend was found (error decaying with increased training duration), but the rate of error decay was not as steep. This difference in rate may reflect that the final error was, on average, larger for the 2-DoF trials. These results are generally consistent with system identification theory, in which the necessary training duration is proportional to the number of fit parameters (2-DoF models have more fit parameters) and that error reduces less than linearly as the training size progressively increases (Ljung 1999).

Second, we researched the specificity of the model (subject-specific vs. DoF-specific vs. universal). A universal model is similar to a Hill model in that the dynamics are pre-assigned. For 1-DoF models, subject-specific models clearly performed best, in general, reducing error by 11–24% compared to universal models. But, for 2-DoF models, universal models actually performed *better* than subject-specific models, in general, by 15–21%. Since model training for 2-DoF models uses twice as many fit parameters, one would expect a

poorer fit (if all other factors are identical). Thus, perhaps it is simply more difficult to identify these more complex models, leading to poorer model fits in the subject-specific models. Additionally, our anecdotal evidence during data collection is that subjects struggled to perform 2-DoF tracking, and may have exhibited greatly reduced tracking accuracy in one of the two DoFs. Thus, the second DoF may have been limited to contractions with a non-uniform distributed range of forces and a colored band-limited spectrum, resulting in poorer per-subject model calibration. However, since the universal model was constructed from 1-DoF trials, it would not suffer from this problem. Note that our universal models were still formed from data specific to our muscles studied, arm pose and training-testing trajectories. Hence, generic models (e.g., Hill style) that are not tuned in this manner (i.e., simply selected, for example, as second-order lowpass dynamics—a common selection) might be expected to perform poorer. Thus, our results do not directly suggest that Hill style models will outperform subject-specific models in all cases.

8.4.2 Limitations and Extensions

First, our sample size was limited and we studied a single joint. Second, we limited our contractions to being constant posture. It is well established that EMG-force varies with joint angle (e.g., the length-tension curve (Rack and Westbury 1969, Vredenbregt and Rau 1973, Doheny, Lowery et al. 2008, Hashemi, Morin et al. 2013, Liu, Liu et al. 2013, Liu, Liu et al. 2015)). Thus, conditions of this work should be extended to varied angle in the future. Third, the method of electrode site selection by backward stepping produces a locally optimum solution, but not necessarily a global optimum. And, this solution is limited by the sites imposed by the original equal-spaced application of the 16 electrodes. Alternative schemes exists, including schemes based on muscle anatomy (Fougner, Stavdahl et al. 2014). Fourth, these results present a conundrum for single-use applications: much fewer than 16 electrodes provide minimum error performance, but the complete set of 16 electrodes must be mounted in order to determine the optimal electrode sites. For single-use applications, it may be as effective to simply use the full 16-channel electrode system and forgo any backward selection of EMG channels. Finally, in order to focus on efficient training of EMG-force models, we limited our models to be linear and did not pre-whiten our EMG data. Non-linear models have been shown to produce better EMG-force relationships (Vredenbregt and Rau 1973, Hashemi, Morin et al. 2012, Dai, Bardizbanian et al. 2017). Further, EMG pre-whitening has been shown to reduce the variance of the EMGσ estimate (Hogan and Mann 1980, Clancy and Hogan 1994), resulting in reduced EMG-force error (Clancy and Hogan 1997, Clancy, Liu et al. 2012, Dai, Bardizbanian et al. 2017). Each of these methods can be incorporated in future work.

8.5 Conclusion

We studied efficient training of 2-DoF EMG-force models using conventional EMG electrodes. We found that EMG-force error reduced as training duration increased, for durations up to 40–60 s. Improvement in performance was greatest at the lower training durations. And, subject-specific models performed best when forming 1-DoF models, but (generally) worst when forming 2-DoF models.

Chapter 9: Optimal Estimation of EMG Standard Deviation (EMGσ) in Additive Measurement Noise: Model-Based Derivations and their Implications

This chapter is published as: Haopeng Wang, Kiriaki J. Rajotte, He Wang, Chenyun Dai, Ziling Zhu, Moinuddin Bhuiyan, Xinming Huang, Edward A Clancy, "Optimal Estimation of EMG Standard Deviation (EMGσ) in Additive Measurement Noise: Model-Based," *IEEE Transactions on Neural Systems and Rehabilitation Engineering*, Volume: 27, Issue: 12, Dec. 2019. Color Versions of one or more of the figures in this paper are available online at: https://ieeexplore.ieee.org/document/8890663.

***Abstract*—Typical electromyogram (EMG) processors estimate EMG signal standard deviation (EMGσ) via moving average root mean square (RMS) or mean absolute value (MAV) filters, whose outputs are used in force estimation, prosthesis/orthosis control, etc. In the inevitable presence of additive measurement noise, some processors subtract the noise standard deviation from EMG RMS (or MAV). Others compute a root difference of squares (RDS)—subtract the noise variance from the square of EMG RMS (or MAV), all followed by taking the square root. Herein, we model EMG as an amplitude-modulated random process in additive measurement noise. Assuming a Gaussian (or, separately, Laplacian) distribution, we derive analytically that the maximum likelihood estimate of EMGσ requires RDS processing. Whenever that subtraction would provide a negative-valued result, we show that EMGσ should be set to zero. Our theoretical models further show that during rest, approximately 50% of EMGσ estimates are non-zero. This result is problematic when EMGσ is used for real-time control, explaining the common use of additional thresholding. We tested our model results experimentally using biceps and triceps EMG from 64 subjects. Experimental results closely followed the Gaussian model. We conclude that EMG processors should use RDS processing and not noise standard deviation subtraction.**

***Index Terms*—Biological system modeling, biomedical signal processing, electromyogram, electromyogram (EMG) amplitude estimation, electromyography, myoelectric signal processing.**

9.1 Introduction

The surface electromyogram (EMG) interference pattern has commonly been processed by the cascade operations of highpass filtering (to remove DC offsets and attenuate motion artifacts); optional pre-whitening (Kaiser and Petersen 1974, Hogan and Mann 1980, Clancy and Farry 2000); and then taking its moving average root mean square (RMS), moving average mean absolute value (MAV), or by rectifying the signal followed by lowpass filtering. If EMG is modeled as an amplitude-modulated random process, then these schemes estimate its time-varying standard deviation (EMGσ). For constant-force, non-fatiguing contractions, it has been shown that RMS processing is the optimal estimate of EMGσ if the *noise-free* EMG signal is modeled as Gaussian distributed (Hogan and Mann 1980, Hogan and Mann 1980, Clancy and Hogan 1994, Clancy and Hogan 1995), and that MAV processing is optimal if the *noise-free* EMG signal is modeled as Laplacian distributed (Clancy and Hogan 1999). EMGσ has been used to estimate torque (Doheny, Lowery et al. 2008, Staudenmann, Roeleveld et al. 2010, Hashemi, Morin et al. 2012, Hashemi, Morin et al. 2015, Dai, Bardizbanian et al. 2017, Dai, Zhu et al. 2019) and mechanical impedance about a joint (Abul-Haj and Hogan 1990, Shin, Kim et al. 2009, Kawase, Kambara et al. 2012, Pfeifer, Vallery et al. 2012, Golkar, Tehrani et al. 2017, Dai, Martel et al. 2019), in motor control research (Ostry and Feldman 2003), and in applications including prosthesis control (Popat, Drebs et al. 1993, Parker, Englehart et al. 2006, Farina, Jiang et al. 2014), ergonomics (Kumar and Mital 1996, Hagg, Melin et al. 2004) and biomechanics (Doorenbosch and Harlaar 2003, Disselhorst-Klug, Schmitz-Rode et al. 2009).

However, EMG is always measured in the presence of additive measurement noise, i.e., noise that exists independent of the level of muscle effort. This noise arises from the measurement apparatus (thermal and active device noise), radiated electromagnetic interference, electrode-to-skin contact resistance (Merletti, Botter et al. 2016), unrelated electrophysiological activity, etc. (Clancy, Morin et al. 2002). This noise has an average RMS intensity that is 1.1–4.5% of the RMS EMG at maximum voluntary contraction (MVC) (Clancy 1999, Clancy and Farry 2000, Clancy, Farina et al. 2005, Liu, Liu et al. 2013, Liu, Liu et al. 2015, Clancy, Martinez-Luna et al. 2017, Dai, Bardizbanian et al. 2017, Dai, Zhu et al. 2019). Consequently, the signal to noise ratio (SNR) is low at low contraction levels.

Thus, researchers have proposed alterations to their EMG processors and/or models to include noise. Kaiser and Peterson (Kaiser and Petersen 1974) found that the shape of their whitening filter should be a function of the contraction level, with lower high-frequency gain during low contraction levels. Parker *et*

al. (Parker, Stuller et al. 1977, Parker and Scott 1986, Zhang, Parker et al. 1991) modeled noise as an additive (white Gaussian) process when *solving* for an optimal multistate EMG classifier, and when *analyzing* (but not *solving*) EMGσ estimators. This additive noise model is now common (e.g., (Baratta, Solomonow et al. 1998, Bonato, D'Alessio et al. 1998, Clancy and Farry 2000, Koirala, Dasog et al. 2015)). Clancy and Farry (Clancy and Farry 2000) whitened the raw EMG, then attenuated additive noise using an adaptive Wiener filter. A Weiner filter is the optimal *linear* filter for attenuating additive noise, but is not necessarily the optimal filter overall. Many papers within the ergonomics literature routinely subtract the standard deviation of the background noise from RMS (or MAV) estimates (Frey Law, Krishnan et al. 2011). However, it has been theoretically *argued* (Ortengren 1996, Hansson 2011) that the root difference of squares (RDS) [i.e., subtracting the noise variance from the square of EMG RMS (or MAV), all followed by taking the square root] is the correct approach. An experimental comparison found that RDS processing performs better than standard deviation subtraction (Frey Law, Avin et al. 2011).

The argument for RDS processing is based on the fact that if the signal and noise are independent, then their variances add—*in theory*. However, to our knowledge, this proposed processor has not been *derived* (i.e., *solved* for, based on a model) as a statistical estimator in the published literature (although one unpublished preliminary result appears in (Clancy 1991)). Solution via an estimator can demonstrate the optimality (or lack thereof) of a processor and expose its statistical properties. Herein, we provide this derivation, some of its properties and experimental evaluation of the derived optimal results, all for the case of constant-effort contraction.

9.2 Mathematical Model of EMG in Additive Noise

Consider an amplitude modulated model of the measured EMG signal, *m[n]*, during constant-effort contraction as (Parker, Stuller et al. 1977, Hogan and Mann 1980, Parker and Scott 1986, Zhang, Parker et al. 1991, Clancy and Hogan 1994):

$$m[n] = s \cdot x[n] + v[n], \quad 0 \le n < N \tag{1}$$

where n is the discrete-time sample index, $s \equiv EMG\sigma$ is the standard deviation (i.e., modulation) of the noise-free EMG, $(s \cdot x[n])$ is the noise-free EMG signal and $v[n]$ is additive noise. Let $x[n]$ be zero mean, unit-variance, wide-sense stationary, correlation-ergodic and have independent samples (i.e., via pre-whitening). Let $v[n]$ be similarly specified, but of variance equal to q^2 and independent of $x[n]$. Let $\underline{m}$, $\underline{x}$ and $\underline{v}$ be vectors comprised of N successive samples of each respective random variable.

A. Gaussian Model—EMGσ Estimate (Clancy 1991, Clancy 2019)

Let both $\underline{x}$ and $\underline{v}$ be jointly Gaussian. Then, $\underline{m}$ is jointly Gaussian with zero mean and covariance matrix: $K_{\underline{mm}} = \sigma_m^2\, I$, where $\sigma_m^2 = s^2 + q^2$ and I is the identity matrix. Thus, the probability density function (PDF) for $\underline{m}$, given that the standard deviation of the noise-free EMG is $s \equiv EMG\sigma$, is:

$$p_{\underline{m}|s}(\underline{M}|s) = \frac{e^{\frac{-\underline{M}^T K_{\underline{mm}}^{-1} \underline{M}}{2}}}{(2\pi)^{N/2} \left|K_{\underline{mm}}\right|^{1/2}} = \frac{e^{\frac{-\sum_{n=0}^{N-1} M^2[n]}{2(s^2+q^2)}}}{[2\pi(s^2+q^2)]^{N/2}}\ , \tag{2}$$

where $\underline{M}$ denotes an instance of the random vector $\underline{m}$.

The maximum likelihood (ML) estimate of s is the value $\hat{s}$ which maximizes the above PDF. A monotonic transformation of the PDF does not alter the location of the maximum. Thus, taking the natural logarithm yields:

$$\ln\left[p_{\underline{m}|s}(\underline{M}|\hat{s})\right] = -\frac{N}{2}\ln(2\pi) - \frac{N}{2}\ln(\hat{s}^2 + q^2) - \frac{\sum_{n=0}^{N-1} M^2[n]}{2(\hat{s}^2+q^2)}. \tag{3}$$

Differentiating the above with respect to $\hat{s}$ gives:

$$\frac{\partial \ln\left[p_{\underline{m}|s}(\underline{M}|\hat{s})\right]}{\partial\, \hat{s}} = -\frac{N}{2}\,\frac{2\hat{s}}{\hat{s}^2+q^2} + \frac{\hat{s}\sum_{n=0}^{N-1} M^2[n]}{(\hat{s}^2+q^2)^2}, \tag{4}$$

Setting this derivative to zero and manipulating leads to a quadratic equation for $\hat{s}^2$, the square root of which provides our intermediate result. The quadratic equation has two solutions. But, one of these solutions is not real-valued, so can be eliminated. The retained intermediate result, written as a discrete-time filter, is:

$$\hat{s}[n] = \sqrt{\left(\frac{\sum_{i=0}^{N-1} M^2[n-i]}{N}\right) - q^2}. \tag{5}$$

The parenthesized term within the square root is the mean square value. Hence, the noise correction is made via RDS processing.

The second derivative of (3) with respect to $\hat{s}$, evaluated at the location of the intermediate result specified by (5) is:

$$\frac{\partial^2 \ln\left[p_{\underline{m}|s}(\underline{M}|\hat{s})\right]}{\partial\, \hat{s}^2} = \left[\frac{2\,N^3}{\left(\sum_{i=0}^{N-1} M^2[n-i]\right)^2}\right]\left[q^2 - \frac{\sum_{i=0}^{N-1} M^2[n-i]}{N}\right]. \tag{6}$$

This second derivative is less than or equal to zero, indicating a local maximum (and not a minimum), when $\frac{1}{N}\sum_{n=0}^{N-1} M^2[n-i]$ exceeds the noise variance q^2. This condition is almost always satisfied during active muscle contraction, but not during low-level contractions or rest. When the condition is not satisfied, maximization with respect to $\hat{s}$ of the PDF occurs at the boundary constraint where $\hat{s} = 0$ (Thomas Jr.,

Weir et al. 2014). Hence, the complete solution for this ML estimate is:

$$\hat{s}_{\mathrm{RMS}}[n] = \sqrt{\max\left[0,\ \left(\frac{\sum_{i=0}^{N-1} M^2[n-i]}{N}\right) - g^2q^2\right]}, \tag{7}$$

where "max" denotes the maximum value operator and the "RMS" subscript emphasizes the use of an RMS processor. Constant scaling factor g has been inserted into this solution, since some applications prefer to artificially inflate the noise threshold. For example, in myoelectric prosthesis control, $g > 1$ helps to insure that the prosthesis is not actuated during rest. For the optimum ML estimate, $g = 1$.

Denote the term in the rounded parenthesis of (7) (i.e., the mean square value of the measured EMG signal) as y. This random variable is Gamma distributed as:

$$p_y(Y) = \frac{Y^{\frac{N}{2}-1}\, e^{\frac{-Y\cdot N}{2\sigma_m^2}}}{\left(\sigma_m\sqrt{\frac{2}{N}}\right)^N \Gamma\left(\frac{N}{2}\right)}\ \mu(Y), \tag{8}$$

where $\Gamma(\cdot)$ is the Gamma function and $\mu(\cdot)$ is the step function. Its cumulative density function (CDF) is:

$$P_{y\leq}(Y) = 1 - \sum_{k=0}^{\frac{N}{2}-1} \frac{\left(\frac{N}{2\,\sigma_m^2}\right)^k Y^k\, e^{\frac{-Y\cdot N}{2\sigma_m^2}}}{k!}\ \mu(Y)\,, N \text{ even} \tag{9}$$

When the muscle is at rest, the true EMGσ is zero ($s = 0$) and the variance of the measured EMG signal is $\sigma_m^2 = q^2$. A fraction of the EMGσ estimates—but not all—will be zero (due to the noise variance subtraction). This probability of estimating a zero value during rest is the CDF of y, evaluated at $Y = g^2q^2$ (with $s = 0$). This probability, for N even, is:

$$P_{y\leq g^2q^2,Rest}(Y) = \left[1 - \sum_{k=0}^{\frac{N}{2}-1} \frac{\left(\frac{N}{2}\right)^k g^{2k}\, e^{\frac{-g^2N}{2}}}{k!}\right] \mu(Y). \tag{10}$$

Note that this probability is *not* a function of the noise variance and is *only* a function of N and g. Fig. 9.1 shows this probability as a function of N for four possible values of g. Equation 10 and Fig. 9.1 show that for $g > 1$, a negative-valued subtraction result within (7) is more likely, producing a higher probability of estimating $\hat{s} = 0$. Conversely, for $g < 1$, a negative-valued subtraction result is less likely, producing a lower probability of estimating $\hat{s} = 0$.

B. Laplacian Model—EMGσ Estimate (Clancy 1991, Clancy 2019)

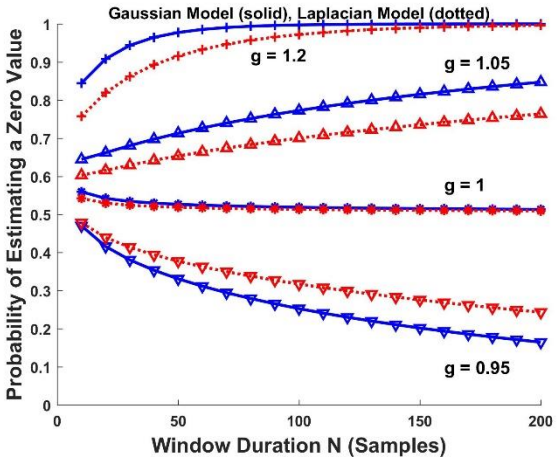

Fig. 9.1. Probability of estimating a zero EMGσ value during rest for theoretical Gaussian model (moving average RMS processing; solid blue) and Laplacian model (moving average MAV processing; dashed red) as a function of number of independent samples *N*, for four different noise gain values "*g*".

MAV processing has been shown to be the ML estimate of EMGσ, if the PDF is Laplacian (Clancy and Hogan 1999). So that the additive noise model has a Laplacian PDF, we directly model the measured EMG samples *m[n]* as being independent and of a Laplacian PDF, without explicit specification of the PDFs of *x[n]* and *v[n]*. (Note that if *x[n]* and *v[n]* are each modeled as Laplacian, then their sum is *not* Laplacian.) Nonetheless, if *x[n]* and *v[n]* are assumed independent, then their variances again add. Thus, the measured EMG again has variance: $s^2 + q^2$, and the PDF for sample *m[n]* is (Drake 1967):

$$p_{m[n]|s}(M[n]|s) = \frac{\sqrt{2}}{2} \cdot \frac{e^{\frac{-\sqrt{2}}{(s^2+q^2)^{1/2}}|M[n]|}}{(s^2+q^2)^{1/2}}. \tag{11}$$

Since the samples of the EMG vector $\underline{m}$ are independent, its joint PDF is the product of the *N* individual PDFs, which simplifies to:

$$p_{\underline{m}|s}(\underline{M}|s) = \left[\frac{\sqrt{2}}{2\,(s^2+q^2)^{1/2}}\right]^N e^{\frac{-\sqrt{2}}{(s^2+q^2)^{1/2}}\sum_{n=0}^{N-1}|M[n]|}. \tag{12}$$

Similar to the Gaussian case above, maximum likelihood estimation of s is found by taking the natural logarithm of the PDF, differentiating with respect to $\hat{s}$, setting this derivative to zero and solving for $\hat{s}$. Again, the second derivative proves this intermediate result to, in fact, be a minimum, subject to the same boundary constraint where $\hat{s} = 0$. The complete filter for this ML estimate, again inserting a scaling factor g for the noise, is:

$$\hat{s}_{MAV}[n] = \sqrt{\max\left[0, \left\{\left(\frac{\sqrt{2}}{N}\sum_{i=0}^{N-1}|M[n-i]|\right)^2\right\} - g^2q^2\right]}. \quad (13)$$

Denote the term in the curly brackets of (13) as *w*. The PDF for this random variable is:

$$p_w(W) = \frac{e^{-\frac{N\sqrt{W}}{\sigma_m}}}{2} \cdot \left[\sum_{k=0}^{N-1}\left(\left\{\frac{N}{\sigma_m\sqrt{W}} - \frac{(N-1-k)}{W}\right\} \cdot \prod_{p=1}^{N-1-k}\left\{\frac{N\sqrt{W}}{\sigma_m p}\right\}\right)\right] \mu(W). \quad (14)$$

Its CDF is:

$$P_{w\leq}(W) = \left\{1 - e^{-\frac{N\sqrt{w}}{\sigma_m}}\left[\sum_{k=0}^{N-1}\left(\prod_{p=1}^{N-1-k}\frac{N\sqrt{W}}{\sigma_m p}\right)\right]\right\} \mu(W). \quad (15)$$

The probability of estimating a zero value during rest is the CDF evaluated at $W = g^2q^2$ (with $s = 0$):

$$P_{w\leq g^2q^2,Rest}(W) = \left\{1 - e^{-Ng}\left[\sum_{k=0}^{N-1}\left(\prod_{p=1}^{N-1-k}\frac{Ng}{p}\right)\right]\right\} \mu(W). \quad (16)$$

Again, the probability of a zero value is only related to *N* and *g*. Fig. 9.1 shows this probability as a function of *N* for four possible values of *g*.

9.3 Experimental Evaluation of the Models

9.3.1 Experimental Data Set

Data from 64 subjects acquired during four prior experiments with overlapping protocols were used for this study (Clancy 1999, Clancy and Farry 2000, Liu, Liu et al. 2015, Dai, Bardizbanian et al. 2017). Re-analysis of these data was exempted from human studies supervision by the WPI Institutional Review Board. Subjects had no known neuromuscular deficits of the right shoulder, arm or hand. In each experiment (see Fig. 9.1 in (Dai, Bardizbanian et al. 2017) for a photograph of the most recently used experimental apparatus), a subject was seated and secured with seat belts. Their right shoulder was abducted 90º, elbow flexed 90º, and hand supinated perpendicular to the floor. Their wrist was cuffed to a load cell to measure constant-posture elbow torque.

The skin above the triceps and biceps muscles was scrubbed with an alcohol wipe. Gel was applied in the latter two studies. Four bipolar EMG electrode-amplifiers were secured over each of the triceps and biceps muscles, in a tightly-spaced transverse row centered on the muscle mid-line, midway between the elbow and the midpoint of the upper arm. Each electrode-amplifier had stainless steel, hemispherical contacts of diameter 4 or 8 mm, separated 10 mm edge-to-edge, oriented along the long axis of the muscle.

A reference electrode was secured alongside the active electrodes. Each EMG channel had selectable gain, a CMRR ≥ 90 dB at 60 Hz, a 10 or 15 Hz highpass filter (second or fourth order), and a 1800 or 2000 Hz lowpass filter (fourth order). EMG and load cell data were sampled at 4096 Hz at 16-bit resolution. Achieved force was fed back in a real-time display, along with a force target.

After a brief warm-up, separate elbow flexion and extension maximum voluntary contraction (MVC) forces were measured, without the use of force feedback. At least 20–30 minutes had elapsed between the time at which the electrodes were mounted and the completion of these MVC measurements. Then, constant-force 50% MVC extension trials, 50% MVC flexion trials and 0% MVC trials (arm at rest, removed from the wrist cuff) were acquired for 5 s each, using force feedback. (Only one of each type of trial was used in our analysis.) Two or three minutes of rest was provided between trials to avoid cumulative fatigue. Each of the eight, 5-s duration EMG signals from a trial was defined as an "epoch." Before any further use off-line, each epoch was highpass filtered (15 Hz cut-off, fourth-order Butterworth); IIR notch filtered at 60 Hz and its harmonics (second-order); when selected, adaptively pre-whitened (Clancy and Farry 2000, Prakash, Salini et al. 2005); and bandlimited to 600 Hz (Dasog, Koirala et al. 2014) (fourth-order Butterworth lowpass). Then the first 500 ms of each epoch was omitted to account for filter start-up transients.

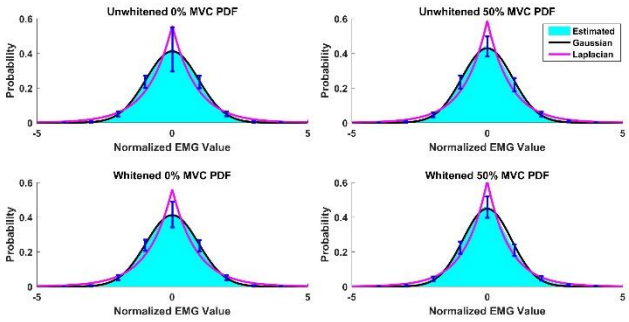

Fig. 9.2. Top shows ensemble-average PDF estimates of *unwhitened* EMG during 0% MVC (left) and 50% MVC (right), as well as best-fit theoretic Gaussian and Laplacian PDFs. Bottom shows corresponding PDF estimates from *whitened* EMG. $N = 512$ epochs from 64 subjects. Error bars in each plot show ±1 std. dev. for the ensemble-average estimates.

9.3.2 Evaluating Model Assumptions—EMG PDF

We evaluated the model assumptions related to the first-order PDF of EMG, both at rest and during 50% MVC trials, with and without whitening. During 50% extension trials, only the four epochs from

TABLE 9.1

ABSOLUTE AREA DIFFERENCES BETWEEN EXPERIMENTAL ENSEMBLE PDFS AND GAUSSIAN/LAPLACIAN PDFS. PARENTHESES LIST STANDARD DEVIATION AT WHICH AREA DIFFERENCE WAS ASSESSED (I.E., STANDARD DEVIATION AT WHICH THE ABSOLUTE ERROR DIFFERENCE BETWEEN EACH ENSEMBLE AND THEORETIC PDF WAS MINIMIZED).

EMG	Gaussian Model		Laplacian Model	
Processing	0% MVC	50% MVC	0% MVC	50% MVC
Unwhite	0.0241 (0.97)	0.0530 (0.93)	0.1981 (1.26)	0.1730 (1.20)
White	0.0188 (0.97)	0.0749 (0.89)	0.2035 (1.26)	0.1532 (1.16)

triceps electrodes were examined; during 50% flexion trials, only the four epochs from biceps electrodes were examined. A total of 512 epochs (64 subjects x 8 electrodes/subject) were available at 0% (rest) and at 50% MVC (combining extension and flexion). Each EMG epoch was normalized to a sample variance of one and a histogram PDF estimate formed (500 bins, equally spaced over the range from –5 to +5). The ensemble histogram sample means and standard deviations are shown in Fig. 9.2.

Best matching between the ensemble vs. theoretic Gaussian/Laplacian PDFs did *not* occur when using theoretic PDFs of unit variances. Thus, the absolute error difference between each ensemble and theoretic PDF was computed for theoretic PDF standard deviations between 0.5 and 2 (increment of 0.01). The minimum area and its corresponding theoretic PDF standard deviation are shown in Table 9.1 (see also Fig. 9.2). In all cases, the data more closely followed the Gaussian model. Kolmogorov-Smirnoff tests between the experimental ensemble PDFs and each of the Gaussian and Laplacian PDFs were not sensitive, finding no statistically significant differences using either the Gaussian model ($p > 0.99$) or the Laplacian model ($p > 0.31$), for the four combinations of effort level (0% MVC, 50% MVC) and whitening. Thus, we computed the absolute area difference between each of the 512 histogram PDF estimates vs. the Gaussian/Laplacian PDFs, finding the best fit standard deviation for each. Paired sign tests (Bonferroni corrected) found the Gaussian PDF to be a better fit ($p < 10^{-6}$) for each of the four combinations.

9.3.3 Evaluating Estimates of EMGσ

Historically, quantitative evaluation of constant-effort EMGσ has used the ratio of the estimate mean to its standard deviation (the inverse of the coefficient of variation), denoted the SNR. With this definition, variations about the mean of EMGσ are considered as "noise." This definition was convenient, as knowledge of neither the "true" EMGσ value nor the EMGσ-force relationship was necessary, and the measure is invariant to signal gain. However, that definition is not as indicative of EMGσ estimate performance once additive noise is modeled. In particular, the noise can cause the EMGσ estimate to incorrectly coalesce about the wrong mean value. In this case, SNR would measure the variation of the processed signal *plus* noise; and not the desired error with respect to the true (noise-free) EMGσ—which is more appropriate for this study.

Thus, root mean square error between the true and estimated EMGσ value was used as the error measure. However, the true value is not known when assessing with real EMG data. Thus, we pursued an approach similar to (Frey Law, Krishnan et al. 2011). Our available 50% MVC trials assume that muscle effort—and therefore EMGσ—is not changing during the contraction. So, we optionally whitened each

EMG epoch, then normalized each 0% and, separately, each 50% MVC epoch to have a standard deviation of one. We treated each 50% MVC epoch as the "true" EMG signal and its 0% MVC epoch from the corresponding electrode as noise. We then multiplied each normalized 50% MVC EMG epoch point-by-point by a ramp (1 s zero, 3 s ramping from 0 to 0.1, 1 s at 0.1). To this signal, we added 0.02 times the respective, normalized 0% MVC epoch. This addition gave a SNR of 5, which is representative of measured EMG (Clancy 1999, Clancy and Farry 2000, Clancy, Farina et al. 2005, Liu, Liu et al. 2013, Liu, Liu et al. 2015, Clancy, Martinez-Luna et al. 2017, Dai, Bardizbanian et al. 2017, Dai, Zhu et al. 2019). We then computed the EMGσ estimate using a 200 ms duration centered (non-causal) window, only using RMS processing (since the Gaussian model was a much better fit to our data), with and without RDS processing. The root mean square error between the EMGσ estimate and the "true" EMGσ (i.e., the ramp pattern) was computed at times 1.0, 1.5, … 4.0 s across the 512 epochs (64 subjects x 8 electrodes per subject). Fig. 9.3 shows summary results. Due to non-normality of the data, we computed paired sign tests (separately for each time) between the root mean square error of all six unique paired combinations of the four factors: unwhitened data, whitened data, without RDS processing, and with RDS processing (Bonferroni corrected). Comparing each method with RDS processing to each method without RDS processing (four comparisons) always resulted in significantly lower errors *with* RDS processing for times $\leq$ 2.5 s ($p < 10^{-5}$), and no differences for times $\geq$ 3 s ($p > 0.1$). When unwhitened vs. whitened processors were compared *without* RDS processing (one combination), there were no statistical differences ($p > 0.1$), except at 1.5 s ($p = 10^{-4}$)—likely an anomoly. When unwhitened vs. whitened processors were compared *with* RDS processing (one combination), whitening had lower error for times $\leq$ 1.5 s ($p < 10^{-5}$), and was not significantly different for times $\geq$ 3.0 s ($p > 0.1$).

9.3.4 Evaluating Probability of a Zero Value at Rest

The theoretical results predict that the probability of estimating a zero value for EMGσ during rest is a function of the window length and the noise gain factor "g". We experimentally evaluated this result using the 512 0% MVC epochs. We again limited analysis to RMS processing. We computed the fraction of zero-valued estimates when using RDS processing for all combinations of: unwhitened vs. whitened processing, window length values ranging from N=2–400 ms, and g values of 0.95, 1, 1.05 and 1.2. The sample variance of each rest epoch was computed (after removing a 400 ms startup transient) and used as the noise variance q^2 to compute its respective RMS estimate of EMGσ.

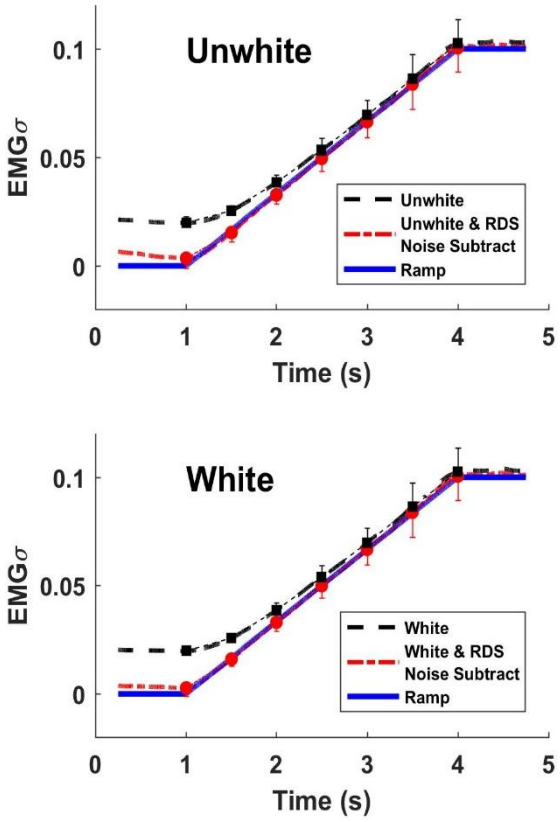

Fig. 9.3. Top shows ensemble averaged *unwhitened* EMGσ estimates along the ramp contraction, with and without RDS processing. Symbols and one-sided error bars show mean and one standard deviation at times 1.0, 1.5, 2.0, …, 4.0. Bottom shows corresponding results for *whitened* EMGσ estimates.

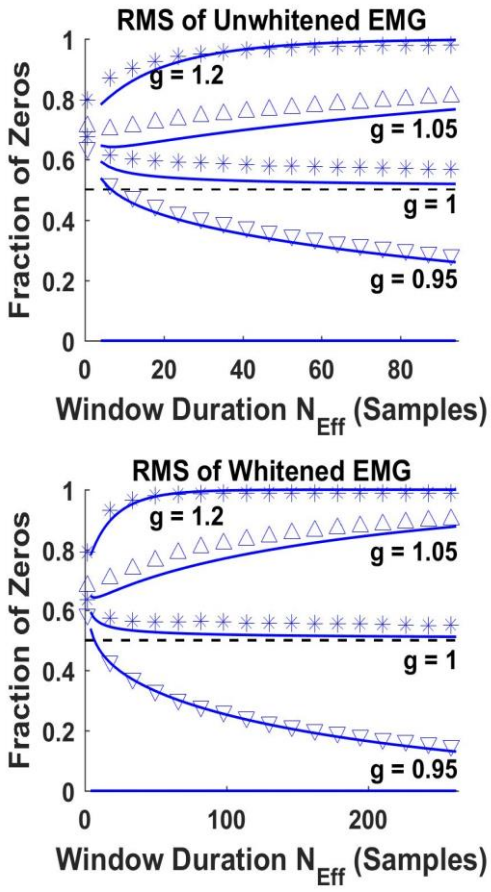

Fig. 9.4. Symbols show fraction of EMGσ values equal to zero during rest contractions for unwhitened (top) and whitened (bottom) experimental moving average RMS estimates as a function of effective number of samples N_{Eff}, for four different noise gain values "g". Solid lines show corresponding theoretic probabilities of zero values (same as Fig. 9.1), for comparison. Dash line show 0.5 probability.

With this method, the selected window length is misleading for comparison to the theoretical results shown in Fig. 9.1, because the experimental EMG signal is correlated (i.e., has finite bandwidth). To resolve this conflict, Bendat and Piersol (Bendat and Piersol 1971, Hogan and Mann 1980) list the number of effective independent samples for a correlated Gaussian process as: $N_{Eff} = 2B_S T$, where B_S is statistical bandwidth (Hz) and T is the window duration (s). Thus, we used the method of (Liu, Liu et al. 2013) to estimate statistical bandwidth from the PSD estimate of each 0% MVC epoch, separately with and without whitening (Welch method, Hamming window, 50% overlap, 614-length DFT). Without whitening we found the 0% MVC bandwidth to be $B_{S,Unwhite} = 118 \pm 72\ Hz$, and with whitening we

found the 0% MVC bandwidth to be $B_{S,White} = 329 \pm 157\ Hz$. Fig. 9.4 plots the fraction of zero values during rest as a function of N_{Eff} and "g".

9.4 Discussion

9.4.1 Maximum Likelihood Estimates of EMGσ

There has been debate in the literature as to the best way in which to suppress the influence of additive noise when estimating EMGσ. While RDS processing has been suggested (as well as other approaches), no model-derived optimal solution has been peer-review published. Herein, we analytically derived, using maximum likelihood estimation, that constant-effort EMG, modeled as either a Gaussian or Laplacian random process, requires RDS processing when additive noise is modeled [equations (7) and (13), respectively, with $g = 1$]. Further, our work shows that when the particular instance of the EMG signal is such that RDS processing would result in a negative value within the square root, then EMGσ should be estimated as EMGσ = 0. While these formulae are derived with constant-effort assumptions, existing EMG processors assume a quasi-stationary EMG signal, even during highly dynamic contractions (Jerard, Williams et al. 1974, D'Alessio 1985, Park and Meek 1995, Clancy 1999, Ranaldi, De Marchis et al. 2018). Thus, a moving average window assumes a constant EMGσ within that window, but an EMGσ that slowly varies between adjacent windows. Hence, these RDS processing results remain valid.

9.4.2 EMG Probability Density Function

It does not appear that the PDF of rest EMG has previously been reported. We found this PDF to closely match the Gaussian PDF.

But, the literature has variously reported the PDF of active EMG as Gaussian or as more peaked near zero than Gaussian (e.g., Laplacian), mostly in small sample size studies. Roesler (Roesler 1974) (sample size not listed, perhaps one subject; biceps, triceps and forearm muscles) found the EMG PDF to be precisely Gaussian across a range of isometric contraction levels. Parker *et al.* (Parker, Stuller et al. 1977) (sample size not listed, likely one trial reported; intramuscular fine wires within the long head of the biceps brachii) found the EMG PDF to be Gaussian during an ~25% MVC and a just perceptible contraction. Hunter *et al.* (Hunter, Kearney et al. 1987) (one subject; biceps brachii muscle) found 30% MVC to have a PDF that is more peaked than Gaussian, as did Bilodeau *et al.* (Bilodeau, Cincera et al. 1997) for 20% MVCs (16 subjects; biceps brachii and brachioradialis muscles). Nazarpour *et al.* (Nazarpour, Al-Timemy

et al. 2013) (four subjects; abductor pollicis brevis and flexor carpi radialis muscles) found evidence that the PDF was more peaked (i.e., closer to Laplacian) at low level contractions, but more bell-shaped/Gaussian at higher contraction levels. They postulated that, since more motor unit firings contribute to the EMG during higher contraction levels, the interference signal more closely obeys the central limit theorem—resulting in a more Gaussian shape.

Our own prior work (Clancy and Hogan 1999) (24 subjects; all distinct from the subjects in the present study) found the PDF from biceps and triceps muscle EMG to be closer to Gaussian than Laplacian, for 10, 25, 50 and 75% constant-force MVCs, using apparatus and methods quite similar to that of the present study. However, this work found that MAV processing produced a higher SNR than RMS processing. A simulation study of constant-effort EMG confirmed that as the EMG PDF is progressively varied from Laplacian to Gaussian, there exists a region wherein the data are more Gaussian in distribution, but MAV processing performs better than RMS.

The present study likely reports the largest sample size to-date. Our EMG exhibited a distribution that closely matched the Gaussian PDF, with a poorer fit to the Laplacian PDF. Since our data were from 50% MVCs (a high contraction level), this result is consistent with the findings of Nazapour *et al.* (Nazarpour, Al-Timemy et al. 2013). Future comparison to data at lower contraction levels (in which (Nazarpour, Al-Timemy et al. 2013) found a more peaked PDF) may be appropriate. The similarity in PDF shapes to our own prior work (Clancy and Hogan 1999) may be due to the similarity in equipment and use of the identical contraction level. In the end, various factors may influence the EMG PDF, including: electrode shape, size and inter-electrode distance; contraction level; and muscle studied.

9.4.3 EMGσ Estimates

Our root mean square error results from the amplitude-modulated ramp contractions show that noise correction is most important at the lowest contractions levels. RDS processing has the advantage of being progressively less noticeable as effort level increases. For example, once the true EMGσ is four times that of the noise standard deviation, the RDS adjustment is only one sixteenth of the true EMGσ. Once the true EMGσ is five times the noise standard deviation, RDS adjustment is only one 25th the true EMGσ. Etc.

9.4.4 Estimator Performance During Rest

For the ML estimate (c.f., $g = 1$ in Fig. 9.1 and Fig. 9.4), we have shown that approximately 50% of EMGσ estimates will be zero, based on either the Gaussian or Laplacian model (excluding unrealistically

small N_{Eff} values). Accordingly, nearly half of all EMGσ estimates will be *greater* than zero during rest! In some applications, this result is problematic. For example, the pose of myoelectrically-controlled prostheses, orthoses and exoskeletons would slowly drift at rest, producing an undesired and potentially dangerous action. Thus, we suggest that undesired non-zero EMGσ estimates during rest be eliminated by accentuating the noise standard deviation (i.e., setting $g > 1$). Fig. 9.1 shows that even modest increases in the gain factor g result in much lower probability of a non-zero value. Indeed, it is common to include threshold subtraction in a prosthesis EMG processor (with zero as the boundary condition), although it is currently applied by subtracting the noise standard deviation from EMG RMS (or MAV) and not via RDS processing (Williams III 1990, Hahne, Schweisfurth et al. 2018).

Note that many biomechanics studies in which the subject is active most of the time might *not* want to increase the gain factor "g". Doing so might create a bias in EMGσ-force estimates.

9.4.5 Limitations

Our theoretical models assumed independent samples, which are approximated in experimental analysis via whitening. However, since signal and noise have some distinctions in their spectral shape (noise exhibits a lower span of power across frequency (Clancy and Farry 2000)), one filter cannot precisely whiten both the noise-free EMG signal and the noise. In particular, whitening filters calibrated to active EMG may contain excessive high frequency gain (Clancy 1991). Thus, some signal correlation will remain. This dissonance may place practical limits on the bandwidth of whitening filters (Dasog, Koirala et al. 2014), and might argue for the use of RDS processing in concert with other noise mitigation techniques such as adaptive whitening (Clancy and Farry 2000) —in which an adaptive Wiener filter provides lowpass filtering with a progressively lower cutoff at lower EMGσ levels.

When evaluating the fraction of zero EMGσ values during a rest contraction, we used that same rest contraction to estimate the noise variance (q^2). In practice, q^2 may vary over time; thus, so would the fraction of zero EMGσ values during rest. Hence, setting the noise gain factor "g" above one might help to mitigate unmeasured changes in q^2.

9.5 Conclusion

Using established stochastic models for EMG in the presence of additive noise, we derived that RDS processing represents the ML estimate of EMGσ, under both Gaussian and Laplacian PDF assumptions. We concomitantly showed that EMGσ should be set to zero whenever RDS processing produces a

negative-valued result. Further, we showed that the ML estimate at rest produces zero EMGσ estimates only 50% of the time (for all but short-duration smoothing windows). Experimentally, our biceps-triceps EMG data more closely followed a Gaussian PDF than a Laplacian PDF. Our EMGσ estimates closely followed theoretical predictions, both during ramp and rest contractions. This work definitively argues that EMG processors should use RDS processing rather than subtracting the noise standard deviation from EMG RMS (or MAV).

Appendix I. Subjects Used in each Experiment

EXPERIMENTS	ABLE-BODIED		LIMB-ABSENT	
CHAPTER	Data Range	Data Used	Data Range	Data Used
CHAPTER 2	LY 01-12	LY 01-12	LY 21-28	LY 21-23, 25-28
CHAPTER 3	LY 01-12	LY 01-12		
CHAPTER 4			LY 21-28	LY 21-23, 25-28
CHAPTER 5	LV 23-32	LV 23-32	LV 41-44	LV 41-44
CHAPTER 6	LZ 01-50	LZ 01-05		
CHAPTER 7	LZ 01-50	LZ 41-43, 45-50		
CHAPTER 8	LZ 01-50	LZ 41-43, 45-50		
CHAPTER 9	LV 00-10	LV 01-10	LV 11-14	LV 11-14
CHAPTER 10				

References

Abul-Haj, C. J. and N. Hogan (1990). "Functional assessment of control systems for cybernetic elbow prosthesis—Part I: Description of the technique." IEEE Trans. Biomed. Eng. **37**(11): 1025–1036.

Al-Timemy, A. H., G. Bugmann, J. Escudero and N. Outram (2013). "Classification of finger movements for the dexterous hand prosthesis control with surface electromyography." IEEE J. Biomed. Health Inform. **17**(3): 608-618.

Alkan, A. and M. Günay (2012). "Identification of EMG signals using discriminant analysis and SVM classifier." Expert Syst. Appl. **39**(1): 44-47.

Ameri, A., E. N. Kamavuako, E. J. Scheme, K. B. Englehart and P. Parker (2014). "Support vector regression for improved real-time, simultaneous myoelectric control." IEEE Trans. Neural Sys. Rehabil. Eng. **22**(6): 1198–1209.

Ameri, A., E. J. Scheme, E. N. Kamavuako, K. B. Englehart and P. A. Parker (2014). "Real-time, simultaneous myoelectric control using force and position-based training paradigms." IEEE Trans. Biomed. Eng. **61**(2): 279–287.

Amsuess, S., P. Goebel, B. Graimann and D. Farina (2014). "A multi-class proportional myocontrol algorithm for upper limb prosthesis control: Validation in real-life scenarios on amputees." IEEE Trans. Neural Syst. Rehabil. Eng. **23**(5): 827-836.

Amsuess, S., I. Vujaklija, P. Goebel, A. D. Roche, B. Graimann, O. C. Aszmann and D. Farina (2016). "Context-dependent upper limb prosthesis control for natural and robust use." IEEE Trans. Neural Sys. Rehabil. Eng. **24**(7): 744–753.

Andison, C. (2011). EMG-based assessment of active muscle stiffness and co-contraction in muscles with primary and secondary actions at the wrist during piano playing. Master of Applied Science, Carleton University.

Atkins, D. J., D. C. Y. Heard and W. H. Donovan (1996). "Epidemilogic overview of individuals with upper-limb loss and their reported research priorities." J. Prosthet. Orthot. **8**(1): 2–11.

Azaria, M. and D. Hertz (1984). "Time delay estimation by generalized cross correlation methods." IEEE Trans. Acoust. Speech Sig. Proc. **32**(2): 280–285.

Babiloni, C., F. Carducci, C. Del Gratta, M. Demartin, G. L. Romani, F. Babiloni and P. M. Rossini (2003). "Hemisperical asymmetry in human SMA during voluntary simple unilateral movements. An fMRI study." Cortex **39**: 293–305.

Bagesteiro, L. B. and R. L. Sainburg (2002). "Handedness: Dominant arm advantages in control of limb dynamics." J. Neurophysiol. **88**: 2408–2421.

Bagesteiro, L. B. and R. L. Sainburg (2003). "Nondominant arm advantages in load compensation during rapic elbow joint movements." J. Neurophysiol. **90**: 1503–1513.

Baratta, R. V., M. Solomonow and B.-H. Zhu (1998). "Methods to reduce the variability of EMG power spectrum estimates." J. Electromyo. Kinesiol. **8**: 279–285.

Barbin, J., V. Seetha, J. Casillas, M., J. Paysant and D. Pérennou (2016). "The effects of mirror therapy on pain and motor control of phantom limb in amputees: A systematic review." Ann. Phys. Rehabil. Med. **59**: 270–275.

Bardizbanian, B., Z. Zhu, J. Li, C. Dai, C. Martinez-Luna, X. Huang, T. Farrell and E. A. Clancy (2018). Calibration of dynamic hand-wrist EMG-force models using a minimum number of electrodes. IEEE SPMB Symposium, Philadelphia, PA.

Bardizbanian, B., Z. Zhu, J. Li, X. Huang, C. Dai, C. Martinez-Luna, B. E. McDonald, T. R. Farrell and E. A. Clancy (2020). Efficiently training two-DoF hand-wrist EMG-force models. Ann. Int. Conf. IEEE EMBS, Montreal, Canada.

Barry, D. (1992). "Vibrations and sounds from evoked muscle twitches." Electromyography and clinical neurophysiology **32**(1-2): 35-40.

Bendat, J. S. and A. G. Piersol (1971). Random Data: Analysis and Measurement Procedures. New York, John Wiley and Sons, Inc.**:** 277–281.

Bertels, T., T. Schmalz and E. Ludwigs (2009). "Objectifying the Functional Advantages of Prosthetic Wrist Flexion." J. Prosthet. Orthot. **21**(2): 74-78.

Bilodeau, M., M. Cincera, A. B. Arsenault and D. Gravel (1997). "Normality and stationarity of EMG signals of elbow flexor muscles during ramp and step isometric contractions." J. Electromyo. Kinesiol. **7**(2): 87–96.

Bonato, P., T. D'Alessio and M. Knaflitz (1998). "A statistical method for the measurement of muscle activation intervals from surface myoelectric signal during gait." IEEE Trans. Biomed. Eng. **45**(3): 287–299.

Boostani, R. and M. H. Moradi (2003). "Evaluation of the forearm EMG signal features for the control of a prosthetic hand." Physiol. Meas. **24**: 309–319.

Boyd, W. J. (2018). EMG Site: A MATLAB-based Application for EMG Data Collection and EMG-based Prosthetic Control M.S. Thesis, Worcester Polytechnic Institute, Worcester, MA.

Buchanan, T. S., D. G. Lloyd, K. Manal and T. F. Besier (2004). "Neuromusculoskeletal modeling: Estimation of muscle forces and joint moments and movements from measurements of neural command." J Appl Biomech **20**(4): 367–395.

Buchthal, F. and H. Schmalbruch (1980). "Motor unit of mammalian muscle." Physiological reviews **60**(1): 90-142.

Burke, R., D. Levine, F. E. Zajac, P. Tsairis and W. Engel (1971). "Mammalian motor units: physiological-histochemical correlation in three types in cat gastrocnemius." Science **174(**4010): 709-712.

Carson, R. G. (1989). "Manual asymmetries: Feeback processing, output variability, and spatial complexity—Resolving some inconsistencies." J. Motor Behav. **21**(1): 38–47.

Cavanaugh, K. T., E. A. Clancy, J. A. Natrillo, R. J. Paquette and F. J. Looft (1983). "Optimal site selection for prosthetic control." IEEE 1983 Frontiers Eng. Comput. Health Care: 565–569.

Chan, B. L., R. Witt, A. P. Charrow, A. Magee, R. Howard, P. F. Pasquina, K. M. Heilman and J. W. Tsao (2007). "Mirror therapy for phantom limb pain." New England J. Med. **357(**21): 2206–2207.

Cipriani, C., C. Antfolk, M. Controzzi, G. Lundborg, M. C. Carrozza and F. Sebelius (2011). "Online myoelectric control of a dexterous hand prosthesis by transradial amputees." IEEE Trans. Neural Sys. Rehabil. Eng. **19**(3): 260–270.

Cipriani, C., F. Zaccone, S. Micera and M. C. Carozza (2008). "On the shared control of an EMG-controlled prosthetic hand: Analysis of user-prosthesis interaction." IEEE Trans. Robotics **24**(1): 170–184.

Clancy, E. A. (1991). Stochastic Modeling of the Relationship Between the Surface Electromygram and Muscle Torque, Ph.D Thesis, Massachusetts Institute of Technology, p. 303–352, 449–469.

Clancy, E. A. (1999). "Electromyogram amplitude estimation with adaptive smoothing window length." IEEE Trans. Biomed. Eng. **46**(6): 717–729.

Clancy, E. A. (2019). Optimal Electromyogram Modeling and Processing During Active Contractions and Rest, Haopeng Wang M.S. Thesis, Worcester Polytechnic Institute**:** 40–58.

Clancy, E. A., O. Bida and D. Rancourt (2006). "Influence of advanced electromyogram (EMG) amplitude processors on EMG-to-torque estimation during constant-posture, force-varying contractions." J. Biomech. **39**: 2690–2698.

Clancy, E. A., D. Farina and R. Merletti (2005). "Cross-comparison of time- and frequency-domain methods for monitoring the myoelectric signal during a cyclic, force-varying, fatiguing hand-grip task." J. Electromyo. Kinesiol. **15**: 256–265.

Clancy, E. A. and K. A. Farry (2000). "Adaptive whitening of the electromyogram to improve amplitude estimation." IEEE Trans. Biomed. Eng. **47**(6): 709–719.

Clancy, E. A. and N. Hogan (1994). "Single site electromyograph amplitude estimation." IEEE Trans. Biomed. Eng. **41**(2): 159–167.

Clancy, E. A. and N. Hogan (1995). "Multiple site electromyograph amplitude estimation." IEEE Trans. Biomed. Eng. **42**(2): 203–211.

Clancy, E. A. and N. Hogan (1997). "Relating agonist-antagonist electromyograms to joint torque during isometric, quasi-isotonic, non-fatiguing contractions." IEEE Trans. Biomed. Eng. **44**(10): 1024–1028.

Clancy, E. A. and N. Hogan (1999). "Probability density of the surface electromyogram and its relation to amplitude detectors." IEEE Trans. Biomed. Eng. **46**(6): 730–739.

Clancy, E. A., L. Liu, P. Liu and D. V. Moyer (2012). "Identification of constant-posture EMG-torque relationship about the elbow using nonlinear dynamic models." IEEE Trans. Biomed. Eng. **59**(1): 205–212.

Clancy, E. A., C. Martinez-Luna, M. Wartenberg, C. Dai and T. Farrell (2017). "Two degrees of freedom quasi-static EMG-force at the wrist using a minimum number of electrodes." J Electromyogr Kinesiol **34**: 24–36.

Clancy, E. A., C. Martinez-Luna, M. Wartenberg, C. Dai and T. Farrell (2017). "Two degrees of freedom quasi-static EMG-force at the wrist using a minimum number of electrodes." J. Electromyogr. Kinesiol. **34**: 24–36.

Clancy, E. A., E. L. Morin and R. Merletti (2002). "Sampling, noise-reduction and amplitude estimation issues in surface electromyography." J. Electromyo. Kinesiol. **12**: 1–16.

Clancy, E. A., F. Negro and D. Farina (2016). Single-channel techniques for information extraction from the surface EMG signal. Surface Electromyography: Physiology, Engineering, and Applications. R. Merletti and D. Farina, John Wiley & Sons, Inc.**:** 91–125.

Coapt, LLC, 222 W. Ontario St., Suite 300, Chicago, IL. Retrieved accessed 6 June 2015, 2015, from http://www.coaptengineering.com.

Coupar, F., A. Pollock, P. Rowe, C. Weir and P. Langhorne (2011). "Predictors of upper limb recovery after stroke: A systematic review and meta-analysis." Clin. Rehabil. **26**(4): 291–313.

D'Alessio, T. (1985). "Analysis of a digital EMG signal processor in dynamic conditions." IEEE Trans. Biomed. Eng. **32**: 78–82.

Dai, C., B. Bardizbanian and E. A. Clancy (2017). "Comparison of constant-posture force-varying EMG-force dynamic models about the elbow." IEEE Trans. Neural Sys. Rehabil. Eng.(9): 1529–1538.

Dai, C., B. Bardizbanian and E. A. Clancy (in press). "Comparison of constant-posture force-varying EMG-force dynamic models about the elbow." IEEE Trans. Neural Sys. Rehabil. Eng.

Dai, C., S. Martel, F. Martel, D. Rancourt and E. A. Clancy (2019). "Single-trial estimation of quasi-static EMG-to-joint-mechanical-impedance relationship over a range of joint torques." J. Electromyo. Kinesiol. **45**: 18–25.

Dai, C., Z. Zhu, C. Martinez-Luna, T. R. Hunt, T. R. Farrell and E. A. Clancy (2019). "Two degrees of freedom, dynamic, hand-wrist EMG-force using a minimum number of electrodes." J. Electromyo. Kinesiol. **47**: 10–18.

Dai, C., Z. Zhu, C. Martinez-Luna, T. R. Hunt, T. R. Farrell and E. A. Clancy (2019). "Two degrees of freedom, dynamic, hand-wrist EMG-force using a minimum number of electrodes." J. Electromyogr. Kinesiol. **47**: 10–18.

Dasog, M., K. Koirala, P. Liu and E. A. Clancy (2014). "Electromyogram bandwidth requirements when the signal is whitened." IEEE Trans. Neural Sys. Rehabil. Eng. **22**(3): 664–670.

Dillingham, T. R., L. E. Pezzin and E. J. MacKenzie (2002). "Limb Amputation and Limb Deficiency: Epidemiology and Recent Trends in the United States." South. Med. J. **95**: 875–883.

Disselhorst-Klug, C., T. Schmitz-Rode and G. Rau (2009). "Surface electromyography and muscle force: Limits in sEMG-force relationship and new approaches for applications." Clin. Biomech. **24**: 225–235.

Doheny, E. P., M. M. Lowery, D. P. FitzPatrick and M. J. O'Malley (2008). "Effect of elbow joint angle on force-EMG relationships in human elbow flexor and extensor muscles." J Electromyogr Kinesiol **18**: 760–770.

Doorenbosch, C. A. M. and J. Harlaar (2003). "A clinically applicable EMG-force model to quantify active stabilization of the knee after a lesion of the anterior cruciate ligament." Clin. Biomech. **18**: 142–149.

Drake, A. W. (1967). Fundamentals of Applied Probability Theory. New York, McGraw-Hill Book Company**:** 103–107, 273–274.

Dyson, M., S. Dupan, H. Jones and K. Nazarpour (2020). "Learning, generalization, and scalability of abstract myoelectric control." IEEE Trans. Neural Syst. Rehabil. Eng. **28**(7): 1539-1547.

Englehart, K. and B. Hudgins (2003). "A robust, real-time control scheme for multifunction myoelectric control." IEEE Trans. Biomed. Eng. **50**(7): 848–854.

Farina, D., N. Jiang, H. Rehbaum, A. Holobar, B. Graimann, H. Dietl and O. C. Aszmann (2014). "The extraction of neural information from the surface EMG for the control of upper-limb prostheses: Emerging avenues and Challenges." IEEE Trans. Neural Sys. Rehabil. Eng. **22**(4): 797–809.

Finch, J. (2011). "The ancient origins of prosthetic medicine." The Lancet **377**(9765): 548-549.

Force, L. L. T. and A. Coalition (2012). "Roadmap for preventing limb loss in america: Recommendations from the 2012 limb loss task force." Knoxville, Tennessee.

Fougner, A., O. Stavdahl, P. J. Kyberd, Y. G. Losier and P. A. Parker (2012). "Control of upper limb prosthesis: Terminology and proportional myoelectric Control—A review." IEEE Trans. Neural Sys. Rehabil. Eng. **20**(5): 663–677.

Fougner, A., Ø. Stavdahl, P. J. Kyberd, Y. G. Losier and P. A. Parker (2012). "Control of upper limb prostheses: Terminology and proportional myoelectric control—A review." IEEE Transactions on neural systems and rehabilitation engineering **20**(5): 663-677.

Fougner, A. L., O. Stavdahl and P. J. Kyberd (2014). "System training and assessment in simultaneous proportional myoelectric prosthesis control." J. NeuroEng. Rehabil. **11:75**.

Frey Law, L., K. Avin and C. Krishnan (2011). "Response to letter to the editor." J. Biomech. **44**: 1637–1638.

Frey Law, L., C. Krishnan and K. Avin (2011). "Modeling nonlinear errors in surface electromyography due to baseline noise: A new methodology." J. Biomech. **44**: 202–205.

Friedmann, L. W. (1978). The psychological rehabilitation of the amputee, Charles C Thomas.

Georgopoulos, A. P., J. F. Kalaska, R. Caminiti and J. T. Massey (1982). "On the relations between the direction of two-dimensional arm movements and cell discharge in primate motor cortex." Journal of Neuroscience **2**(11): 1527-1537.

Gilroy, A. M., B. R. MacPherson, L. M. Ross, J. Broman and A. Josephson (2008, p. 328–336). Atlas of Anatomy. Germany, Thieme.

Girden, E. R. (1992). ANOVA: Repeated Measures, Sage Publications**:** 21.
Girden, E. R. (1992, p. 21). ANOVA: Repeated Measures, Sage Publications.
Goble, D. J. and S. H. Brown (2008). "The biological and behavioral basis of upper limb asymmetries in sensorimotor performance." Neurosci. Biobehav. Rev. **32**: 598–610.
Goble, D. J. and S. H. Brown (2008). "Upper limb asymmetries in the matching of proprioceptive versus visual targets." J. Neurophysiol. **99**: 3063–3074.
Golkar, M. A., E. S. Tehrani and R. E. Kearney (2017). "Linear parametric varying identification of dynamic joint stiffness during time-varying voluntary contractions." Front. Comput. Neurosci. **11**: 35.
Graupe, D. and W. K. Cline (1975). "Functional separation of EMG signals via ARMA identification methods for prosthesis control purposes." IEEE Trans. Sys. Man Cyber. **5**(2): 252–259.
Graziano, M. S. and T. N. Aflalo (2007). "Mapping behavioral repertoire onto the cortex." Neuron **56**(2): 239-251.
Gribble, P. L., L. I. Mullin, N. Cothros and A. Mattar (2003). "Role of cocontraction in arm movement accuracy." J. Neurophysiol. **89**(5): 2396-2405.
Haaland, K. Y., J. L. Prestopnik, R. T. Knight and R. R. Lee (2004). "Hemispheric asymmetries for kinetic and positional aspects of reaching." Brain **127**: 1145–1158.
Hagg, G. M., B. Melin and R. Kadefors (2004). Applications in ergonomics. Electromyography: Physiology, Engineering, and Noninvasive Applications. R. Merletti and P. A. Parker, IEEE Press/Wiley-Interscience**:** 343–363.
Hahne, J. M., Biebmann, F., N. Jiang, H. Rehbaum, D. Farina, F. C. Meinecke, K.-R. Muller and L. C. Parra (2014). "Linear and nonlinear regression techniques for simultaneous and proportional myoelectric control." IEEE Trans. Neural Sys. Rehabil. Eng. **22**(2): 269–279.
Hahne, J. M., Biessmann, F., N. Jiang, H. Rehbaum, D. Farina, F. C. Meinecke, K.-R. Muller and L. C. Parra (2014). "Linear and nonlinear regression techniques for simultaneous and proportional myoelectric control." IEEE Trans. Neural Sys. Rehabil. Eng. **22**(2): 269–279.
Hahne, J. M., S. Dahne, H.-J. Hwang, K.-R. Muller and L. C. Parra (2015). "Concurrent adaptation of human and machine improves simultaneous and proportional myoelectric control." IEEE Trans. Neural Sys. Rehabil. Eng. **24**(4): 618–627.
Hahne, J. M., M. Markovic and D. Farina (2017). "User adaptation in myoelectric man-machine interfaces." Sci. Reports **7**: 4437.
Hahne, J. M., M. A. Schweisfurth, M. Koppe and D. Farina (2018). "Simultaneous control of multiple functions of bionic hand prostheses: Performance and robustness in end users." Sci. Robot. **3**: eaat3630.
Hahne, J. M., M. A. Wilke, M. Koppe, D. Farina and A. F. Schilling (2020). "Longitudinal case study of regression-based hand prosthesis control in daily life." Front. Neurosci. **14**: 600.
Hansson, G.-A. (2011). "Letter to the editor." J. Biomech. **44**: 1637.
Hashemi, J., E. Morin, P. Mousavi and K. Hashtrudi-Zaad (2013). "Surface EMG force modeling with joint angle based calibration." J Electromyogr Kinesiol **23**: 416–424.
Hashemi, J., E. Morin, P. Mousavi and K. Hashtrudi-Zaad (2015). "Enhanced dynamic EMG-force estimation through calibration and PCI modeling." IEEE Trans. Neural Sys. Rehabil. Eng. **23**(1): 41–50.
Hashemi, J., E. Morin, P. Mousavi, K. Mountjoy and K. Hashtrudi-Zaad (2012). "EMG-force modeling using parallel cascade identification." J Electromyogr Kinesiol **22**: 469–477.
Hashemi, J., E. Morin, P. Mousavi, K. Mountjoy and K. Hashtrudi-Zaad (2012). "EMG-force modeling using parallel cascade identification." J. Electromyogr. Kinesiol. **22**: 469–477.

Hof, A. L. and J. Van den Berg (1981). "EMG to force processing I: An electrical analogue of the Hill muscle model." J. Biomech. **14**(11): 747–758.

Hogan, N. and R. W. Mann (1980). "Myoelectric signal processing: Optimal estimation applied to electromyography—Part I: Derivation of the optimal myoprocessor." IEEE Trans. Biomed. Eng. **27**(7): 382–395.

Hogan, N. and R. W. Mann (1980). "Myoelectric signal processing: Optimal estimation applied to electromyography—Part II: Experimental demonstration of optimal myoprocessor performance." IEEE Trans. Biomed. Eng. **27**(7): 396–410.

Howell, D. C. (p. 366, 2010). Statistical Methods for Psychology, 7th Ed. Belmont, CA, Cengage Wadsworth.

Hrysomallis, C. (2011). "Balance ability and athletic performance." Sports medicine **41**(3): 221-232.

Huang, H.-P. and C.-Y. Chen (1999). "Development of a myoelectric discrimination system for a multi-degree prosthetic hand." Proc. IEEE Int. Conf. Robotics Automat.: 2392–2397.

Hudgins, B., P. Parker and R. N. Scott (1993). "A new strategy for multifunction myoelectric control." IEEE Trans. Biomed. Eng. **40**(1): 82–94.

Hunter, I. W., R. E. Kearney and L. A. Jones (1987). "Estimation of the conduction velocity of muscle action potentials using phase and impulse response function techniques." Med. Biol. Eng. Comput. **25**: 121–126.

Hussaini, A. and P. Kyberd (2017). "Refined clothespin relocation test and assessment of motion." Prosthet. Orthot. Int. **41**(3): 294-302.

Igual, C., J. Igual, J. M. Hahne and L. C. Parra (2019). "Adaptive auto-regressive proportional myoelectric control." IEEE Trans. Neural Syst. Rehabil. Eng. **27**(2): 314-322.

Inman, V. T., H. J. Ralston, J. B. Saunders, B. Feinstein and E. W. Wright (1952). "Relation of human electromyogram to musculuar tension." EEG Clin. Neurophysiol. **4**(2): 187–194.

Jegatheeswaran, G., M. Vesia, R. Isyama, C. Gunraj and R. Chen (2018). "Increases in motor cortical excitability during mirror visual feedback of a precision grasp is influenced by vision and movement of the opposite limb." Neurosci. Let. **681**: 31–36.

Jerard, R. B., T. W. Williams and C. W. Ohlenbusch (1974). Practical design of an EMG controlled above elbow prosthesis. Proc. 1974 Conf. Eng. Devices Rehabil., Boston, MA.

Jiang, N., S. Dosen, K.-R. Muller and D. Farina (2012). "Myoelectric control of artificial limbs—Is there a need to change focus?" IEEE Signal Proc. Mag. **29**(5): 152–150.

Jiang, N., K. B. Englehart and P. A. Parker (2009). "Extracting simultaneous and proportional neural control information for multiple-DOF prostheses from the surface electromyographic signal." IEEE Trans. Biomed. Eng. **56**(4): 1070–1080.

Jiang, N., S. Muceli, B. Graimann and D. Farina (2013). "Effect of arm position on the prediction of kinematics from EMG in amputees." Med. Biol. Eng. Comput. **51**: 143–151.

Jiang, N., H. Rehbaum, I. Vujaklija, B. Graimann and D. Farina (2014). "Intuitive, online, simultaneous, and proportional myoelectric control over two degrees-of-freedom in upper limb amputees." IEEE Trans. Neural Sys. Rehabil. Eng. **22**(3): 501–510.

Jiang, N., J. L. G. Vest-Nielsen, S. Muceli and D. Farina (2012). "EMG-based simultaneous and proportional estimation of wrist/hand kinematics in uni-lateral trans-radial amputees." J. NeuroEng. Rehabil. **9:42**.

Jiang, N., I. Vujaklija, H. Rehbaum, B. Graimann and D. Farina (2014). "Is accurate mapping of EMG signals on kinematics needed for precise online myoelectric control?" IEEE Trans. Neural Sys. Rehabil. Eng. **22**(3): 549–558.

Johansen-Berg, H. and P. Matthews (2002). "Attention to movement modulates activity in sensori-motor areas, including primary motor cortex." Exp. Brain Res. **142**(1): 13-24.

Kaiser, E. and I. Petersen (1974). Adaptive Filter for EMG Control Signals. The Control of Upper-Extremity Prostheses and Orthoses. P. Herberts, R. Kadefors, R. Magnusson and I. Petersen. Springfield, IL, Charles C. Thomas**:** 54–57.

Kamen, G. (2004). "Research methods in biomechanics." Champaign, IL, Human Kinetics Publ.

Kang, N. and J. H. Cauraugh (2017). "Bilateral synergy as an index of force coordination in chronic stroke." Exp. Brain Res. **235**: 1501–1509.

Kawase, T., H. Kambara and Y. Koike (2012). "A power assist device based on joint equilibrium point estimation from EMG signals." J. Robot. Mechatron. **24**(1): 205–218.

Kearney, R., E., R. B. Stein and L. Parameswaran (1997). "Indentification of intrinsic and reflex contributions to human ankle stiffness dynamics." IEEE Trans. Biomed. Eng. **44**(6): 493–504.

Kelly, M. F., P. A. Parker and R. N. Scott (1990). "The application of neural networks to myoelectric signal analysis: A preliminary study." IEEE Trans. Biomed. Eng. **37**(3): 221-230.

Kelso, J. S. (1982). Human motor behavior: An introduction, Psychology Press.

Kenway, L. C., L. M. Bisset and J. J. Kavanagh (2015). "Removing visual feedback for a single limb alters between-limb force tremor relationships during isometric bilateral contractions." Exp. Brain Res. **233**: 115–124.

Kestner, S. (2006). "Defining the relationship between prosthetic wrist function and its use in performing work tasks and activities of daily living." J. Prosthet. Orthot. **18**(3): 80-86.

Khushaba, R. N., S. Kodagoda, M. Takruri and G. Dissanayake (2012). "Toward improved control of prosthetic fingers using surface electromyogram (EMG) signals." Exp. Sys. App. **39**: 10731–10738.

Koirala, K., M. Dasog, P. Liu and E. A. Clancy (2015). "Using the electromyogram to anticipate torques about the elbow." IEEE Trans. Neural Sys. Rehabil. Eng. **23**(3): 396–402.

Kuiken, T. A., G. A. Dumanian, R. D. Lipschutz, L. A. Miller and K. A. Stubblefield (2004). "The use of targeted muscle reinnervation for improved myoelectric prosthesis control in a bilateral shoulder disarticulation amputee." Prosthet. Orthot. Int. **28**: 245–253.

Kuiken, T. A., G. Li, B. A. Lock, R. D. Lipschutz, L. A. Miller, K. A. Stubblefield and K. B. Englehart (2009). "Targeted muscle reinnervation for real-time myoelectric control of multifunction artificial arms." J. Am. Med. Assoc. **301**(6): 619–628.

Kuiken, T. A., L. A. Miller, K. Turner and L. J. Hargrove (2016). "A comparison of pattern recognition control and direct control of a multiple degree-of-freedom transradial prosthesis." IEEE J. Transl. Eng. Health Med. **4**: 1-8.

Kumar, S. and A. Mital (1996). Electromyography in Ergonomics. Briston, PA, Taylor & Francis.

Light, C. M., P. H. Chappell and P. J. Kyberd (2002). "Establishing a standardized clinical assessment tool of pathologic and prosthetic hand function: Normative data, reliability, and validity." Arch. Phys. Med. Rehabil. **83**: 776–783.

Lin, C., B. Wang, N. Jiang and D. Farina (2018). "Robust extraction of basis functions for simultaneous and proportional myoelectric control via sparse non-negative matrix factorization." J. Neural. Eng. **5**: 026017.

Lipschutz, R. D., T. A. Kuiken, L. A. Miller and G. A. Dumanian (2006). "Shoulder disarticulation externally powered prosthetic fitting following targeted muscle reinnervation for improved myoelectric control." J. Prosthet. Orthot. **18**: 28–34.

Liu, H., S. M. Stufflebeam, J. Sepulcre, T. Hedden and R. L. Buckner (2009). "Evidence from intrinsic activity that asymmetry of the human brain is controlled by multiple factors." PNAS **106**(48): 20499–20503.

Liu, L., P. Liu, E. A. Clancy, E. Scheme and K. B. Englehart (2013). "Electromyogram whitening for improved classification accuracy in upper limb prosthesis control." IEEE Trans. Neural Sys. Rehabil. Eng. **21**(5): 767–774.

Liu, M. M., W. Herzog and H. H. C. M. Savelberg (1999). "Dynamic muscle force predictions from EMG: An artificial neural network approach." J. Electromyo. Kinesiol. **9**: 391–400.

Liu, P., D. R. Brown, E. A. Clancy, F. Martel and D. Rancourt (2013). "EMG-force estimation for multiple fingers." IEEE Sig. Proc. Med. Biol. Symp.

Liu, P., L. Liu and E. A. Clancy (2015). "Influence of joint angle on EMG-torque model during constant-posture, torque-varying contractions." IEEE Trans. Neural Sys. Rehabil. Eng. **23**(6): 1039–1046.

Liu, P., L. Liu, F. Martel, D. Rancourt and E. A. Clancy (2013). "Influence of joint angle on EMG-torque model during constant-posture quasi-constant-torque contractions." J. Electromyo. Kinesiol. **23**: 1020–1028.

Ljung, L. (1999). System Identification: Theory for the User. Upper Saddle River, NJ, Prentice-Hall**:** 408–452, 491–519.

Ljung, L. (1999). System Identification: Theory for the User. Upper Saddle River, NJ, Prentice-Hall**:** 1–8, 408–452, 491–519.

Lodha, N., S. K. Naik, S. A. Coombes and J. H. Cauraugh (2010). "Force control and degree of motor impairments in chronic stroke." Clin. Neurophysiol. **121**: 1952–1961.

Lovely, D. F. (2004). Signals and Signal Processing for Myoelectric Control. Powered Upper Limb Prostheses: Control, Implementation and Clinical Application. A. Muzumdar. Berlin, Heidelberg, Springer Berlin Heidelberg**:** 35-54.

Luce, R. D. (1986, p. 209–210). Response Times: Their Role in Inferring Elementary Mental Organization, Oxford University Press.

Luh, J.-J., C. Gwo-Ching, C.-K. Cheng, J.-S. Lai and e.-S. Kuo (1999). "Isokinetic elbow joint torques estimation from surface EMG and joint kinematic data: Using an artificial neural network model." J. Electromyo. Kinesiol. **9**: 173–183.

Maat, B., G. Smit, D. Plettenburg and P. Breedveld (2018). "Passive prosthetic hands and tools: A literature review." Prosthetics and orthotics international **42**(1): 66-74.

MacDonald, M., D. Losier, V. L. Chester and U. Kuruganti (2014). "Comparison of bilateral and unilateral contractions between swimmers and nonathletes during leg press and hand grip exercises." Applied Physiology, Nutrition, and Metabolism **39**(11): 1245-1249.

MacPhee, B. J. (2007). Examining the prosthetic function and body behavior of prosthesis users performing activities of daily living, University of New Brunswick, Department of Mechanical Engineering.

Mann, R. W. (1981). "Cybernetic limb prosthesis: The ALZA distinguished lecture." Ann. Biomed. Eng. **9**: 1–43.

Mann, R. W. and S. D. Reimers (1970). "Kinesthetic sensing for the EMG controlled "Boston Arm"." IEEE Trans. Man-Mach. Sys. **11**(1): 110–115.

Mathiowetz, V., G. Volland, N. Kashman and K. Weber (1985). "Adult norms for the Box and Block Test of manual dexterity." Am. J. Occup. Ther. **39**(6): 386-391.

McGimpsey, G. and T. C. Bradford (2008). "Limb prosthetics services and devices." Bioengineering Institute Center for Neuroprosthetics Worcester Polytechnic Institution.

McGimpsey, G. and T. C. Bradford (2008). "Limb prosthetics services and devices." Bioengineering Institute Center for Neuroprosthetics Worcester Polytechnic Institute.

Mercier, C., K. T. Reilly, C. D. Vargas, A. Aballea and A. Sirigu (2006). "Mapping phantom movement representations in the motor cortex of amputees." Brain **129**(8): 2202–2210.

Merletti, R., A. Botter and U. Barone (2016). Detection and conditioning of surface EMG signals. Surface Electromyography; Physiology, Engineering, and Applications. R. Merlett and D. Farina. Hoboken, New Jersey, John Wiley & Sons, Inc.**:** 54–90.

Messier, R. H., J. Duffy, H. M. Litchman, P. R. Raslay, J. F. Soechting and P. A. Stewart (1971). "The electromyogram as a measure of tension in the human biceps and triceps muscles." Int. J. Mech. Sci. **13**: 585–598.

Mozaffarian, D., E. J. Benjamin, A. S. Go, D. K. Arnett, M. J. Blaha, M. Cushman, S. R. Das, S. de Ferranti, J.-P. Després, H. J. Fullerton and e. al. (2016). "Executive summary: Heart disease and stroke statistics—2016 update. A report from the American Heart Association." Circulation **133**: 447–454.

Muceli, S. and D. Farina (2012). "Simultaneous and proportional estimation of hand kinematics from EMG during mirrored movements at multiple degrees-of-freedom." IEEE Trans. Neural Sys. Rehabil. Eng. **20**(3): 371–378.

Muceli, S., N. Jiang and D. Farina (2010). Multichannel surface EMG based estimation of bilateral hand kinematics during movements at multiple degrees of freedom. Ann. Int. Conf. IEEE EMBS, Buenos Aires, Argentina.

Muceli, S., N. Jiang and D. Farina (2014). "Extracting signals robust to electrode number and shift for online simultaneous and proportional myoelectric control by factorization algorithms." IEEE Trans. Neural Sys. Rehabil. Eng. **22**(3): 623–633.

Muzumdar, A. (2004). Powered upper limb prostheses: control, implementation and clinical application; 11 tables, Springer Science & Business Media.

Nazarpour, K., A. Al-Timemy, G. Bugmann and A. Jackson (2013). "A note on the probability distrubution function of the surface electromyogram signal." Brain Res. Bull. **90**: 88–91.

Neilson, C. (2002). "Issues affecting the future demand for orthotists and prosthetists: update 2002." Alexandria, VA: National Commission on Orthotic and Prosthetic Education.

Nielsen, J. L., S. Holmgaard, N. Jiang, K. B. Englehart, D. Farina and P. Parker (2011). "Simultaneous and proportional force estimation for multifunction myoelectric prostheses using mirrored bilateral training." IEEE Trans. Biomed. Eng. **58**(3): 681–688.

Nikolajsen, L. and T. S. Jensen (2001). "Phantom limb pain." Br. J. Anaesthesia **87**(1): 107–116.

Noble, J. W., J. J. Eng and L. A. Boyd (2013). "Effect of visual feedback on brain activation during motor tasks: an FMRI study." Motor Control **17**(3): 298.

Olsson, A. E., N. Malešević, A. Björkman and C. Antfolk (2021). "Learning regularized representations of categorically labelled surface EMG enables simultaneous and proportional myoelectric control." J. Neuroeng. Rehabil. **18**(1): 1-19.

Ortengren, R. (1996). Noise and artefacts. Electromyography in Ergonomics. S. Kumar and A. Mital. London, Taylor & Francis**:** 97–107.

Oskouei, H. A., M. G. Paulin and A. B. Carman (2013). "Intra-session and inter-day reliability of forearm surface EMG during varying hand grip forces." J. Electromyo. Kinesiol. **23**: 216–222.

Ostry, D. J. and A. G. Feldman (2003). "A critical evaluation of the force control hypothesis in motor control." Exp. Brain Res. **153**: 275–288.

Pan, L., D. L. Crouch and H. Huang (2018). "Myoelectric control based on a generic musculosketal model: Toward a multi-user neural-machine interface." IEEE Trans. Neural Sys. Rehabil. Eng. **26**(7): 1435–1442.

Park, E. and S. G. Meek (1995). "Adaptive filter of the electromyographic signal for prosthetic control and force estimation." IEEE Trans. Biomed. Eng. **42**: 1048–1052.

Parker, P., K. Englehart and B. Hudgins (2006). "Myoelectric signal processing for control of powered limb prostheses." J. Electromyogr. Kinesiol. **16**(6): 541-548.

Parker, P., K. Englehart and B. Hudgins (2006). "Myoelectric signal processing for control of powered limb prostheses." J. Electromyo. Kinesiol. **16**: 541–548.
Parker, P., K. Englehart and B. Hudgins (2006). "Myoelectric signal processing for control of powered limb prostheses." J. Electromyogr. Kinesiol. **16**: 541–548.
Parker, P. A. and R. N. Scott (1986). "Myoelectric control of prostheses." CRC Crit. Reviews Biomed. Eng. **13**(4): 283–310.
Parker, P. A., J. A. Stuller and R. N. Scott (1977). "Signal processing for the multistate myoelectric channel." Proc. IEEE **65**(5): 662–674.
Peerdeman, B., D. Boere, H. Witteveen, H. Hermens, S. Stramigioli, H. Rietman, P. Veltink and S. Misra (2011). "Myoelectric forearm prostheses: state of the art from a user-centered perspective." J. Rehabil. Res. Dev. **48**(6).
Pfeifer, S., H. Vallery, M. Hardegger, R. Riener and E. J. Perreault (2012). "Model-based estimation of knee stiffness." IEEE Trans. Biomed. Eng. **59**(9): 2604–2612.
Popat, R. A., D. E. Drebs, J. Mansfield, D. Russell, E. Clancy, K. M. Gill-Body and N. Hogan (1993). "Quantitative assessment of four men using above-elbow prosthetic control." Arch. Phys. Med. Rehabil. **74**: 720–729.
Popović, M. B. (2003). "Control of neural prostheses for grasping and reaching." Med. Eng. Phys. **25**(1): 41-50.
Powell, M. A., R. R. Kaliki and N. V. Thakor (2014). "User training for pattern recognition-based myoelectric prostheses: Improving phantom limb movement consistency and distinguishability." IEEE Trans. Neural Sys. Rehabil. Eng. **22**(3): 522–532.
Pradhan, A., U. Kuruganti, W. Hill, N. Jiang and V. Chester (2020). Robust Simultaneous and Proportional Myoelectric Control Scheme for Individuals with Transradial Amputations. 2020 42nd Ann. Int. Conf. IEEE Eng. Med. Biol. Soc., IEEE.
Prakash, P., C. A. Salini, J. A. Tranquilli, D. R. Brown and E. A. Clancy (2005). "Adaptive whitening in electromyogram amplitude estimation for epoch-based applications." IEEE Trans. Biomed. Eng. **52**(2): 331–334.
Press, W. H., B. P. Flannery, S. A. Teukolsky and W. T. Vetterling (1994). Numerical Recipies in C. New York, Cambridge Univ. Press**:** 671–681.
Rack, P. M. H. and D. R. Westbury (1969). "The effects of length and stimulus rate on tension in the isometric cat soleus muscle." J. Physiol. **2014**: 443–460.
Ramachandran, V. S. and E. L. Altschuler (2009). "The use of visual feedback, in particular mirror visual feedback, in restoring brain function." Brain **132**: 1693–1710.
Ramachandran, V. S. and D. Rogers-Ramachandran (1996). "Synaesthesia in phantom limbs induced with mirrors." Proc. R. Soc. Lond. B **263**(1369): 377–386.
Ranaldi, S., C. De Marchis and S. Conforto (2018). "An automatic, adaptive, information-based algorithm for the extraction of the sEMG envelope." J. Electromyo. Kinesiol. **42**: 1–9.
Rancourt, D. and N. Hogan (2001). "Dynamics of pushing." J. Motor Behavior **33**(4): 351–362.
Reilly, K. T., C. Mercier, M. H. Schieber and A. Sirigu (2006). "Persistent hand motor commands in the amputees' brain." Brain **129**(8): 2211–2223.
Robertson, D. G. E. and J. J. Dowling (2003). "Design and responses of Butterworth and critically damped digital filters." J. Electromyogr. Kinesiol. **13**(6): 569-573.
Roesler, H. (1974). Statistical analysis and evaluation of myoelectric signals for proportional control. The Control of Upper-Extremity Prosthesis and Orthoses. Springfield, IL, Thomas**:** 44–53.
Rojas-Martínez, M., M. A. Mañanas and J. F. Alonso (2012). "High-density surface EMG maps from upper-arm and forearm muscles." J. Neuroeng. Rehabil. **9**(1): 1-17.

Ross, M. P. (2007). Development of a quantitative test for prosthetic function using motion analysis and activities of daily living, ProQuest.
Sainburg, R. L. (2002). "Evidence for a dynamic-dominance hypothesis of handedness." Exp. Brain Res. **142**: 241–258.
Sainburg, R. L., D. Good and A. Przybyla (2013). "Bilateral synergy: A framework for post-stroke rehabilitation." J. Neurol. Transl. Neurosci. **1**(3): 1025.
Schaefer, S. Y., K. Y. Haaland and R. L. Sainburg (2001). "Ipsilesional motor deficits following stroke reflect hemispherical specializations for movement control." Brain **130**: 2146–2158.
Schmidt, R. A. (1975). "A schema theory of discrete motor skill learning." Psych. Rev. **82**(4): 225–260.
Sherman, E. D. (1964). "A Russian bioelectric-controlled prosthesis: Report of a research team from the Rehabilitation Institute of Montreal." Can. Med. Assoc. J. **91**(24): 1268.
Sherwood, D. E. (2014). "Aiming accuracy in preferred and non-preferred limbs: Implications for programming models of motor control." Front. Psychol. **5**: 1236.
Shin, D., J. Kim and Y. Koike (2009). "A myokinetic arm model for estimating joint torque and stiffness from EMG signals during maintained posture." J. Neurophysiol. **101**: 387–401.
Simon, A. M., L. J. Hargrove, B. A. Lock and T. A. Kuiken (2011). "Target achievement control test: Evaluating real-time myoelectric pattern-recognition control of multifunctional upper-limb prostheses." J. Rehabil. Res. Devel. **48**(6): 619–628.
Simon, A. M., B. A. Lock and K. A. Stubblefield (2012). "Patient training for functional use of pattern recognition-controlled prostheses." J. Prosthet. Orthot. **24**(2): 56–64.
Smith, L. H., T. A. Kuiken and L. J. Hargrove (2014). "Real-time simultaneous and proportional myoelectric control using intramuscular EMG." J. Neural. Eng. **11**: 066013.
Smith, L. H., T. A. Kuiken and L. J. Hargrove (2016). "Evaluation of linear regression simultaneous myoelectric control using intramuscular EMG." IEEE Trans. Biomed. Eng. **63**(4): 737–746.
Smith, R. J., D. Huberdeau, F. Tenore and N. V. Thakor (2009). "Real-time myoelectric decoding of individual finger movements for a virtual target task." Ann. Int. Conf. IEEE EMBS: 2376–2379.
Smith, R. J., F. Tenore, D. Huberdeau, R. Etienne-Cummings and N. V. Thakor (2008). "Continuous decoding of finger position from surface EMG signals for the control of powered prostheses." Ann. Int. Conf. IEEE EMBS: 197–200.
Soares, A., A. Andrade, E. Lamounier and R. Carrijo (2003). "The development of a virtual myoelectric prosthesis controlled by an EMG pattern recognition system based on neural networks." J. Intell. Inf. Syst. **21**(2): 127-141.
Spanias, J. A., E. J. Perreault and L. J. Hargrove (2015). "Detection of and compensation for EMG disturbances for powered lower limb prosthesis control." IEEE Trans. Neural Syst. Rehabil. Eng. **24**(2): 226-234.
Staudenmann, D., I. Kingma, A. Daffertshofer, D. F. Stegeman and J. H. Van Dieen (2006). "Improving EMG-based muscle force estimation by using a high-density EMG grid and principal component analysis." IEEE Trans. Neural Sys. Rehabil. Eng. **53**(4): 712–719.
Staudenmann, D., K. Roeleveld, D. F. Stegeman and J. H. van Dieen (2010). "Methodological aspects of EMG recordings for force estimation—A tutorial and review." J Electromyogr Kinesiol **20**: 375–387.
Swinnen, S. P. (2002). "Intermanual coordination: From behavioral principles to neural-netwok interactions." Nature Rev. **3**: 350–361.
Tabor, A., S. Bateman and E. Scheme (2018). "Evaluation of myoelectric control learning using multi-session game-based training." IEEE Trans. Neural Sys. Rehabil. Eng. **26**(9): 1680–1688.
Thieme, H., J. Mehrholz, M. Pohl, J. Behrens and C. Doyle (2012). "Mirror therapy for improving motor function after stroke." Stroke **44**(1): e1–e2.

Thomas Jr., G. B., M. D. Weir, J. Hass and C. Heil (2014). Thomas' Calculus. Boston, MA, Pearson**:** 185–193.

Todor, J. I. and T. Doane (1978). "Handedness and hemispheric asymmetry in the control of movements." J. Motor Behav. **10**(4): 295–300.

Tracy, B. L., L. N. Hitchcock, S. J. Welsh, R. J. Paxton and C. E. Feldman-Kothe (2015). "Visuomotor correction is a robust contributor to force variability during index finger abduction by older adults." Front. Aging Neurosci. **7**: 229.

Triggs, W. J., B. Subramanium and F. Rossi (1999). "Hand preference and transcranial magnetic stimulation asymmetry of cortical motor representation." Brain Re. **835**: 324–329.

Vredenbregt, J. and G. Rau (1973). "Surface electromyography in relation to force, muscle length and endurance." New Developments Electromyogr. Clin. Neurophysiol. **1**: 607–622.

Weir, J. P., L. L. Wagner and T. J. Housh (1992). "Linearity and reliability of the IEMG v torque relationship for the forearm flexors and leg extensors." American journal of physical medicine & rehabilitation **71**(5): 283-287.

Whitall, J., S. M. Waller, K. H. C. Silver and R. F. Macko (2000). "Repetitive bilateral arm training with rhythmic auditory cueing improves motor function in chronic hemiparetic stroke." Stroke **31**: 2390–2395.

Williams III, T. W. (1990). "Practical methods for controlling powered upper-extremity prostheses." Assist. Technol. **2**: 3–18.

Winter, D. A. (2005). Biomechanics and Motor Control of Human Movement, 3rd edition. Hoboken, NJ, John Wiley & Sons, Inc.**:** 203–260.

Winter, D. A. (2009, pp. 250–280). Biomechanics and Motor Control of Human Movement. New Jersey, John Wiley & Sons, Inc.

Winter, D. A. and H. J. Yack (1987). "EMG profiles during normal human walking: Stride-to-stride and inter-subject variability." Electroenceph Clin Neurophysiol **67**: 402–411.

Wirta, R. W., D. R. Taylor and F. R. Finley (1978). "Pattern-recognition arm prosthesis: a historical perspective-a final report." Bull. Prosthet. Res **10**(30): 8-35.

Xing, K., P. Yang, J. Huang, Y. Wang and Q. Zhu (2014). "A real-time EMG pattern recognition method for virtual myoelectric hand control." Neurocomputing **136**: 345-355.

Zhang, Y. T., P. A. Parker and R. N. Scott (1991). "Control performance characteristics of myelectric signal with additive interference." Med. Biol. Eng. Comput. **29**: 84–88.

Zhu, Z., C. Martinez-Luna, J. Li, B. E. McDonald, C. Dai, X. Huang, T. R. Farrell and E. A. Clancy (2020). "EMG-Force and EMG-Target Models During Force-Varying Bilateral Hand-Wrist Contraction in Able-Bodied and Limb-Absent Subjects." IEEE Trans. Neural Syst. Rehabil. Eng.

Zhu, Z., C. Martinez-Luna, J. Li, B. E. McDonald, C. Dai, X. Huang, T. R. Farrell and E. A. Clancy (2020). "EMG-Force and EMG-Target Models During Force-Varying Bilateral Hand-Wrist Contraction in Able-Bodied and Limb-Absent Subjects." IEEE Transactions on Neural Systems and Rehabilitation Engineering.

Zhu, Z., C. Martinez-Luna, J. Li, B. E. McDonald, C. Dai, X. Huang, T. R. Farrell and E. A. Clancy (in press). "EMG-force and EMG-target models during force-varying bilateral hand-wrist contraction in able-bodied and limb-absent subjects." IEEE Trans. Neural Sys. Rehabil. Eng.

Ziegler-Graham, K., E. J. MacKenzie, P. L. Ephraim, T. G. Travison and R. Brookmeyer (2008). "Estimating the prevalence of limb loss in the United States: 2005 to 2050." Arch. Phys. Med. Rehabil. **89**: 422–429.